AD NUMBER

AD865317

NEW LIMITATION CHANGE

TO

Approved for public release, distribution unlimited

FROM

Distribution authorized to U.S. Gov't. agencies and their contractors; Administrative/Operational Use; Dec 1969. Other requests shall be referred to Air Force Materials Lab., Attn: MAMC, Wright-Patterson AFB, OH 45433.

AUTHORITY

AFML ltr, 29 Mar 1972

AD 865317

AFML-TR-69-84
PART II. VOLUME I

STABILITY CHARACTERIZATION OF REFRACTORY MATERIALS UNDER HIGH VELOCITY ATMOSPHERIC FLIGHT CONDITIONS

PART II. VOLUME I: FACILITIES AND TECHNIQUES EMPLOYED FOR CHARACTERIZATION OF CANDIDATE MATERIALS

LARRY KAUFMAN
HARVEY NESOR
ManLabs, Inc.

TECHNICAL REPORT AFML-TR-69-84, PART II, VOLUME I

DECEMBER 1969

This document is subject to special export controls and each transmittal to foreign governments or foreign nationals may be made only with prior approval of the Air Force Materials Laboratory (MAMC), Wright-Patterson Air Force Base, Ohio 45433.

AIR FORCE MATERIALS LABORATORY
AIR FORCE SYSTEMS COMMAND
WRIGHT-PATTERSON AIR FORCE BASE, OHIO

101

NOTICE

When Government drawings, specifications, or other data are used for any purpose other than in connection with a definitely related Government procurement operation, the United States Government thereby incurs no responsibility nor any obligation whatsoever; and the fact that the government may have formulated, furnished, or in any way supplied the said drawings, specifications, or other data, is not to be regarded by implication or otherwise as in any manner licensing the holder or any other person or corporation, or conveying any rights or permission to manufacture, use, or sell any patented invention that may in any way be related thereto.

This document is subject to special export controls and each transmittal to foreign governments or foreign nationals may be made only with prior approval of the Air Force Materials Laboratory (MAMC), Wright-Patterson Air Force Base, Ohio 45433.

Distribution of this report is limited for the protection of technology relating to critical materials restricted by the Export Control Act.

Copies of this report should not be returned unless return is required by security considerations, contractual obligations, or notice on a specific document.

700 - January 1970 - CO455 - 105-2334

STABILITY CHARACTERIZATION OF REFRACTORY MATERIALS UNDER HIGH VELOCITY ATMOSPHERIC FLIGHT CONDITIONS

PART II. VOLUME I: FACILITIES AND TECHNIQUES EMPLOYED FOR CHARACTERIZATION OF CANDIDATE MATERIALS

LARRY KAUFMAN

HARVEY NESOR

FOREWORD

This report was prepared by ManLabs, Inc. with the assistance of the Non-Destructive Testing Group at Avco Missile Systems Division, Lowell, Massachusetts. Avco personnel involved in this study included E.A. Proudfoot, R. Gaudette, G. Lockyear and Dr. R. Stinebring. This contract was initiated under Project 7312, "Metal Surface Deterioration and Protection", Task 731201, "Metal Surface Protection" and Project 7350, "Refractory Inorganic Nonmetallic Materials", Task Nos. 735001, "Refractory Inorganic Nonmetallic Materials: Nongraphitic", and 735002, "Refractory Inorganic Nonmetallic Materials: Graphitic", under AF33 (615)-3859 and was administered by the Metals and Ceramics Divisions of the Air Force Materials Laboratory, Air Force Systems Command, with J. D. Latva, J. Krochmal, and N. M. Geyer acting as project engineers.

This report covers the period from April 1966 to July 1969.

ManLabs personnel participating in this study included L. Kaufman, H. Nesor, H. Bernstein, E. Peters, J.R. Baron, G. Stepakoff, R. Pober, R. Hopper, R. Yeaton, S. Wallerstein, E. Sybicki, J. Davis, K. Meaney, K. Ross, J. Dudley, E. Offner, A. Macey, A. Silverman, and A. Constantino.

The manuscript of this report was released by the authors September 1969 for publication. This technical report has been reviewed and is approved.

W. G. Ramke
Chief, Ceramics and Graphite Branch
Metals and Ceramics Division
Air Force Materials Laboratory

The following reports will be issued under this contract:

Part/Volume	
I-I	Summary of Results
II-I	Facilities and Techniques Employed for Characterization of Candidate Materials
II-II	Facilities and Techniques Employed for Cold Gas/Hot Wall Tests
II-III	Facilities and Techniques Employed for Hot Gas/Cold Wall Tests
III-I	Experimental Results of Low Velocity Cold Gas/Hot Wall Tests
III-II	Experimental Results of High Velocity Cold Gas/Hot Wall Tests
III-III	Experimental Results of High Velocity Hot Gas/Cold Wall Tests
IV-I	Theoretical Correlation of Material Performance with Stream Conditions
IV-II	Computer Calculation of the General Surface Reaction Problem

ABSTRACT

The oxidation of refractory borides, graphites, and JT composites, hypereutectic carbide-graphite composites, refractory metals, coated refractory metals, metal oxide composites and iridium coated graphites in air over a wide range of conditions was studied over the spectrum of conditions encountered during reentry or high velocity atmospheric flight as well as those employed in conventional furnace tests. Elucidation of the relationship between hot gas/cold wall (HG/CW) and cold gas/hot wall (CG/HW) surface effects in terms of heat and mass transfer rates at high temperatures was a principal goal of this investigation.

This report describes the candidate materials which were obtained from commercial sources and represent state of the art materials. Available processing information is included. Characterization of materials was performed by qualitative spectrographic, wet chemical and vacuum (or inert gas) fusion, metallographic, X-ray, electron microprobe and pycnometric analysis. Standard analysis of refractory boride, carbide and silicide composites were employed. However, considerable difficulties were encountered in the chemical analysis of JT graphite composites due to formation of $ZrSiO_4$ or $HfSiO_4$ on combustion. In order to avoid this complication a novel method was developed.

Nondestructive testing of candidate materials included radiography, gamma radiometry, die penetrant inspection and measurement of ultrasonic velocity. Film radiography was used to detect the presence of voids, inclusions and local gross changes in composition. Radiometric density gauging used to measure local densities within each specimen and alcohol penetrant tests were employed to disclose tight surface cracks which are not visible at moderate magnifications.

The measurement of ultrasonic velocity was utilized for establishing correlations between quantitative NDT measurements and material properties. Process variations leading to modulus changes, (such as preferred orientation in elastically anisotropic materials or small amounts of "stiffening" impurities) change sound velocity. These techniques are capable of a precision of about 1%. Moreover, ultrasonic energy is reflected at solid material/air interfaces. Such interfaces exist at cracks, bursts, voids, etc., present in solids.

The results of nondestructive testing of samples prior to arc plasma testing is reported. Test results are provided for a series of hemispherical shells of diboride composites. Graphite composites, silicon carbide and hafnium-tantalum alloy were also tested prior to exposure. In several instances, flaws which caused failures on exposure were detected by means of dye penetrant and radiographic techniques. The latter methods proved to be most effective of the NDT techniques employed in this study.

TABLE OF CONTENTS

LIST OF FIGURES

LIST OF TABLES

I. INTRODUCTION AND SUMMARY

A. Introduction

The response of refractory materials to high temperature oxidizing conditions imposed by furnace heating has been observed to differ markedly from the behavior in arc plasma "reentry simulators". The former evaluations are normally performed for long times at fixed temperatures and slow gas flows with well defined solid/gas-reactant/product chemistry. The latter on the other hand are usually carried out under high velocity gas-flow conditions in which the energy flux rather than the temperature is defined and significant shear forces can be encountered. Consequently, the differences in philosophy, observables and techniques used in the "material centered" regime and the "environment centered-reentry simulation" area differ so significantly as to render correlation of material responses at high and low speeds difficult if not impossible in many cases. Under these circumstances, expeditious utilization of the vast background of information available in either area for optimum matching of existing material systems with specific missions or prediction and synthesis of advanced material systems to meet requirements of projected missions is sharply curtailed.

In order to progress toward the elimination of this gap, an integrated study of the response of refractory materials to oxidation in air over a wide range of time, gas velocity, temperature and pressure has been designed and implemented. This interdisciplinary study spans the heat flux and boundary-layer-shear spectrum of conditions encountered during high velocity atmospheric flight as well as conditions normally employed in conventional materials centered investigations. In this context, significant efforts have been directed toward elucidating the relationship between hot gas/cold wall (HG/CW) and cold gas/hot wall (CG/HW) surface effects in terms of heat and mass transfer rates at high temperatures, so that full utilization of both types of experimental data can be made. In gaseous and solid oxide formation, the elucidation of various mass transfer reaction regimes have been studied.

The principal goal of this study is the coupling of the material-centered and environment-centered philosophies in order to gain a better insight into systems behavior under high-speed atmospheric flight conditions. This coupling function has been provided by an interdisciplinary panel composed of scientists representing the component philosophies. The coupling framework consists of an intimate mixture of theoretical and experimental studies specifically designed to overlap temperature/energy and pressure/velocity conditions. This overlap has provided a means for the evaluation of test techniques and the performance of specific materials systems under a wide range of flight conditions. In addition, it provides a base for developing an integrated theory or modus operandi capable of translating reentry systems requirements such as velocity, altitude, configuration and lifetime into requisite materials properties as vaporization rates, oxidation kinetics, density, etc., over a wide range of conditions.

The correlation of heat flux, stagnation enthalpy, Mach Number, stagnation pressure and specimen geometry with surface temperature through the utilization of thermodynamic, thermal and radiational properties of the material and environmental systems used in this study was of prime importance in defining the conditions for overlap between materials-centered and environment-centered tests.

Significant practical as well as fundamental progress along the above mentioned lines necessitated evaluation of refractory material systems which exhibit varying gradations of stability above 2700°F. Emphasis was placed on candidates for 3400° to 6000°F exploitation. Thus, borides, carbides, boride-graphite composites (JTA), JT composites, carbide-graphite composites, pyrolytic and bulk graphite, PT graphite, coated refractory metals/alloys, oxide-metal composites, oxidation resistant refractory metal alloys and iridium-coated graphites were considered. Similarly, a range of test facilities and techniques including oxygen pickup measurements, cold sample hot gas and hot sample cold gas devices at low velocities, as well as different arc plasma facilities capable of covering the 50-2500 BTU/ft^{2}sec flux range under conditions equivalent to speeds up to Mach 12 at altitudes up to 200,000 ft were employed. Stagnation pressures between 0.001 and 10 atmospheres were covered. Splash and pipe tests were performed in order to evaluate the effects of aerodynamic shear. Based on the present results, this range of heat flux and stagnation enthalpy produced surface temperatures between 2000° and 6500°F.

B. Summary

The candidate materials employed in the current study were obtained from commercial sources and represent state of the art materials. An attempt was made to obtain processing information from each supplier. This was not possible in all cases due to requirements for preserving proprietary manufacturing information. However, manufacturing procedures were obtained on some cases.

Characterization of candidate materials was performed by means of qualitative spectrographic, wet chemical and vacuum (or inert gas) fusion, metallographic, X-ray, electron microprobe and pycnometric analysis. In most cases, these analyses were performed at ManLabs, Inc. In addition, some wet chemical analyses were performed at the Department of Metallurgy, M.I.T. Qualitative spectrographic analysis was performed by Jarrell-Ash Co. of Waltham, Massachusetts, while M.I.T. and Luvak, Inc. of Newton, Massachusetts, carried out vacuum (or inert gas) fusion analysis.

Standard methods for analysis of refractory boride, carbide and silicide composites have been employed in performing the wet chemical analysis. However, considerable difficulties were encountered in the chemical analysis of JT graphite composites due to formation of $ZrSiO_4$ or $HfSiO_4$ on combustion. In order to avoid this complication, a novel method was employed for analysis. The details of this method are reported.

The results of characterization analysis for all of the candidate materials is provided in the form of tabular data on chemistry, density, phase analysis by X-ray diffraction and metallography. Photomicrographs of all the candidate materials are provided.

Nondestructive testing of candidate materials was performed at Avco/SSD. Test methods included radiography, gamma radiometry, die penetrant inspection and measurement of ultrasonic velocity.

Film radiography was used to detect the presence of voids, inclusions and local gross changes in composition such as gross segregation. The through transmission method is used with the X-ray source on one side of the specimen and a film (detector) on the other side. Absorption is a function of the chemistry, the density and thickness. When several elemental components are present, the absorption coefficient depends on the density and the percentage of each element present and the wavelength or "voltage" of the incident radiation. If chemistry, density and thickness are constant, the amount of radiation passing through the specimen will be constant and the film will be uniformly exposed. However, if foreign included material or segregation is present, or if the thickness changes (as in the case of a void) then the amount of radiation impinging on the film is less than the surrounding image. Radiographic sensitivity depends on the source and the detector system used, but optimum combinations yield intensity differences of the order of 1% with resolution down to $\pm$ 0.001 inch.

Gamma radiometry is similar to radiography. In radiometric density gauging, a collimated source of radiation is used, and a confined beam is directed through the specimen impinging on a scintillation detector. The utility of such measurements for later application to large specimens or parts has been demonstrated; further, if density appears to be an important variable with respect to oxidation behavior, resolution can be further improved and local densities determined within each specimen.

Penetrant tests were used to disclose tight surface cracks which may not be visible to the naked eye or even at moderate magnifications. In practice, any one of a number of low viscosity fluids is applied to the surface. The low viscosity fluid is either drawn out by the use of "developers" or permitted to seep out naturally to provide an easily recognisable and enlarged indication of the crack. Alcohol was used in the present case because it is unlikely to result in any contamination (some procedures may leave a residue in the crack or pores present).

The measurement of velocity presents a means for determining properties of interest by direct calculation using well known relations, and by establishing correlations between quantitative NDT measurements and material properties. In regard to elastic properties, for example, relationships exist between wave velocities, density and elastic moduli.

Consequently, process variations leading to modulus changes, either total or in a given direction (such as preferred orientation in elastically anisotropic materials or small amounts of "stiffening" impurities) will show up as a change in sound velocity. In some materials, depending on the stress-strain relationship, variation in internal stress levels will also be indicated. These techniques are capable of determining velocity to a precision of about 1%. Moreover, due to the very large ultrasonic impedence differences between gases and solid materials, ultrasonic energy is very efficiently reflected at solid material/air interfaces. Such interfaces occur when cracks, bursts, voids, etc., are present in solids and ultrasonic detection of such flaws is quite common.

Variations in chemical composition, phases present, distribution of phases, hardness and internal stress result in changes in the electromagnetic properties of electrically conductive materials. Thus, the measurement of electromagnetic properties especially in the near surface layers, could provide a measure of relative oxidation resistance. This measurement was made by a coil carrying an alternating electrical signal which is brought into proximity with the electrically conductive specimen. Eddy currents induced in the specimen were dissipated through the action of the resistivity of the material encountered. Reflection to the exciting coil results in a coil current related to the electromagnetic properties of the material in the field induced by the coil.

The results of nondestructive testing of $HfB_{2.1}$(A-2), ZrB_2 (A-3), HfC+C(C-11), ZrC+C(C-12), JTA(D-13), JT0981(F-16) and Ir/C(I-24) samples prior to arc plasma testing is reported. In addition, test results are provided for a series of diboride composites exposed in the Ten Megawatt Arc facility. Hemispherical shells of diboride composites, graphite composites, silicon carbide and hafnium-tantalum alloy were also tested prior to exposure in the CAL Wave Superheater. In several instances, flaws were detected by means of dye penetrant and radiographic techniques which caused failures on exposure. The latter methods proved to be most effective of the NDT techniques employed in this study.

II. PROCUREMENT OF CANDIDATE MATERIALS

The candidate materials employed in the present study are listed in Table 1. This listing includes the code number assigned to each material as well as the source. An attempt was made to obtain processing information from each supplier. This was not possible in all cases due to requirements for preserving proprietary manufacturing information. The processing techniques employed in the fabrication of diborides (A-6), (A-7), (A-8), (A-9) and (A-10) by hot pressing techniques are contained in reports generated under AF33(615)-3671 (1)*. The following listing summarizes the remaining information which was made available by various suppliers.

1. $HfB_{2.1}$(A-2) was prepared by Carborundum from 3 lots of powder having the following composition:

Lot No.	4	3	2
Soluble (Hf + Zr)	87.39	87.60	87.32
Insoluble (HfO_2)	0.99	0.54	1.64
C	0.44	0.64	0.10
B	9.86	10.36	10.53
N	0.14	-----	-----
Gross B/Me	1.87	1.95	1.99

This powder together with a SiC addition was employed to fabricate HfB_2+SiC(A-4).

2. ZrB_2(A-3) was prepared by Carborundum from powder having the following composition:

Soluble (Zr)	80.43
Insoluble (ZrO_2)	0.17
C	1.07
B	18.51
N	1.20

3. LMSC Glassy Carbon (B-11) was supplied by Lockheed Palo Alto Research Laboratory as finished samples suitable for arc plasma testing. The preparation involved molding of a thermosetting resin to shape with allowance for shrinkage, and a pyrolysis operation. The maximum heat treatment temperature is either 2000° or 3000°F and materials are designated as Grades 2000 or 3000, accordingly.

4. HfC+C(C-11) billets were fabricated by Battelle Memorial Institute. Nuclear-grade graphite and good quality hafnium sponge were the starting materials. Charges were first pre-alloyed by skull-arc melting in a helium atmosphere. Both the electrode and crucible were graphite so that little contamination was introduced. Next, the charges

*Underscored numbers in parentheses indicate References given at the end of this report.

were remelted and then drop-cast into an induction heated graphite mold, once again in a helium atmosphere. The rough billets were machined to 1 inch diameter by 4 inches long to eliminate surface flaws and end effects.

5. ZrC+C(C-12) billets were fabricated by Battelle Memorial Institute utilizing identical procedures as described above for HfC+C (C-11). Starting materials were nuclear-grade graphite and zirconium chunklets.

6. W+Zr+Cu(G-20) rods were supplied from material, fabricated by Rocketdyne (2). The material was fabricated by infiltration of zirconium-25% copper into a porous tungsten lattice.

7. W+Ag(G-21) rods were supplied from material fabricated by Wah Chang Corp. The material was fabricated by infiltration of silver into a porous tungsten lattice.

8. SiO_2+68.5W(H-22) was prepared by Bjorksten Research Labs. Samples were prepared from intimate and uniform mixtures of fine powders of high purity W and SiO_2 by first degassing and fusing under vacuum and then collapsing the resulting void-filled mass by application of an atmosphere of argon. Of the fifty specimens supplied, half of these were given a post-heat treatment to increase their viscosity.

9. Hf-20Ta-2Mo(I-23) was prepared by Wah Chang in the following manner:

(a) One-half inch diameter rod was double arc-melted and skull cast into 5/8" diameter rod and machined to final size.

	Ingot Chemistry		
	Top	Middle	Bottom
Ta	19.17 w/o	19.13 w/o	19.25 w/o
Mo	2.11 w/o	2.16 w/o	2.07 w/o
Hf	Balance	Balance	Balance
Zr	2.55 w/o	2.65 w/o	2.55 w/o
C	110 ppm	---------	120 ppm
N	62 ppm	---------	74 ppm
O	360 ppm	---------	240 ppm

(b) One inch rod was double arc-melted, hot forged annealed, hot rolled to final size, and vacuum annealed one hour at 2100°F.

	Ingot Chemistry		
	Top	Middle	Bottom
Ta	19.17 w/o	19.13 w/o	19.25 w/o
Mo	2.11 w/o	2.16 w/o	2.07 w/o
Hf	Balance	Balance	Balance
Zr	2.55 w/o	2.65 w/o	2.55 w/o
C	70 ppm	70 ppm	80 ppm
N	30 ppm	40 ppm	35 ppm
O	100 ppm	------	90 ppm
H	2.4 ppm	------	3.6 ppm

MIT Analysis	Jarrell-Ash (Qualitative Spectrography)
Hf-79.4 Ta-19.6 Mo-1.4 O_2-0.0075 and 0.0078	0.01 - 0.001 Ti, Fe

10. Ir/Graphite (I-24) specimens for arc plasma testing were coated with iridium by Battelle Memorial Institute. The coating process is described in reports under AF33(615)-3706 (3). Briefly, outgassed specimens of graphite were iridium coated by plasma-arc deposition and the coating was then outgassed. Coated specimens were wrapped in graphite foil, welded into a vacuum tight steel container, and pressure bonded at 10,000-15,000 psi for two hours at 1090°C. Poco Graphite (B-10) was used to fabricate arc plasma specimens. All speciments, except Nos. 2, 3, 4 and 6 were processed by outgassing the substrate at 1370°C, outgassing the coating at 2000°C, wrapping in graphite foil, and bonding at 1090°C for two hours under a pressure of 15,000 psi. Specimens 2, 3, 4 and 6 had the substrate outgassed at 1200°C, with no outgas of the coating. They were wrapped in tantalum foil and bonded at 1090°C for two hours under a pressure of 10,000 psi. These specimens were rusted, probably by contamination during bonding due to lack of sufficient outgassing.

Ir/C(I-24) samples were also supplied from material fabricated by General Technologies Corp. Whereas the Ir/C samples supplies by Battelle were coated by means of a high pressure bonding technique, the GTC samples were prepared utilizing the fused-salt electrodeposited coating process. This process produced coatings with an average thickness of about 4 mils as compared with 33 mils for the pressure-bonded coatings (4).

III. CHARACTERIZATION OF CANDIDATE MATERIALS

A. Introduction

Characterization of candidate materials was performed by means of qualitative spectrographic, wet chemical and vacuum (or inert gas) fusion, metallographic, X-ray, electron microprobe and pycnometric analysis. In most cases, these analyses were performed at ManLabs, Inc. by Dr. Edward Peters, Messrs. Raymond Yeaton and Joseph Davis. In addition, Mr. Donald Guernsey, Department of Metallurgy, M.I.T. performed some of the wet chemical analysis. Qualitative spectrographic analysis was done by Jarrell-Ash Co. of Waltham, Massachusetts, while Donald Guernsey at M.I.T. and Luvak, Inc. of Newton, Massachusetts carried out vacuum (or inert gas) fusion analysis.

B. Chemical Analysis Procedures Employed for Refractory Composite Materials

Standard methods for analysis of refractory boride, carbide and silicide composites (5-8) have been employed in performing the wet chemical analysis. However, considerable difficulties were encountered in the chemical analysis of JT graphite composites due to formation of $ZrSiO_4$ or $HfSiO_4$ on combustion. In order to avoid this complication, the following procedure was employed. The composite is burned on a bed of RR alundum covered with a tin or copper accelerator (approximately one gram for a one hundred milligram sample). The mixture is covered with a layer of alundum and burned for 45 minutes at 1300°C. The resulting CO_2 is collected and weighed to determine total carbon.

A second 200 mg sample is employed for determination of zirconium (or hafnium) and silicon. The sample is reduced to -200 mesh powder and boiled in 5-10 ml of H_2SO_4 in a covered beaker. About 2 ml HNO_3 is added drop-wise at intervals until all of the graphite is removed and the ZrC or HfC is in solution. Solution takes place in about 30 minutes. This procedure dissolves ZrC or HfC leaving SiC behind. Following evaporation and resolution in 50 ml of 3NHC*l*, the mixture is filtered and washed in hot water with 2% NH_4NO_3 added. The precipitate is then ignited. At this point, an approximate value can be obtained by weighing the SiC. Subsequently, the SiC is fused in two grams of Na_2CO_3 (and 100 mg of KNO_3, if necessary). Fifteen or twenty minutes of this treatment is sufficient to effect fusion. The fused mass is leached in hot water with cautious addition of 10 ml of 50% H_2SO_4 solution. This procedure converts SiC to SiO_2. Following evaporation the silicon is determined by standard procedures.

The filtrate from the SiC separation which contains zirconium or hafnium is evaporated, redissolved in 50 ml of 3NHC*l* and reacted with mandelic acid. The precipitate contains the zirconium or hafnium. This procedure can only tolerate traces of the SO_4 radical*. Subsequently, the mandelate is ignited to the zirconium or hafnium dioxide and weighed.

If the composite contains ZrB_2 or HfB_2 in place of the transition metal carbides, the procedure is identical except that a third sample is employed for boron analysis. If boron is present as ZrB_2 or HfB_2, fusion with Na_2CO_3 is employed to form $Na_4B_4O_7$.

C. Summary of Characterization Results

The results of the characterization studies of all of the candidate materials listed in Table 1 are shown in Tables 2-14 and in Figures 1-64. As indicated in Table 1, $HfB_{2.1}$(A-2), ZrB_2(A-3), $HfB_{2.1}$+20 v/o SiC(A-4) and Boride Z(A-5) were obtained from Carborundum Company, Niagara Falls, New York. The hot pressed samples (1/2 inch diameter x 1 inch long, and 1 inch diameter x 2 inches long cylinders) were fabricated from powders produced by Carborundum Company as indicated in Section II. The $HfB_{2.1}$+20v/o SiC(A-4) composite was designed to reproduce the properties of HfB_2+SiC(F-2) first synthesized under AF33(657)-8635 (4). Figures 1-8 show the microstructural characteristics of $HfB_{2.1}$(A-2), ZrB_2 (A-3), HfB_2+20v/oSiC(A-4) and Boride Z(A-5).

This analysis indicates that (A-2) is boron rich B/(Hf+Zr) = 2.07 and low in oxygen. The (A-3) material contains more oxygen than does (A-2) but is slightly metal rich, B/Zr=1.97. The present (A-3) material is lower in oxygen and slightly less dense (5.58 vs 5.70 gms/ cm^3) than the Carborundum ZrB_2 evaluated earlier (4). However, the boron to metal ratio is nearly the same (1.97 vs. 1.95). The chemical pycnometric and metallographic results indicate that (A-2), (A-3) and (A-4) are all 90-95% dense. Reference to Figures 1-6 show that (A-2) and (A-3) are more prone to "pull out" of second phase (oxide or carbide) during metallographic preparation than (A-4). Finally, it should be noted that (A-2), $HfB_{2.1}$ was far more susceptible to chipping and cracking during cutting and grinding than (A-3), (A-4) or high pressure-hot pressed hafnium diboride.

Tables 3 and 4 and Figures 9-18 show the characterization results for the borides and boride composites $HfB_{2.1}$(A-6), $HfB_{2.1}$+ 20v/oSiC(A-7), $ZrB_{2.1}$+20v/oSiC(A-8), $HfB_{2.1}$+35v/oSiC(A-9) and ZrB_2+14%SiC+30%C(A-10) prepared by ManLabs and Avco under AF33 (615)-3671. Comparison of the microstructural features of $HfB_{2.1}$ (A-2) and $HfB_{2.1}$(A-6) shown in Tables 2 and 3 and in Figures 1, 2 and 9 show little difference between the two. A similar comparison of the results obtained for HfB_2+20v/oSiC(A-4) and HfB_2+20v/oSiC(A-7) is shown in Tables 2 and 3 and Figures 5, 6 and 11. The zirconium-base analog

*Alternately the zirconium or hafnium may be determined in a 0.3-0.6 mol hot solution of HNO_3 by titration with (0.05 molar) EDTA using xylenol orange as an indicator. In this case the SO_4 does not interfere.

of (A-4) and (A-7) synthesized earlier (4) is ZrB_2+20v/oSiC(A-8) whose structure is shown in Figure 13. Figure 15 shows the hafnium diboride base composite HfB_2+35v/oSiC(A-9) containing larger quantities of SiC than (A-4) and (A-7). The final diboride composite which was included for evaluation was ZrB_2+14%SiC+30%C(A-10) characterized in Table 4 and Figures 17 and 18.

The graphites investigated in the current program included RVA(B-5), Pyrolytic (PG(B-6)), Boron-Doped Pyrolytic (BPG(B-7)), Siliconized RVC(B-8), PT0178(B-9), AXF-5Q Poco(B-10) and Glassy Carbon (B-11). The characterization data and structural information for these materials are shown in Tables 4-6 and Figures 19-34.

The pyrolytic materials shown in Figures 20-23 are more dense than the RVA and display the typical oriented microstructures with the "C" direction perpendicular to the transverse sections. The RVA(B-5) material, illustrated in Figure 19, was supplied by AFML in the form of a 6 inch diameter x 12 inch high cylinder. Pyrolytic graphite plate, 1 inch x 2 inches x 1/2 inch was purchased from the Metallurgical Products Division, General Electric Co., Detroit, Michigan. The High Temperature Materials Division, Union Carbide Corp. of Lowell, Mass., supplied one inch diameter disks which were one half inch thick. In the latter cases, the half inch thickness was parallel to the "C" planes of the graphite. The chemical analyses and microstructures presented here for (B-5), (B-6) and (B-7) are quite typical. Electron microprobe and chemical analyses of BPG(B-7) were performed and difficulties were encountered in obtaining accurate analysis of the boron level in BPG. The boron level indicated by the supplier was 2%.

Siliconized RVC(Si/RVC(B-8)) was obtained from the Union Carbide Corp. Table 5 provides characterization data, while Figures 24-27 illustrate the microstructural features of the matrix and the 4 mil coating of SiC. The RVC graphite is employed as the matrix due to the fact that it exhibits a coefficient of thermal expansion which is compatible with SiC.

Table 5 also provides characterization data for PT0178 (B-9). This fibrous graphite obtained from Union Carbide Corp. is fabricated by chopping a resin-impregnated graphite cloth and molding the resultant fibers. The molded shape is then cured under pressure at high temperatures to obtain a solid form. The molded part is then graphitized near 5000°F yielding a low density product. This product is then impregnated with a furane-resin system, which has a low viscosity and a high carbon content. The impregnated structure is baked at 1400°F to carbonize the resin. After regraphitization at 5000°F, a fully stabilized PT0178 product is obtained. Figures 28 and 29 show the microstructural features of PT0179(B-9).

The characteristics of AXF-5Q Poco Graphite (B-10) are shown in Figues 30-33 and in Table 5. Figures 32 and 33 are electron micrographs illustrating the fine grain structure of this graphite which contains substructures at the 0.05 and 0.002 mil levels.

Glassy Carbon (B-11) was supplied by Lockheed Missile/ Space Company, Palo Alto Research Laboratory. Characterization information is provided in Table 6. Figure 34 shows the clear microstructure of this material.

Characterization data for arc cast hypereutectic carbides (HfC+C(C-11) and ZrC+C(C-12) are contained in Tables 5, 7 and 8. Typical microstructures are shown in Figures 35-38 which illustrate the flake graphite in a eutectic matrix. Figure 39 shows radiographs of several of the hypereutectic carbide billets in which internal voids were detected.

Tables 7-10 and Figures 40-48 show the result obtained for KT silicon carbide (E-14) and graphite composites JTA(D-13), JT0992(F-15), JT0981(F-16) and JT-PT. The latter is an experimental composition with the same composition as JTA(D-13) except for the fact that the carbon is present in the form of fibers. Sample quantities of JT-PT were supplied for evaluation by AFML. The KT silicon carbide (E-14) was obtained from Carborundum Company, while the JT composites (D-13), (F-15) and (F-16) were purchased from Union Carbide Corp. (see Table 1). The chemical analysis, pycnometric, X-ray and metallographic results obtained for these materials (Tables 7-10) do not differ materially from those obtained earlier (9) except in the cases of KT-Silicon Carbide (E-14) and JT-0992(F-15). In the former case, the present (E-14) material appears to have more free silicon than previously (9). The current JT0992(F-15) analysis indicates a greater percentage of hafnium (56 vs. 35 w/o) and smaller amounts of carbon (32 vs. 48 w/o) and silicon (11 vs. 17 w/o) than reported earlier. It should be pointed out, however, that the values reported earlier were based on suppliers' analyses. The microstructure of JT0992 shown in Figures 45 and 46 are far more uniform than observed earlier (9). Previously, large particles of hanium carbide were observed to be agglomerated in the graphite matrix. The JT-PT composite shown in Figure 44 has a lower density (1.65 vs. 3.00) than JTA (D-13). The graphite fibers which form the JT-PT matrix appear to be 5-10 microns in diameter.

Table 10 and Figures 49-52 describe the General Electric Type MK, cold pressed and sintered tungsten, purchased for WSi_2 coating by TRW. Reference to Figures 49-51 shows that the one inch diameter bar (970 mils in diameter) exhibits a nonuniform grain structure owing to the fact that it did not receive any substantial reduction in area during forging. By contrast, the microstructure of the 1/2 inch diameter rod shown in Figure 52 which was forged from 1 inch sintered rod is much more uniform. Cylinders were cut from both 1 inch and 1/2 inch rod. Surface preparation of the 1 inch material prior to coating disclosed an array of "Heat-checking" cracks which necessitated surface machining prior to coating. This cracking was not present on the 1/2 inch rod. The 4.5 mil WSi_2 coating applied by TRW to form WSi_2/W(G-18) is shown in Figure 53.

The Ta-10W substrate for Sn-Al on Ta-10W(G-19) was obtained from National Research Corp. Chemical analysis data from the supplier is shown in Table 10. Figures 54 and 55 show the 8 mil slurry coating of Sn-27Al-6.9 Mo applied by Sylcor to form Sn-Al/Ta-10W(G-19).

Table 11 and Figures 56 and 57 contain characterization data and illustrate the microstructural features of the infiltrated tungsten composites obtained from Rocketdyne (2) and Wah Chang. The W+Zr+Cu (G-20), and W+Ag(G-21) materials are fabricated by powder metallurgy techniques as indicated in Section II.

Analytical information for the silica-tungsten composites SiO_2+68w/oW(H-22) supplied by Bjorksten Laboratories, SiO_2+60w/oW (H-23) and SiO_2+35w/oW(H-24) are contained in Tables 10 and 12. Figures 58-61 show the tungsten particles in a silica matrix.

Characterization data for Hf-20Ta-2Mo(I-23) rod obtained from Wah Chang Corp. are shown in Table 12 and Figures 62-65. The microstructure 1 inch diameter rod shows α(hcp) hafnium-rich plates in a β(bcc) tantalum-rich matrix, while the 1/2 inch diameter rod shows only the β(bcc) structure.

Tables 12-14 and Figures 66 and 67 provide characterization information and illustrate the microstructural features of Ir/C(I-24) supplied by Battelle.

IV. APPLICATION OF NONDESTRUCTIVE TEST METHODS TO ANALYSIS OF TEST SAMPLES

During the past several years, the NDT Development Group at Avco/SSD, Lowell, Massachusetts, has been actively pursuing development of methods for nondestructively defining the characteristics of refractory materials and coating systems (10-12) for applications under high temperature conditions. Although the Avco experience does not extend to all of the candidate materials, (10-12) examination of these materials could be informative and at the same time provide destructive test feed back for comparison with the NDT results. This feed back comparison may lead to NDT/destructive test correlations which may be useful in the future. Accordingly, nondestructive test methods including radiography, gamma radiometry, die penetrant inspection and ultrasonic velocity were applied to analysis of selected materials. Subsequent parts of this section describe the techniques employed in these tests and provide a description of the results.

A. Description of Nondestructive Test Methods

1. Radiography

Film radiography was used to detect the presence of voids, inclusions and local gross changes in composition such as gross segregation. The through transmission method is used with the X-ray source on one side of the specimen and a film (detector) on the other side. The equation describing X-ray (and gamma-ray) absorption in traveling through the specimen material is:

$$I = I_o e^{-(\mu/\rho)\rho t} \tag{1}$$

It will be noted that absorption is a function of the chemistry (upon which the value of μ depends), the density and the thickness. When several elemental components are present, the value of μ observed depends on the density and the percentage of each element present and the wavelength or "voltage" of the incident radiation. Since monochromatic beams are not easily obtainable, the value of μ/ρ usually observed is an effective value for polychromatic beams. If chemistry, density and thickness are constant, the amount of radiation passing through the specimen will be constant and the film will be uniformly exposed. However, if μ changes locally, as in the case of foreign included material or of segregation of the elemental constituents, or if the thickness changes (as in the case of a void) then the amount of radiation impinging on the film is less than the surrounding image. Hence, voids, inclusions and segregations can be detected by this procedure. Radiographic sensitivity depends on the source and the detector system used, but optimum combinations yield intensity differences of the order of 1%. Radiographic resolution down to $\pm.001$ inch is obtainable.

2. Gamma Radiometry

Radiometric density gauging is basically similar to radiography, consequently an equation similar to (1) applies. In radiometric density gauging, a collimated source of radiation (gamma rays, for this application) is used, and a confined beam is directed through the specimen impinging on a scintillation detector. The output of the detector is fed to a scintillation counter. By accurately counting scintillation over a fixed time interval, small differences in radiation intensity from point-to-point or from specimen to specimen can be detected. Through suitable calibration procedures, specimen or local density can be determined. In practice, most radiometric gauging applications are based on the assumption of constant chemistry and only concern themselves with the thickness and/or density aspects of Eq. 1. Since the value of transmitted intensity (I) is a function of both of these, it is necessary that one be fixed or known if the other is to be unambiguously determined. Hence, it can be quite important to radiograph materials, prior to density gauging, if voids, inclusions, etc., are likely to occur. Sensitivity of gauging devices to transmitted intensity changes is again about 1% and while normal operations usually have resolution of the order of 0.5 square inches, resolution much greater than this is attainable, depending on materials, configurations, reasonable counting times, etc. The entire volume of each 1/2" diameter by 1" long cylinders is gauged at once by adjusting the resolution capability down to the diameter of the specimens. Obviously, these density measurements yield no more information than gravimetric values. However, the feasibility of such measurements for later application to large specimens or parts has been demonstrated; further, if density appears to be an important variable with respect to oxidation behavior, resolution can be further improved and local densities determined within each specimen.

3. Visual Examination

Visual techniques, often not recognized as NDT, are probably the most common and surprisingly most often neglected of nondestructive tests. In studies of problems like oxidation resistance, conditions existing at the surface of the specimen may be of paramount importance. Because of this importance, specimens are examined visually with the naked eye and at 40X for color variations, which could be associated with oxide formation or surface contamination, for texture differences, which could be associated with processing, for presence of nonuniformity or surface porosity and for surface cracks all of which could be significant with respect to oxidation behavior.

4. Penetrant Inspection

Penetrant tests are used to disclose tight surface cracks which may not be visible to the naked eye or even at moderate magnifications. In practice, any one of a number of low viscosity fluids is applied to the surface. The low viscosity fluid is either drawn out by the use of "developers" or permitted to seep out naturally to provide an easily recognizable and enlarged indication of the crack. Alcohol is being used in the present case because it is unlikely to result in any contamination (some procedures may leave a residue in the crack or pores present).

5. Ultrasonic Velocity Measurements

The measurement of velocity presents a means for determining properties of interest by direct calculation using well known equations where applicable, and by establishing correlations between quantitative NDT measurements and material properties. In regard to elastic properties, for example, the relationship between wave velocities and physical properties can be seen from several equations such as:

$$V_L = \left[\frac{Y}{\rho} \frac{(1-\sigma)}{(1+\sigma)(1-2\sigma)} \right]^{1/2} = \left[\frac{K + 3/4\mu}{\rho} \right]^{1/2} \qquad (2)$$

$$V_T = \left[\frac{Y}{\rho} \frac{1}{2(1+\sigma)} \right]^{1/2} = \left[\frac{\mu}{\rho} \right]^{1/2} \qquad (3)$$

where:

V_L = longitudinal wave velocity
V_T = transverse wave velocity
Y = Young's modulus
σ = Poisson's ratio
ρ = density
K = bulk modulus
μ = shear modulus

While the above equations are written for an extended isotropic media and represent an over simplification when "non-ideal" materials are considered, empirical correlations between the nondestructively determined wave velocities and the destructively determined physical properties are to be expected. Eq. 2 is of particular interest. Since V_L is primarily responsive to the modulus/density ratio, process variation leading to modulus changes, either total or in a given direction (such as preferred orientation in elastically anisotropic materials or small amounts of "stiffening" impurities) will show up as a change in sound velocity. In some materials, depending on the stress-strain relationship, variation in internal stress levels will also be indicated. While not of immediate interest in this program velocity tensile strength determinations are also common for brittle materials. The present velocity measuring system is capable of making velocity determinations to a precision of about 1%. Again, if test results indicate a relationship between velocity and oxidation resistance, more refined techniques, capable of greater precision, are available if required.

6. Ultrasonic Defect Detection

Because of the very large ultrasonic impedence differences between gases and solid materials, ultrasonic energy is very efficiently reflected at solid material/air interfaces. Such interfaces occur when cracks, bursts, voids, etc., are present in solids and ultrasonic detection of such flaws is quite common. All specimens are being examined in this manner.

7. Eddy Current Test

Variations in chemical composition, phases present, distribution of phases, hardness and internal stress result in changes in the electromagnetic properties of electrically conductive materials. These same factors may well have an influence on oxidation resistance; hence, the measurement of electromagnetic properties, especially in the near surface layers, could provide a measure of relative oxidation resistance. This measurement is made by a coil carrying an alternating electrical signal which is brought into proximity with the electrically conductive specimen. Eddy currents are induced in the specimen, and some of the energy contained in them is dissipated through the action of the resistivity of the material encountered. That energy remaining is reflected back to the exciting coil and is seen by it as a back impedence. Hence, by measuring the coil current (phase, amplitude, or both) information is obtained regarding the electromagnetic properties of the material in the field induced by the coil. The depth of penetration of this field is defined as the depth at which the induced field strength falls to 1/e (37%) of its value at the surface and can be calculated from:

$$\delta = \frac{3.5}{f^{1/2}} \left[\frac{\rho}{\mu_{rel}\rho_o} \right]^{1/2} \qquad (4)$$

where:

δ = depth of penetration

f = exciting frequency in cps

$\rho\rho_o$ = ratio of resistivity of material to that of copper

μ_{rel} = relative permeability of material

The first group of 10 ZrB_2 specimens were examined at frequencies of 60 kilocycles per second (kc), 500 kc and 8 megacycles per second (mc).

These frequencies correspond to penetration depths of about 0.030 inch, 0.011 inch and 0.003 inch, respectively. Significant differences were noted between ends and between specimens at 60 kc, but not at the higher frequences. Since different instruments were used at the different frequencies, it is probable that the tests were conducted using different sensitivities; normally, however, one would expect the 60 kc results to be enhanced at the higher frequencies, and they were not. As indicated above, failure to observe differences at the higher frequencies may be due to instrument difference, or it may be that the extreme surface layers are more uniform than the immediate subsurface layers. In any event, the 60 kc results should be compared with oxidation behavior.

B. Nondestructive Test Results for ZrB_2(A-3)

The results obtained on samples ZrB_2(A-3), Nos. 1-30 are as follows:

1. Radiography

150 PkV, 10 mA for 2 minutes; film-foca' distance equal to 24 inches, Eastman Kodak Type AA film with screens. All 30 specimens were exposed in the axial and 90° separated radial directions. The radiographs exhibited a complete lack of image resulting from insufficient penetration. Samples 11-30 were radiographed at 300 PkV, 10 mA for 1 minute; film-focal distance equals 36 inches; Eastman Kodak Type AA film with screens. These specimens all appear free of radiographically detectable gross defects (voids, inclusions, gross segregation). The radiographs exhibited satisfactory penetration in the axial and radial directions as a result of the 300 PkV exposure.

2. Ultrasonic Defect Detection

The pulse echo technique at 1 MHz was used in the axial direction. No significant discontinuities were observed.

3. Surface Visual and Crack Inspection

Binocular microscope (40X) and alcohol wipe inspection of all specimens gave no indication of cracks.

4. Ultrasonic Velocity

The through transmission technique at 1.0 MHz was used to obtain transit time values, from which longitudinal wave velocities (V_L) in the axial direction could be obtained. These values are listed in Table 15. This test is responsive to modulus (consequently preferred orientation) and density variations. It will also indicate changes in internal stress condition from specimen to specimen. The accuracy of this technique is +1%, and A-3-15, 16, 20 and 23 exhibited values of V_L which are significantly outside these limits.

5. Radiation Gauging

The through transmission gamma radiation technique (10 millicurie cobalt 60) was employed to measure the densities shown in Table 15. The calculated mass attenuation coefficient (μ/ρ) of ZrB_2 at an energy of 1.1 Mev is 0.047 cm^2/gm. The experimentally determined value was 0.044 cm^2/gm. The statistical precision is 0.33% for a 30 second counting time (102,000 counts). It was assumed that a radiometrically determined density difference of approximately 1% is adequate. This difference is greater than the precision of measurement so that a density difference of 1% is meaningful. To achieve this level of density difference detection, the criterion for the minimum value of the linear attenuation coefficient for a material is that it exceeds 0.12 cm^{-1} for a nominal thickness of one inch. The linear attenuation coefficient of ZrB_2 for gamma rays at 0.246 Mev is 0.246 cm^{-1} or twice the value required by the minimum observability criterion. Specimens A-3-1, A-3-11 and A-3-22 were the only cases where the observed density differed by more than $\pm 1\%$ from the mean.

6. Eddy Current Measurements

Probe coil measurements at 500 kHz and 8 MHz provided no indications of significant variability. Probe coil measurements at 60 kHz using the Magnatest FM-100 conductivity meter did provide significant variation in the percent International Annealed Copper Standard (%IACS) values. The measurements obtained on both ends of each cylindrical specimen are shown in Table 15. The range of values exceeds the 0.05 (%IACS) measurement precision. This test is sensitive to change in chemistry, microstructure and internal stress levels. Specimens numbered A-3-18 and A-3-12 represent the extreme deviations from the mean.

C. Nondestructive Test Results for $HfB_{2.1}$(A-2), JTA(D-13) and JT0981(F-16)

Nondestructive testing of a series of twenty-four $HfB_{2.1}$ (A-2) cylinders numbered (A-2)-1 through (A-2)-24, ten JTA(D-13) cylinders numbered (D-13)-1 through (D-13)-10 and eleven JT0981 (F-16) cylinders numbered (F-16)-1 through (F-16)-11 have been performed. The JTA(D-13) cylinders were all cut from billet 5/E/17/2 while the JT0981 (F-16) cylinders were cut from billet 5/F/2/1. All cylinders were oriented with their axis parallel to the pressing direction. In addition, nondestructive testing of a series of twenty models exposed in the Cornell Aeronautical Laboratory-Wave Superheater Tunnel was performed. Radiographic, gamma radiometric, ultrasonic, magnetic, and visual methods employing dye penetrants were employed. These methods have been described in Section B. Nondestructive testing of $HfB_{2.1}$(A-2), JTA(D-13) and JT0981(F-16) was initiated when it was noted that the $HfB_{2.1}$(A-2) material exhibited nonuniform density regions near the center of the one-half inch diameter by one inch long cylinder and chipped and cracked easily on machining. This behavior was not noted in earlier studies (1) and was attributed to Carborundum's limited experience in pressing hafnium diboride. The ZrB_2(A-3) and HfB_2+SiC(A-4) material supplied by Carborundum did not show similar features and was machined without incident. Testing of JTA(D-13) and JT0981(F-16) was initiated when the first series of arc plasma tests on these materials produced a high frequency of thermal shock failures (see Section IIB, Part III-Vol.III) JTA(D-13)-21M, 22M, 23M, 24M and JT0981 (F-16)-21M, 22M, 23M, 24M. The general results of the nondestructive testing are discussed below. Detailed quantitative test values are shown in Tables 16 through 18.

1. Ultrasonic Velocity

Longitudinal wave velocity values were determined at a frequency of 1 MHz for the $HfB_{2.1}$, JTA and JT0981 specimens, both in the axial and radial directions. The overall test accuracy and precision were each approximately 1 percent. Consequently, those specimens exhibiting a variability exceeding 1 percent from the average velocity value should be examined to determine if velocity measurements reveal a useful correlation with destructive test results. The ranges noted in the Tables for each specimen type exceed 1 percent, so that at least the extremes should be examined. In particular, $HfB_{2.1}$ specimens numbered 17 and 21 gave extreme values in both axial and radial directions. JTA specimens numbered 1, 6 and 9 and JT0981 specimens numbered 1, 4 and 11 also gave extreme values.

2. Eddy Current Measurements

Probe coil measuremens were performed at 60 KHz, 500 KHz and 8 MHz for the $HfB_{2.1}$ specimens, and at 500 KHz for the JTA and JT0981 specimens. Sixty KHz and eight MHz measurements were insensitive to the JTA and JT0981 specimens. Relative values of current were obtained; the extreme values were found to be much greater than the precision of measurement noted in the tables for each frequency. In particular, examination for possible correlations should be given to at least $HfB_{2.1}$ specimens numbered 19, 21 and 24, where frequencies of 500 KHz and 8 MHz are found to yield the most sensitive tests. Also JTA specimens numbered 6 and 9, and JT0981 specimens numbered 1, 4 and 9 should be given special attention.

3. Radiography

The $HfB_{2.1}$ specimens were inspected by Arnold Greene Testing Labs. The JTA and JT0981 specimens were inspected at Avco/SSD. All $HfB_{2.1}$ specimens exhibit low density regions that extend radially from the axis at a cylinder's midsection. No nonuniformities were observed for the JTA and JT0981 specimens.

4. Surface Crack/Porosity Inspection

Dye penetrants were used to observe surface cracks and open porosity for the $HfB_{2.1}$ specimens. Circumferential porous bands were noted for all specimens except those numbered 4, 9 and 21. Surface cracks were noted for specimens numbered 4, 5, 6, 9, 11, 12, 14, 15 and 21. The alcohol-wipe technique was used to observe surface cracks for the JTA and JT0981 specimens. All specimens appeared free of cracks.

5. Surface Visual Inspection

All specimens were visually observed under magnification. Surface cracks were observed for $HfB_{2.1}$ specimens numbered 6, 9, 14, 15, 16 and 24. All $HfB_{2.1}$ were noted to be chipped. For the JTA and JT0981 specimens, no surface cracks were observed but small scratches and chipping were noted for most of the cylinders.

D. Nondestructive Testing of CAL-Wave Superheater Models

A total of twenty specimens have been nondestructively evaluated employing techniques similar to those used previously. These specimens were finished in various geometries and consisted of various compositions of hafnium, tungsten, zirconium and silicon and of graphite. Of the five techniques used, only X-ray radiography and visual and penetrant inspections yielded meaningful results. Ultrasonic velocity and eddy current measurements were influenced to a much greater degree by specimen geometry than they were by material variability for these geometries exhibiting extreme curvatures relative to probe dimensions. Consequently, it is appropriate that at least part of the nondestructive evaluation in the future be performed on flat-faced specimens prior to their final machining.

Radiography at 1.0 Mev was performed by Arnold Greene Testing Laboratories, Inc. on the hafnium and tungsten composites. Avco radiographed the zirconium and silicon composites and the graphite specimens at 150 kv. The detailed results are included in Tables 19 and 20. The tables also contain comments on the specimen geometries as interpreted visually and radiographically. Of the eight hafnium and tungsten composite specimens, only specimen number Hf-Ta-Mo(I-23)-3-0 contained a possible serious nonuniformity, this being a 0.040 inch diameter low density region located at the tip. The remaining twelve specimens all exhibited apparent geometrical irregularities as indicated in Table 24. High density flecks or particles were observed in specimen numbers ZrB_2(A-3)-24-3, JT0992(F-15)-X-9, JTA (D-13)-X-7 and JT0981(F-16)-X-10). The latter three specimens contained these flecks throughout their volume.

Specimen ZrB_2(A-3)-24-3 contained three 25 mil high density particles, two of which were located near the tip. Failure of this model in thermal shock may possibly be traced to these inhomogeneities.

Fluorescent dye penetrants were used to detect surface cracks and open porosity for the hafnium, tungsten, and zirconium composite specimens. Specimen $HfB_{2.1}$(A-2)-X-1 exhibited a band of porosity on the wall, as well as two cracks at the base. Specimens HfB_2+SiC(A-4)-X-4 and ZrB_2(A-3)-24-3 each exhibited two 1/4 inch long cracks at their base, while specimen ZrB_2(A-3)-1-2 exhibited three 1/4 inch long cracks at its base and wall. No imperfections were noted for the remaining composites in the group.

An alcohol wipe test was used to locate surface cracks in the composites and graphite specimens. All specimens appeared free of cracks except as noted above.

Results of visual examination of the twenty specimens using 40X magnification are listed in Table 19. Several specimens were observed to have the edges of their bores chipped. Specimen RVA(B-5)-X-5 has a large pit and a few porous areas on its hemispherical cap. Specimens PG(B-6)-X-6 and BPG(B-7)-X-16 have porous areas on their walls, while BPG(B-7)-X-16 also has a chipped base and a flattened side.

E. Nondestructive Testing of Models Employed in Ten-Megawatt Arc Tests

A series of thirty-eight boride and boride-silicon carbide composite cylinders prepared for high flux testing in the Avco 10 Megawatt Arc facility have undergone nondestructive testing both before and after exposure to the arc. The materials were subjected to ultrasonic velocity, eddy current measurement, dye penetrant, and visual tests. The materials tested were $HfB_{2.1}$(A-2) and (A-6), ZrB_2 (A-3) and (ManLabs-Avco), $HfB_{2.1}$+20v/oSiC(A-4) and (A-7), Boride Z in numerical order along with results of the nondestructive tests performed. All cylinders were 0.875" diameter by 0.750" long except for the $HfB_{2.1}$+20v/oSiC(A-4) and (A-7-HF-32,33,34) specimens. The general results of the nondestructive testing are discussed below.

1. Ultrasonic Velocity

Longitudinal wave velocities were measured for specimens Hf-1 through HF-24, at a test frequency of 1.0 MHz, in both the axial and radial directions. Transverse wave velocities were measured for this group in the axial direction at frequencies of 1.0 MHz and 2.25 MHz. Table 21 lists quantitative results of ultrasonic velocity determinations for these specimens. The over-all test accurracy and precision were each approximately one percent. All specimens tested fall within this range of accuracy with the possible exception of Boride Z(A-5-HF-11) which exhibited a low longitudinal wave velocity in the axial direction relative to the other Boride Z specimens tested. While the significance of ultrasonic attenuation measurements in these materials has not been established, results of these measurements are included in Table 21. A concurrent laboratory development of attenuation measuring techniques and their significance in these materials is planned.

2. Eddy Current Measurements

Probe coil measurements were performed on the flat faces of specimens HF-1 through HF-24 at frequencies of 60 KHz, 500 KHz, and 8 MHz. The 60 KHz measurements are reported in percent of the International Annealed Copper Standard, while the 500 KHz and 8 MHz measurements are in arbitrary units. Table 21 lists quantitative results for these measurements. The precision for these tests is better than 3% at 60 KHz and better than 20% at 500 KHz and 8 MHz. As in the ultrasonic velocity measurements, the most obvious inconsistency was for Boride Z(A-5-HF-11) on the top face of the specimen. Tests at all frequencies gave significantly different results from the other Boride Z specimens. Most of the other materials again showed no significant differences.

3. Other NDT Results

Visual inspection of specimens HF-1 through HF-24 revealed that virtually all had chipped edges. A large chip was found in Boride Z(A-5-HF-12). Specimen Boride Z(A-5-HF-9) had a crack on one face while specimens ZrB_2(ManLabs-Avco HF-17) and $HfB_{2.1}$ (A-6-HF-20) had microcracks on their surfaces. Fluorescent penetrant inspection did not reveal additional information on this group of specimens. However, all of the $HfB_{2.1}$+20v/oSiC(A-4) specimens inspected showed a circumferential porous band near their center, approximately 1/4" wide. This band is a result of a low density region within the billet from which these specimens were core drilled. Table 22 shows visual, fluorescent penetrant and radiographic results for some of the specimens before and after exposure to the arc.

F. NDT Results for Hypereutectic Carbide HfC+C(C-11) and ZrC+C(C-12) Billets

The surfaces of the thirteen HfC+C(C-11) and seven ZrC+C(C-12) billets were examined at ManLabs, Inc. upon receipt from Battelle Memorial Institute. Most of the HfC+C billets and all of the ZrC+C billets were found to have surface flaws, primarily holes and voids. Such flaws can only be attributed to gas bubbles becoming entrapped during the drop casting process. Radiographs supplied by Battelle showed that many billets contained internal gas holes and several billets contained centerline pipes up to 1/2" long. A summary of the visual and radiographic inspection results are given in Table 22. Figure 39 shows the appearance of some of the defects found within the billets. Wherever possible, such defects will be avoided in preparation of specimens from the billets in question.

G. NDT Results for Crosscut JTA(D-13) Cylinders

An attempt was made to systematically eliminate some of the variables which might be contributing to the high frequency of thermal shock failures observed in the arc plasma testing of JTA(D-13) and JT0981(F-16). A series of eleven JTA(D-13) cylinders numbered D-13-31M through D-13-41M have been prepared for testing in the Model 500 Arc facility by core drilling the cylinders perpendicular to the billet axis rather than parallel, as was the case for all previous specimens. These specimens are currently undergoing arc plasma tests, and results should indicate whether or not inhomogeneities introduced by the fabrication process contribute to thermal shock failures. Radiographic and alcohol wipe tests showed no nonuniformities existed in any of these cylinders.

H. NDT Results for Ir/Graphite (I-24) Cylinders

Nineteen Ir/Graphite (I-24) cylinders received from Battelle Memorial Institute were examined visually at ManLabs, Inc. Specimens 2, 3, 4 and 6 appeared rusted in color rather than metallic. X-ray analysis of these specimens revealed α-Fe_2O_3 to be present, indicating that the lack of outgassing of these specimens caused a reaction with the steel container to occur during pressure bonding. The results of fluorescent penetrant and radiographic inspections of all cylinders are summarized in Table 22. The coating exhibited porosity in all specimens at the junction of the front face and side wall, while specimens 13 and 18 had cracks in their coatings. Other specimens were found to have low density regions, scales, and spotty surface build-up of their coatings. Attempts to measure the thickness of the coatings were inconclusive due to surface irregularities.

Specimens were tested at Avco/SSD using a 60 KHz eddy current conductivity meter and comparing the results with an iridium foil standard. A calibration curve was established by stacking 0.010" thick iridium shims and making eddy current readings on several thicknesses. The shims were placed upon a graphite block to see the influence of the graphite and to more closely simulate the actual test specimens. It was found, however, that the graphite exerted negligible effect on the eddy current reading. Figure 68 shows the calibration curve obtained at 0.010", 0.020" and 0.030" thicknesses. After calibration, the specimens were tested and the data recorded. Several specimens showed a severely irregular front surface and could not be adequately tested because of the need for a 1/4" flat face to suit the transducer requirements.

Results of these tests are given in Table 14 for the GTC material and Table 22 for the Battelle material. Although the eddy current technique does not give precise thickness measurements, it does seem to yield a fair approximation of the front face thickness of the iridium coatings on graphite.

REFERENCES

1. Clougherty, E.V. et al., "Research and Development of Refractory Oxidation-Resistant Diborides" Part II-Volume II "Processing and Characterization" AFML-TR-68-190 Part II-Volume II, Man-Labs, Inc., Cambridge, Mass., June 1969.
2. Schwartzkopf, P., "Evaluation of Tungsten Composites for Hypersonic Vehicles" AFML-TR-67-272, Rocketdyne Division of North American Aviation, Inc., Canoga Park, California, June 1967.
3. Wright, T.R., Braecket, T.R., Kizer, D.E. et al., "The Fabrication of Iridium-Alloy Coatings on Graphite by Plasma-Arc Deposition and Gas-Pressure Bonding" AFML-TR-68-6, Battelle Memorial Institute, Columbus, Ohio, February 1968.
4. Macklin, B.A. and LaMar, P.A., "Development of Improved Methods of Depositing Iridium Coatings on Graphite" AFML-TR-68-195 Parts I and II, General Technologies Corp., Alexandria, Va., August 1967 and October 1968.
5. Kriege, O.H., "The Analysis of Refractory Borides, Carbides, Nitrides and Silicides" LA-2036, Los Alamos Scientific Laboratory of the University of California, August 1959.
6. McKinley, G.J. and Wendt, H.F., "The Determination of Boron in Refractory Borides by Pyrohydrolysis" Union Carbide Research Institute, Tarrytown, New York, January 1965, Technical Report No. C-28, ARPA Contract DA-30-069-ORD-2787.
7. Elinson, S.V. and Petrov, K.I., Analytic Chemistry of Zirconium and Hafnium, Israel Program for Scientific Translations, Daniel Davey and Co., New York, N.Y., 1965.
8. Pribil, R. and Vesely, V., Chemist-Analyst (Published by J.T. Baker Chemical Co., Philipsburg, N.J.) 1964, 53 43.
9. Kaufman, L. and Clougherty, E.V., "Investigation of Boride Compounds for Very High Temperature Applications" RTD-TDR-63-4096 Part III, ManLabs, Inc., Cambridge, Mass., March 1966.
10. Lafyatis, P.G. and Carter, M.B., "Exploratory Development of Graphite Materials" AFML-TR-65-324, Avco Corporation, Lowell, Mass., June 1966.
11. Lockyer, G.E. and Proudfoot, E.A., "Nondestructive Determination of the Mechanical Properties of Refractory Materials" Space Systems Division Avco Corporation, Lowell, Mass., June 1966, AVSSD-0068-66-PP USAF Contract AF33(615)-1601.
12. Stinebring, R.C. and Sturiale, T., "Development of Nondestructive Methods for Evaluating Diffusion Formed Coatings on Metallic Substrates", AFML-TR-66-221, Avco Corporation, Lowell, Mass., September 1966.

Etched with 10 Glycerine 5 HNO_3 3HF 250X

Figure 1. $HfB_{2.1}$ (A-2), 1/2" Diam. Bar, Longitudinal Section.

Etched with 10 Glycerine 5 HNO_3 3HF 250X

Figure 2. $HfB_{2.1}$ (A-2), 1/2" Diam. Bar, Transverse Section.

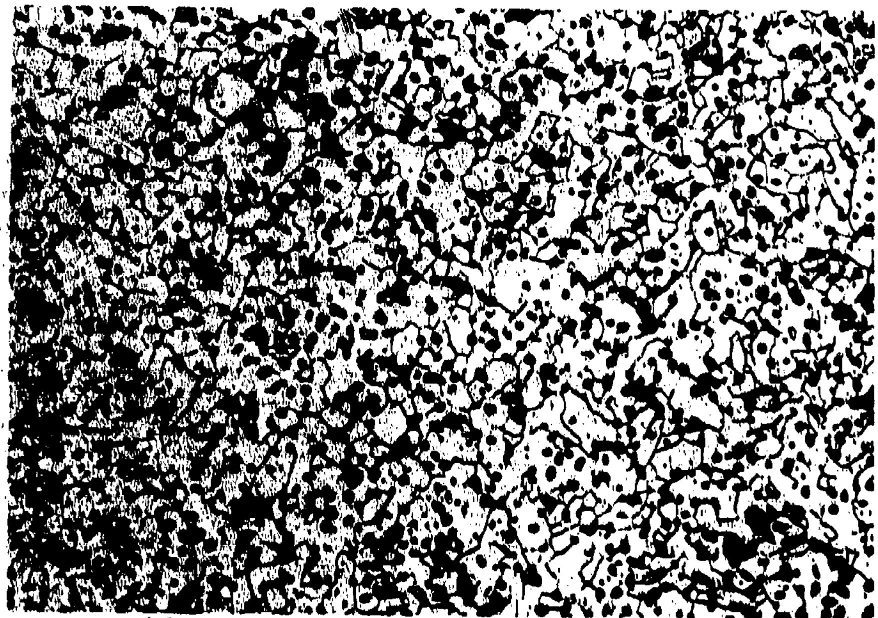

Plate No. 4303

Etched with 10 Glycerine 5 $HNO_3$3HF 250X

Figure 3. ZrB_2 (A-3), 1/2" Diam. Bar, Longitudinal Section.

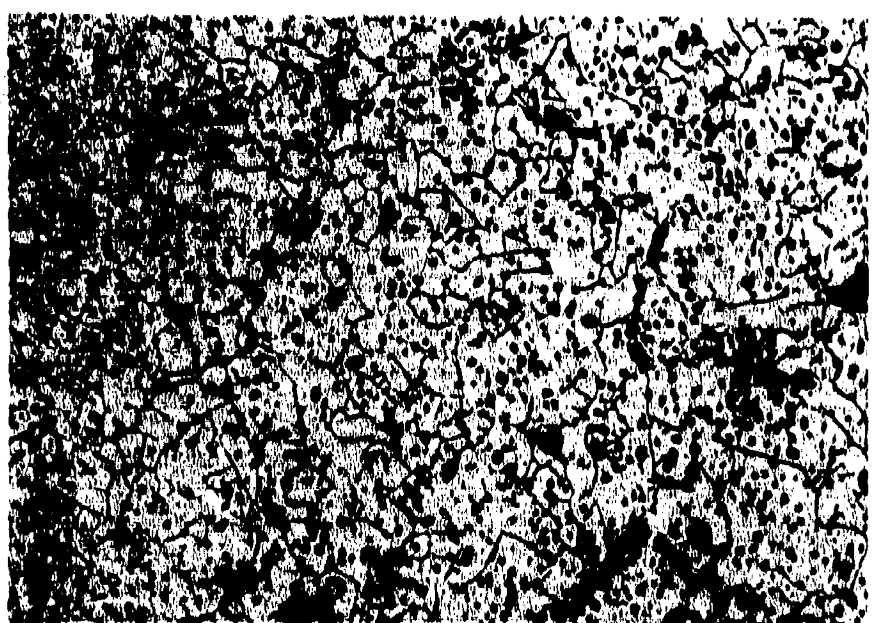

Plate No. 4305

Etched with 10 Glycerine 5$HNO_3$3HF 250X

Figure 4. ZrB_2 (A-3), 1/2" Diam. Bar, Transverse Section.

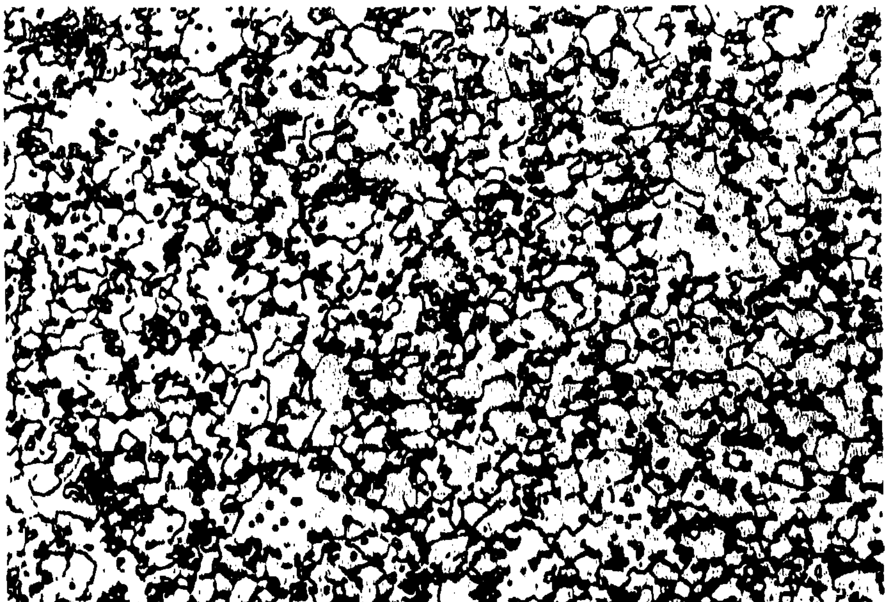

Plate No. 4394a

Etched with 10 Glycerine $5HNO_3$ 3HF 250X

Figure 5. HfB_2 + SiC (A-4), 1/2" Diam. Bar, Longitudinal Section.

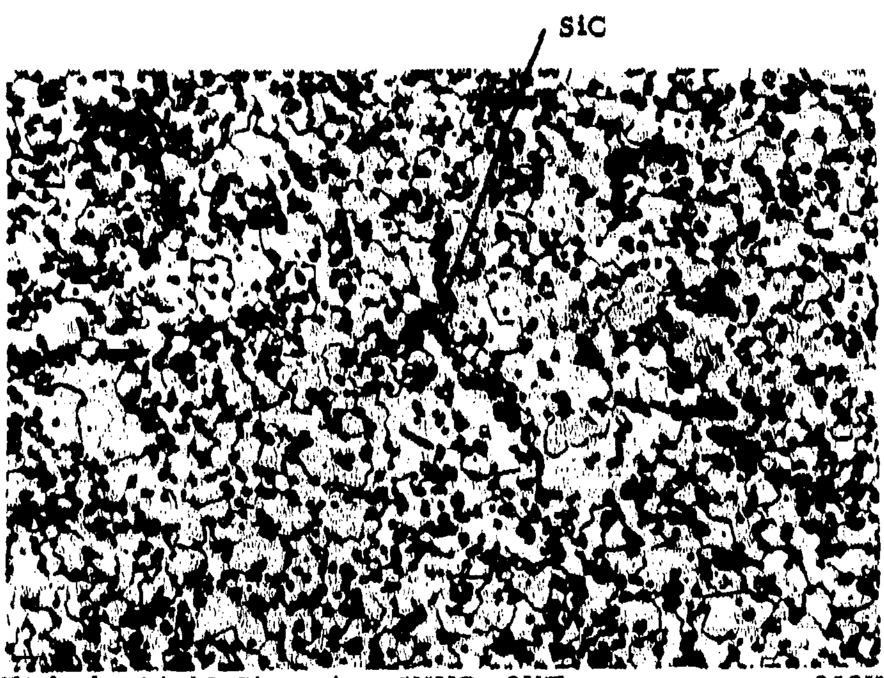

Plate No. 4441a

Etched with 10 Glycerine $5HNO_3$ 3HF 250X

Figure 6. HfB_2 + SiC (A-4), 1/2" Diam. Bar, Transverse Section.

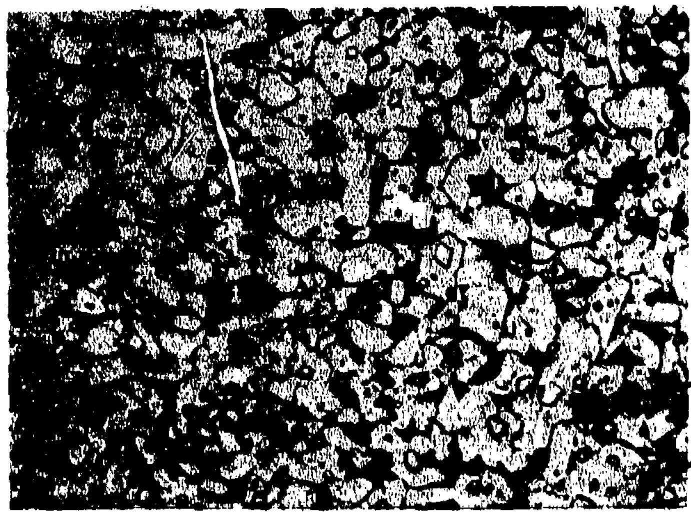

Etched with 10 Glycerine $5HNO_3$ **X250**

Figure 7. Microstructural Characteristics of Large Bar (1.0" diameter x 2.0" long) Carborundum Boride Z (A-5).

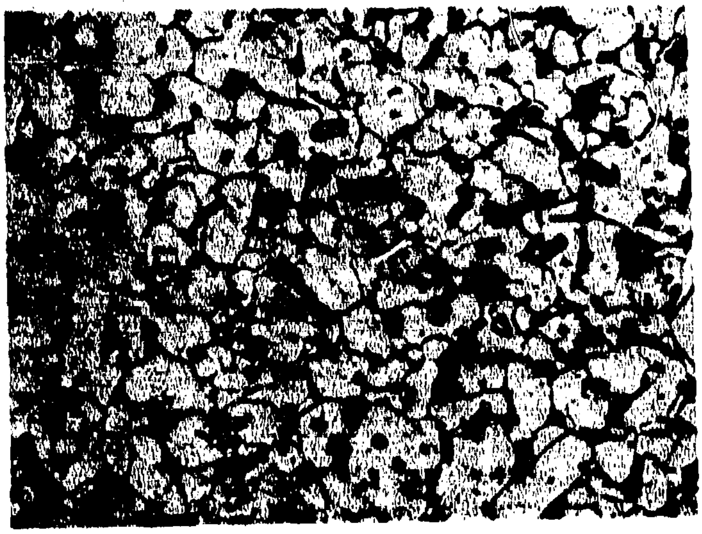

Etched with 10 Glycerine $5HNO_3$ 3HF **X250**

Figure 8. Microstructural Characteristics of Small Bar (0.5" diameter x 1.0" long) Carborundum Boride Z (A-5).

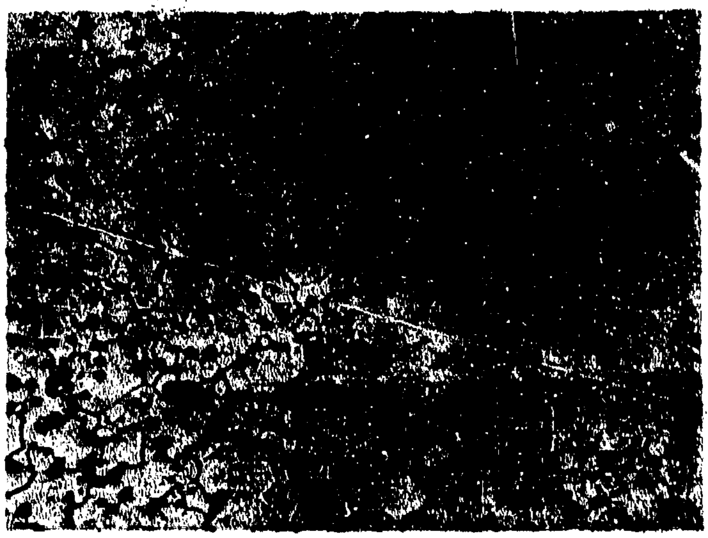

Plate 4739

Etched with 10 Glycerine $5HNO_3$ 3HF X250

Figure 9. Microstructural Characteristics of $HfB_{2.1}$ (A-6) Density = 10.25 gms/cm^3, 95.9% of Theoretical Density.

Plate 4738

Etched with 10 Glycerine $5HNO_3$ 3HF X250

Figure 10. Microstructural Characteristics of $HfB_{2.1}$ (A-6) Density = 9.53 gms/cm^3, 89.1% of Theoretical Density.

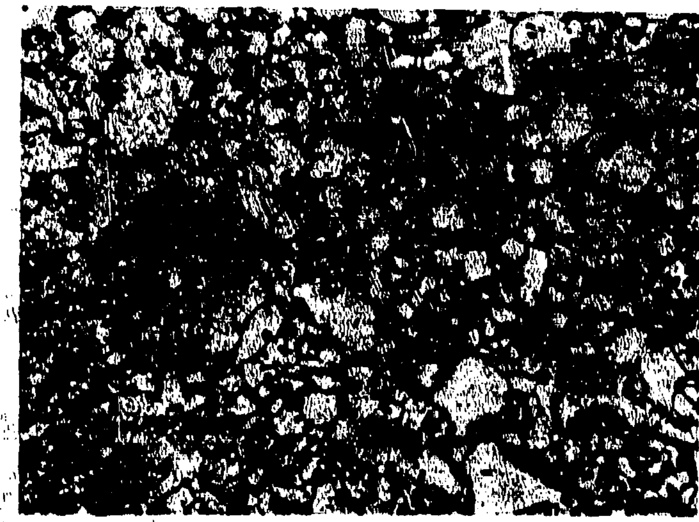

SiC

Plate 4495

Etched with 10 Glycerine $5HNO_3$ 3HF X250

Figure 11. Microstructural Characteristics of $HfB_{2.1}$ + SiC (A-7) (Twenty Volume Per Cent SiC) Density = 9.26 gms/cm^3, 97.5% of Theoretical Density.

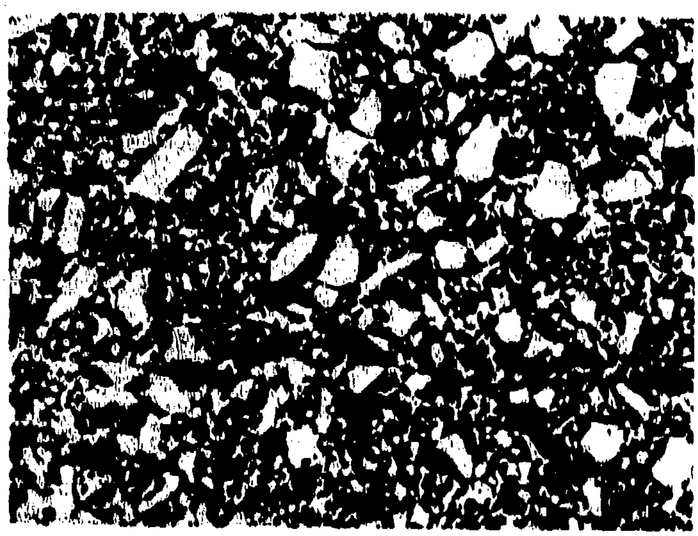

Porosity

Plate 4737

Etched with 10 Glycerine $5HNO_3$ 3HF X250

Figure 12. Microstructural Characteristics of $HfB_{2.1}$ + SiC (A-7) (Twenty Volume Per Cent SiC) Density = 7.84 gms/cm^3, 82.5% of Theoretical Density.

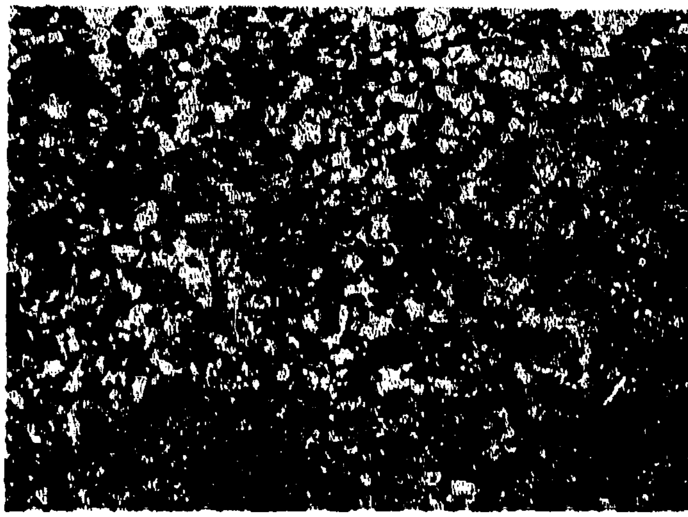

Plate 4736

Etched with 10 Glycerine 5HNO$_3$ 3HF X250

Figure 13. Microstructural Characteristics of ZrB_2 + SiC (A-8) (Twenty Volume Per Cent SiC) Density =5.47 gms/cm^3, 100% of Theoretical Density.

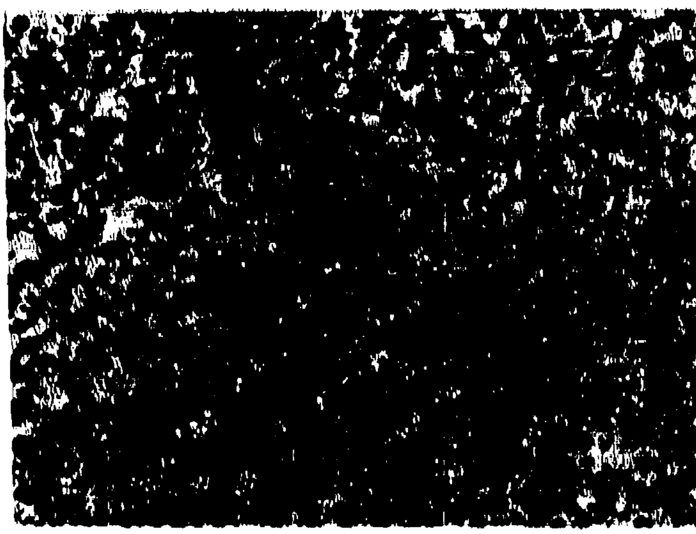

Plate 4521

Etched with 10 Glycerine 5HNO$_3$ 3HF X250

Figure 14. Microstructural Characteristics of ZrB_2 + SiC (A-8) (Twenty Volume Per Cent SiC) Density =5.02 gms/cm^3, 91.8% of Theoretical Density.

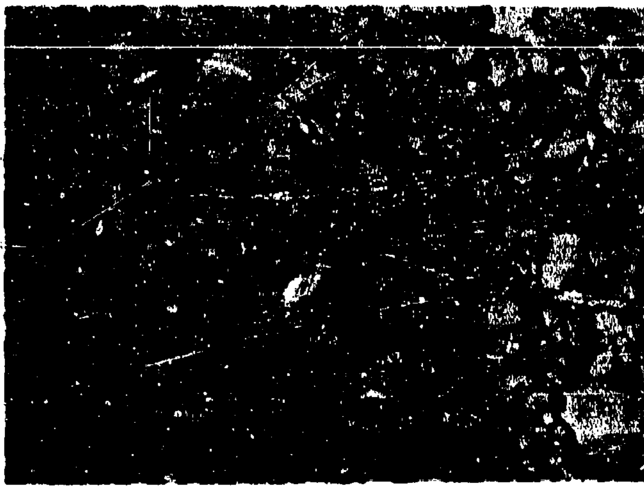

SiC

Plate 4454

Etched with 10 Glycerine $5HNO_3$ 3HF X250

Figure 15. Microstructural Characteristics of HfB_2 + SiC (A-9) (Thirty-Five Volume Per Cent SiC) Density=8.57gms/cm^3, 99.4% of Theoretical Density.

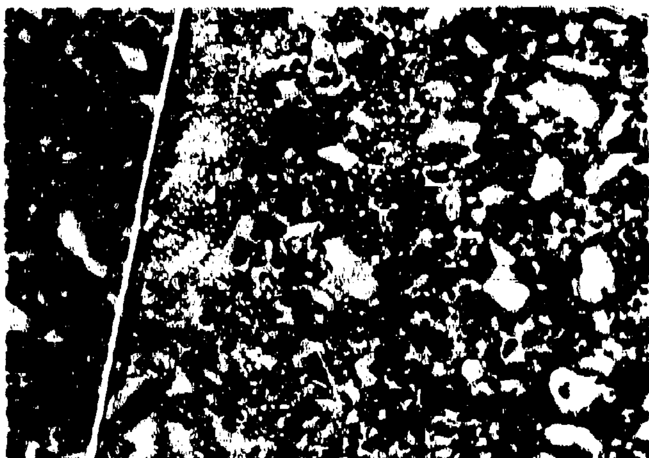

Porosity

Plate 4552

Etched with 10 Glycerine $5HNO_3$ 3HF X250

Figure 16. Microstructural Characteristics of HfB_2 + SiC (A-9) (Thirty-Five Volume Per Cent SiC) Density=7.78gms/cm^3, 90.3% of Theoretical Density.

Plate No. 5059

Unetched X500

Figure 17. Microstructural Characteristics of ZrB_2 + 14%SiC + 30%C(A-10) Longitudinal Section.

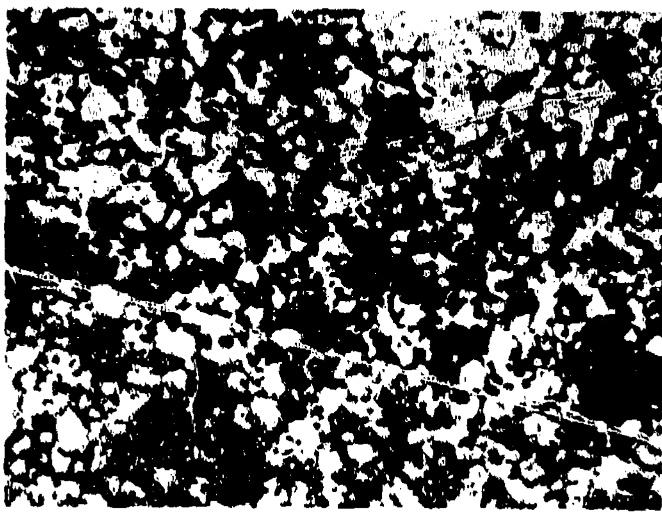

Plate No. 5057

Unetched X500

Figure 18. Microstructural Characteristics of ZrB_2 + 14%SiC + 30%C(A-10) Transverse Section.

Figure 19. RVA Graphite (B-5).

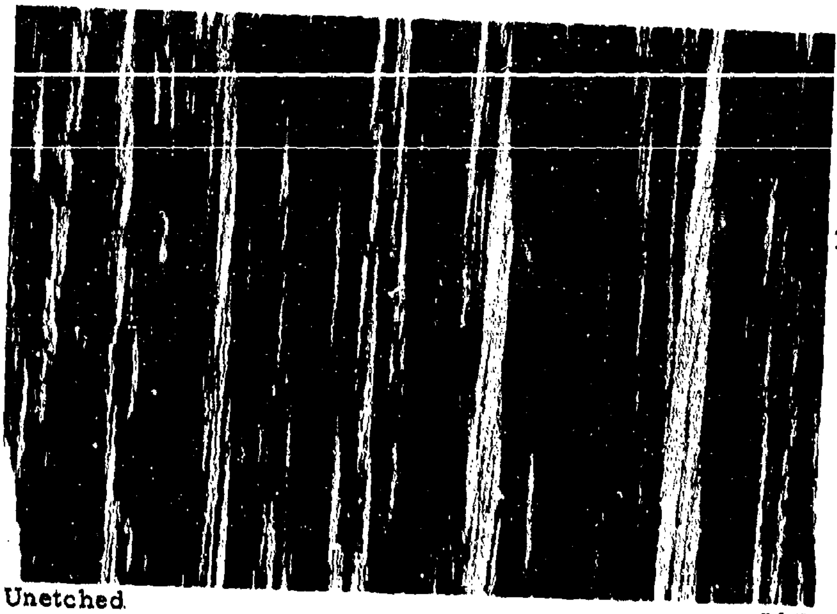

Plate No. 8162

Unetched

50X

Figure 20. Pyrolytic Graphite (B-6), Longitudinal Section, Polarized Light.

Plate No. 8159

Unetched

50X

Figure 21. Pyrolytic Graphite (B-6), Transverse Section, Polarized Light.

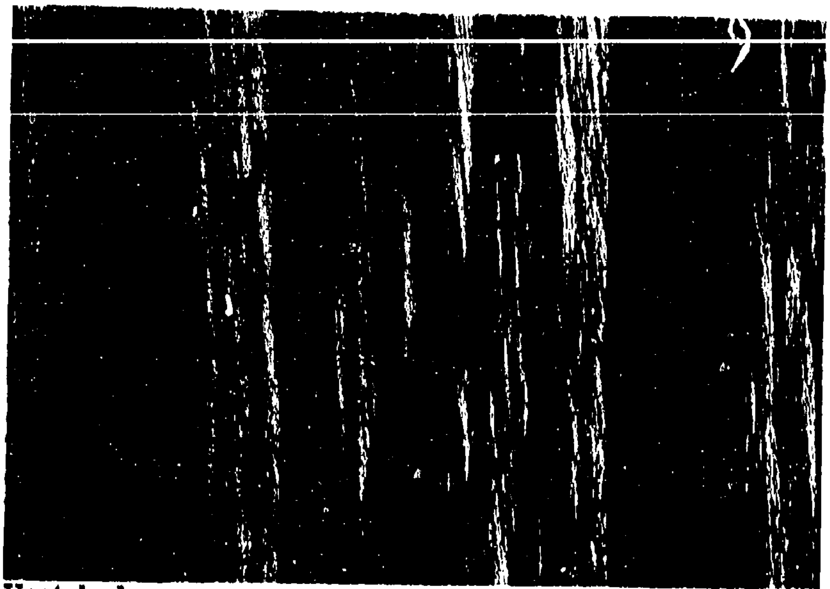

Plate No. 8146a

Unetched

50X

Figure 22. Boron Pyrolytic Graphite (B-7), Longitudinal Section, Polarized Light.

Plate No. 8147

Unetched

50X

Figure 23. Boron Pyrolytic Graphite (B-7), Transverse Section, Polarized Light.

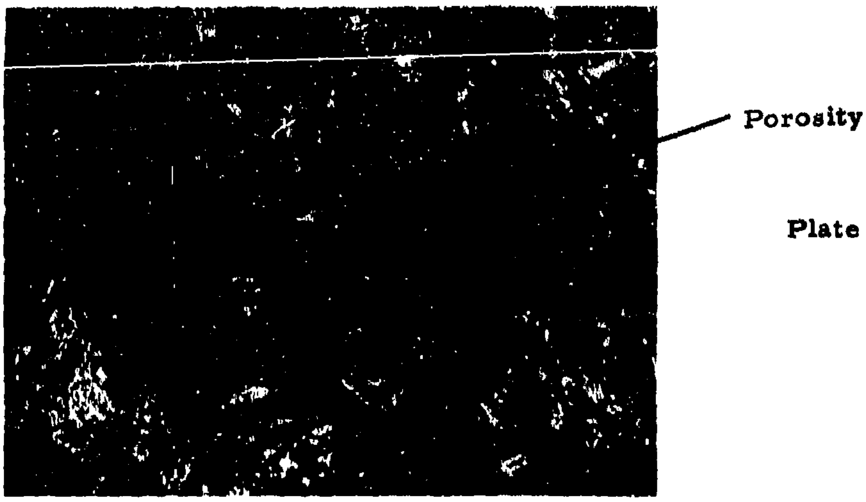

Unetched X250

Figure 24. Microstructural Characteristics of RVC Graphite (B-8) Longitudinal Section.

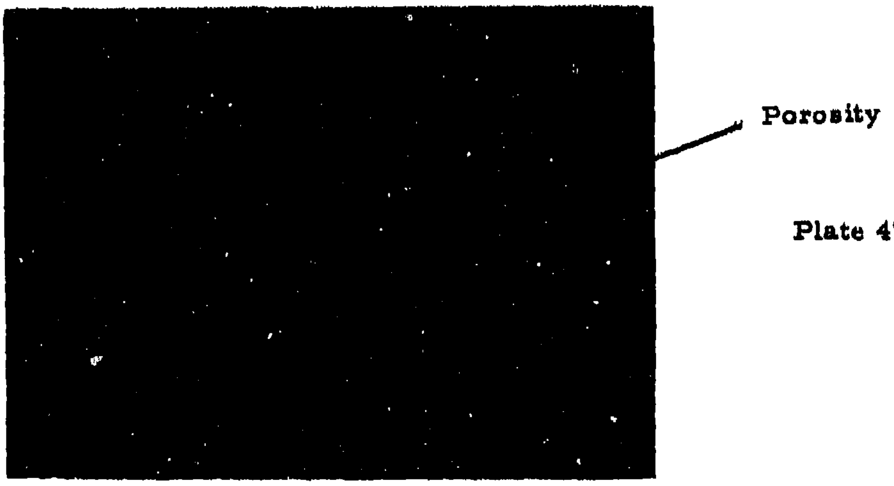

Unetched X250

Figure 25. Microstructural Characteristics of RVC Graphite (B-8) Transverse Section.

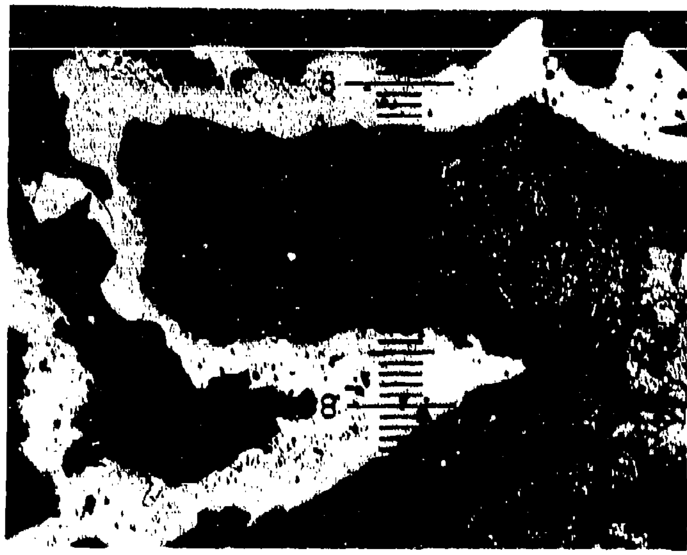

SiC

Plate No. 4947

RVC
Graphite

Unetched X175

Figure 26. SiC Coating on RVC(B-8) Longitudinal Section. Distance between Numbered Divisions Equals 3.94 Mils.

Plate No. 4950

Unetched X250

Figure 27. SiC Coating on RVC(B-8), Transverse Section.

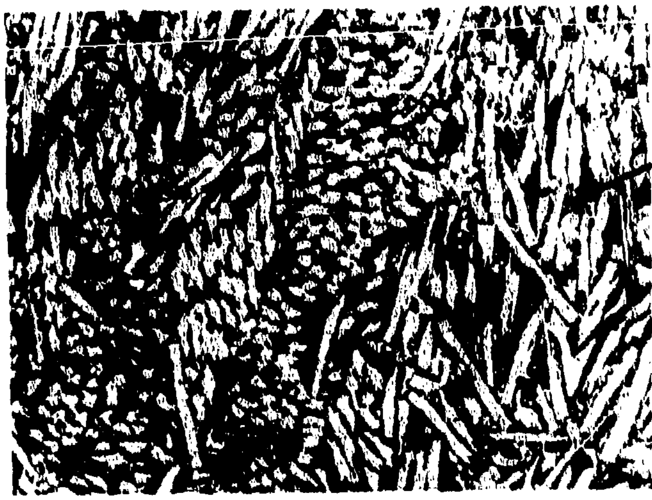

Unetched X250

Figure 28. Microstructural Characteristics of PT0178 Graphite (B-9) Longitudinal Section.

Unetched X250

Figure 29. Microstructural Characteristics of PT0178 Graphite (B-9) Transverse Section.

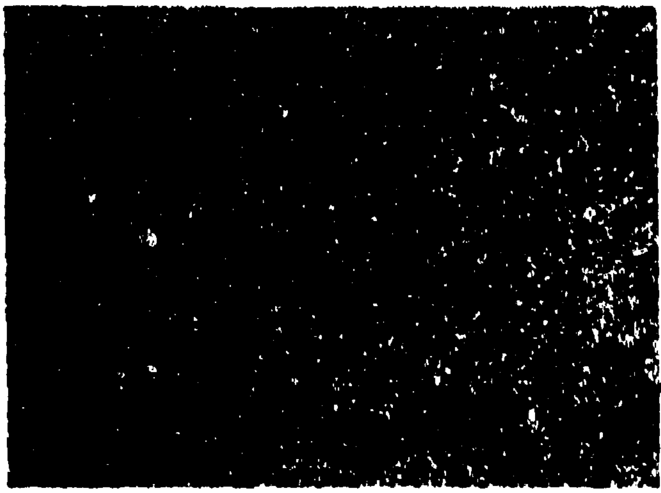

Unetched (a) X250

Figure 30. Microstructural Characteristics of Poco Graphite (B-10) Transverse Section.

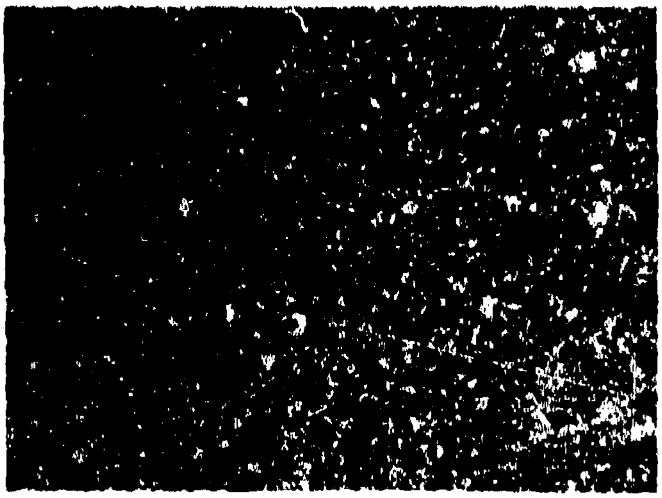

Unetched (b) X500

Figure 31. Microstructural Characteristics of Poco Graphite (B-10) Transverse Section.

Plate No. 3813C

Unetched X13,000

Figure 32. Microstructural Characteristics of AXF-5Q Poco Graphite (B-10). 1.5% Parlodion Replica Shadowed with Chromium at 60° Angle.

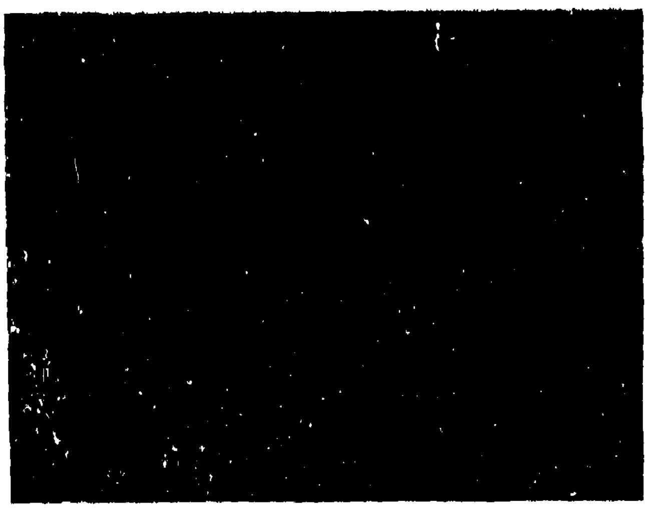

Plate No. 3813D

Unetched X13,000

Figure 33. Microstructural Characteristics of AXF-5Q Poco Graphite (B-10). 1.5% Parlodion Replica Shadowed with Chromium at 60° Angle.

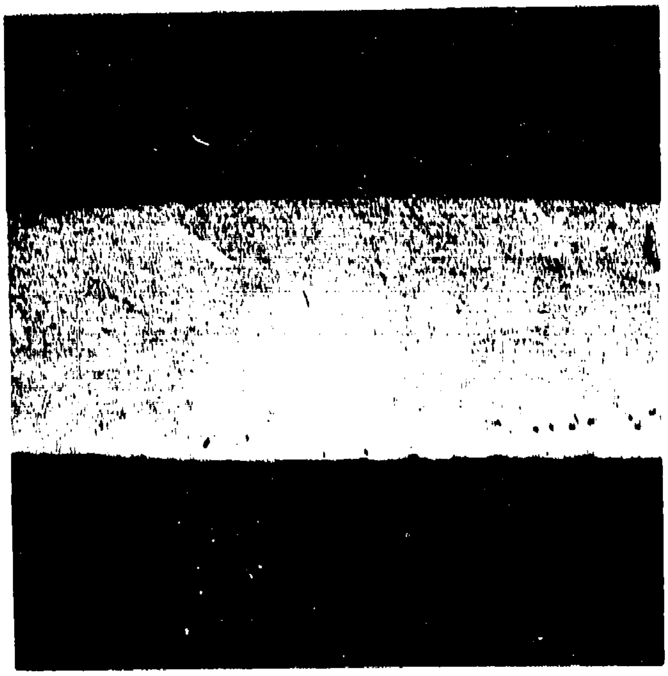

Plate No. 1-8063

Unetched X50

Figure 34. Microstructure of Glassy Carbon(B-11).

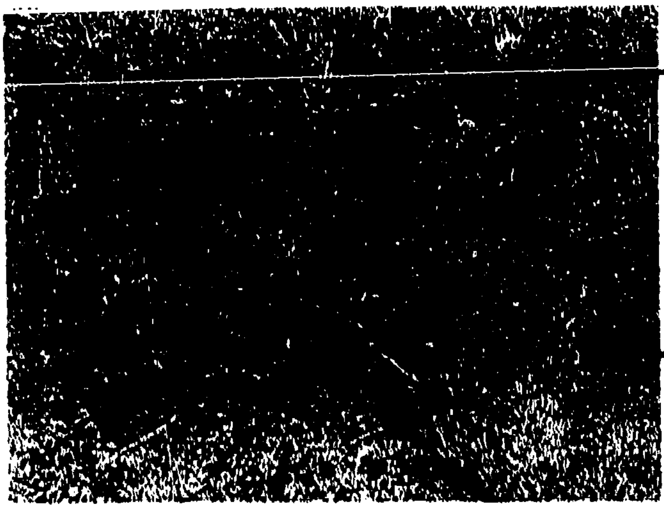

Unetched X100

Figure 35. Microstructural Characteristics of HfC + C (C-11), Longitudinal Section.

Unetched X100

Figure 36. Microstructural Characteristics of HfC + C (C-11), Transverse Section.

Plate No. 4868

Unetched X100

Figure 37. Microstructural Characteristics of ZrC + C (C-12), Longitudinal Section.

Plate No. 4870

Unetched X100

Figure38. Microstructural Characteristics of ZrC + C (C-12), Transverse Section.

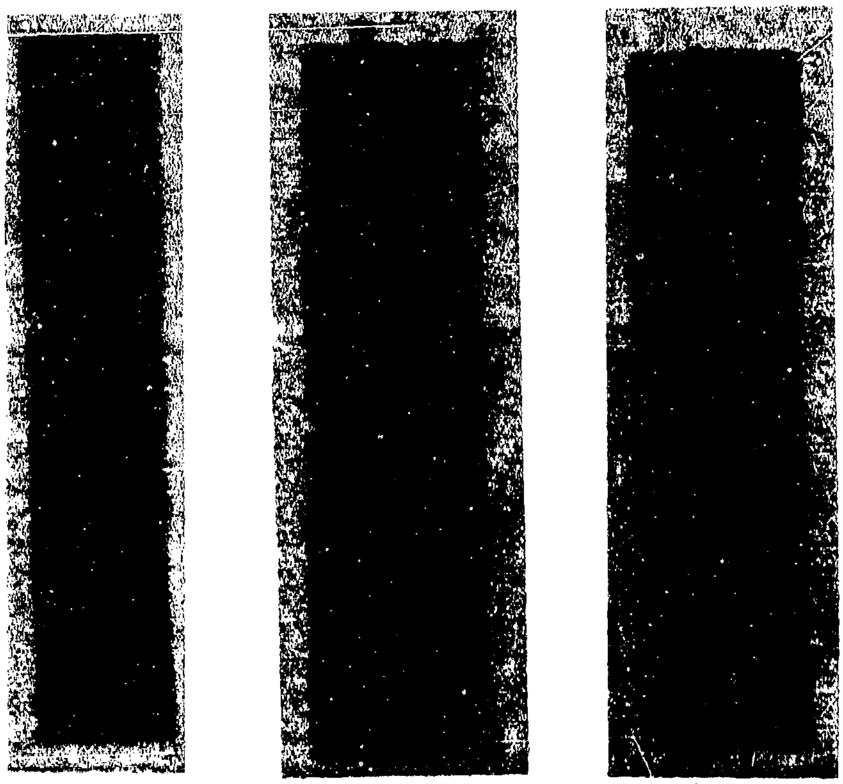

(a) (b) (c)

Figure 39. Radiographs of Hypereutectic Carbide Billets: (a) $HfC + C$(C-11) Billet 1416A with Internal Gas Holes, (b) $ZrC + C$(C-12) Billet 1467A with Center-line Pipe, (c) $ZrC + C$ Billet 1420A with No Internal Voids. (Full Scale)

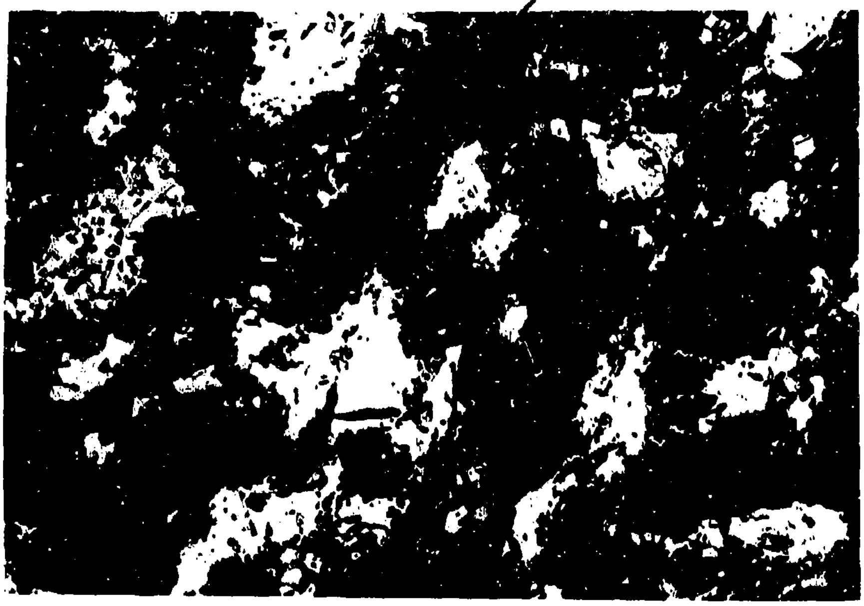

Figure 40. JTA (D-13), Longitudinal Section.

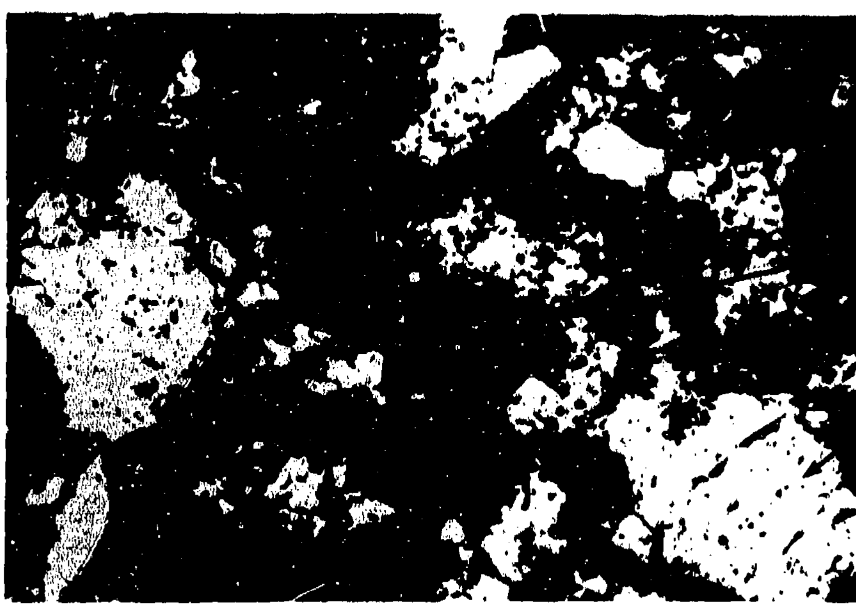

Figure 41. JTA (D-13), Transverse Section.

Figure 42. "KT" SiC (E-14), Longitudinal Section. While Most of the Black Areas Are Probably Pull-Out, Some Have Been Found to Be Carbon.

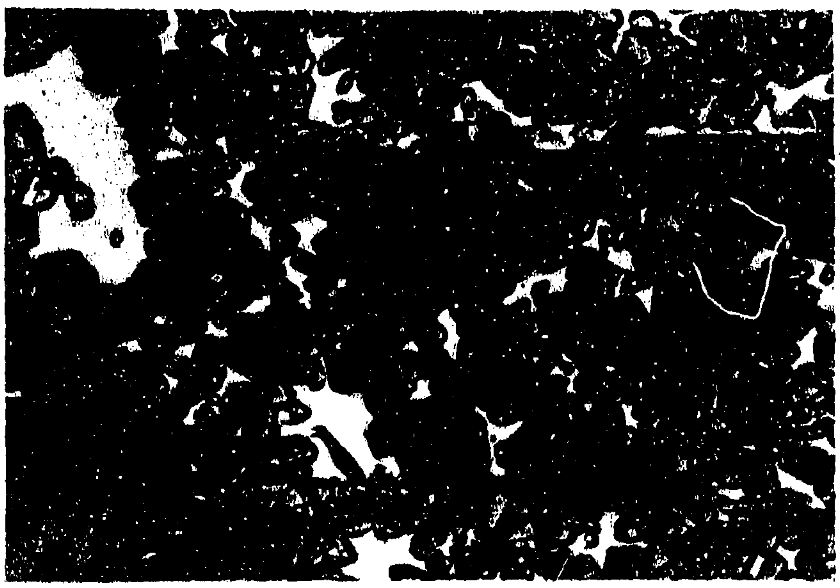

Figure 43. "KT" SiC (E-14), Transverse Section.

Graphite Fibers

ZrB_2

Plate No.

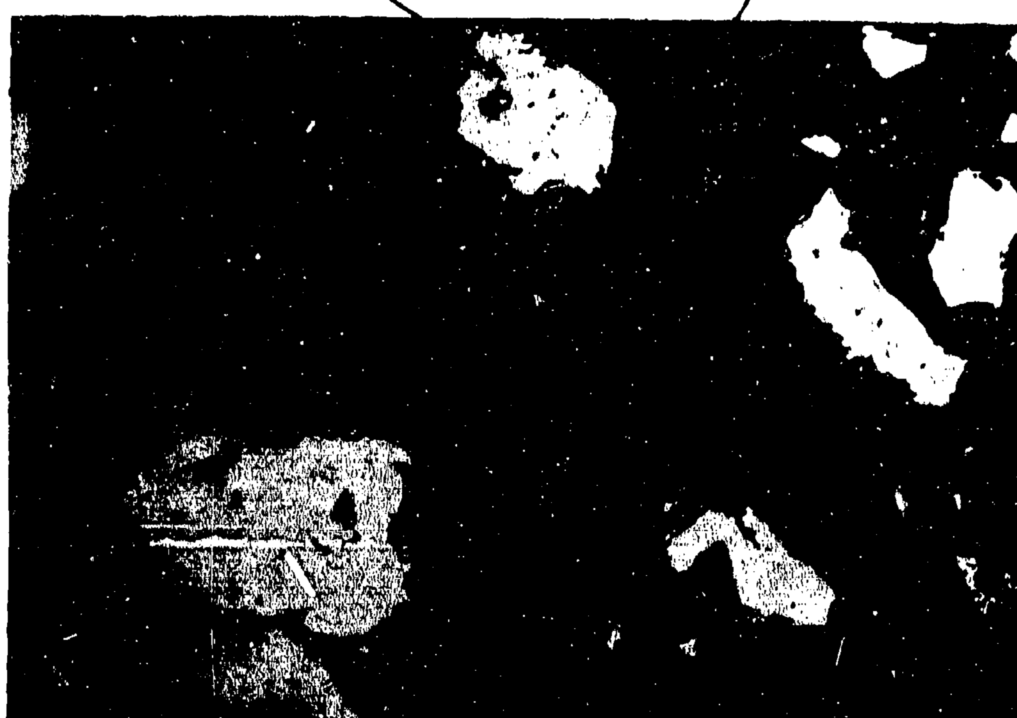

Unetched

500X

Figure 44. JT-PT (F-1) Showing Grains of ZrB_2 in a Graphite Fiber Matrix.

Plate No. 4336

Unetched 500X

Figure 45. JT0992 (F-15), Longitudinal Section.

Plate No. 4338

Unetched 500X

Figure 46. JT0992 (F-15), Transverse Section.

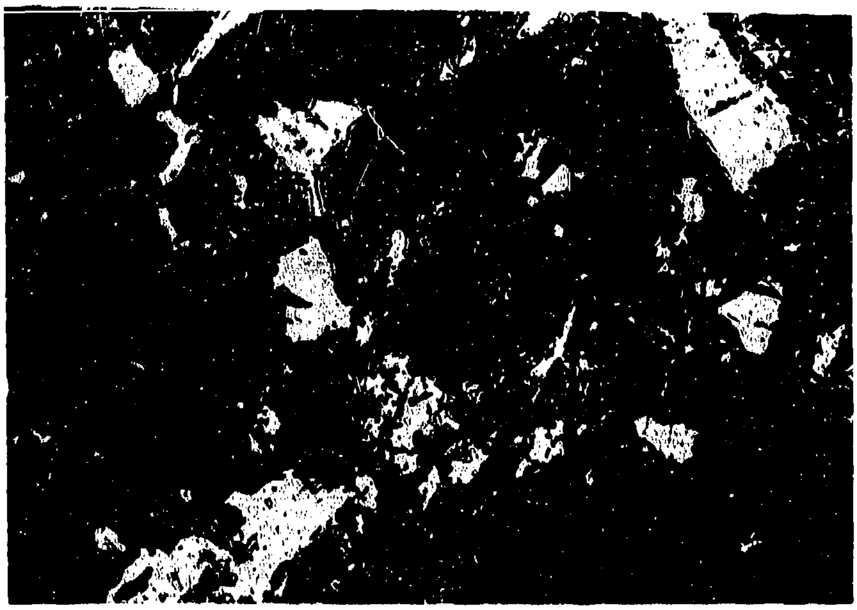

Plate No. 4332

Unetched 500X

Figure 47. JT0981 (F-16), Longitudinal Section.

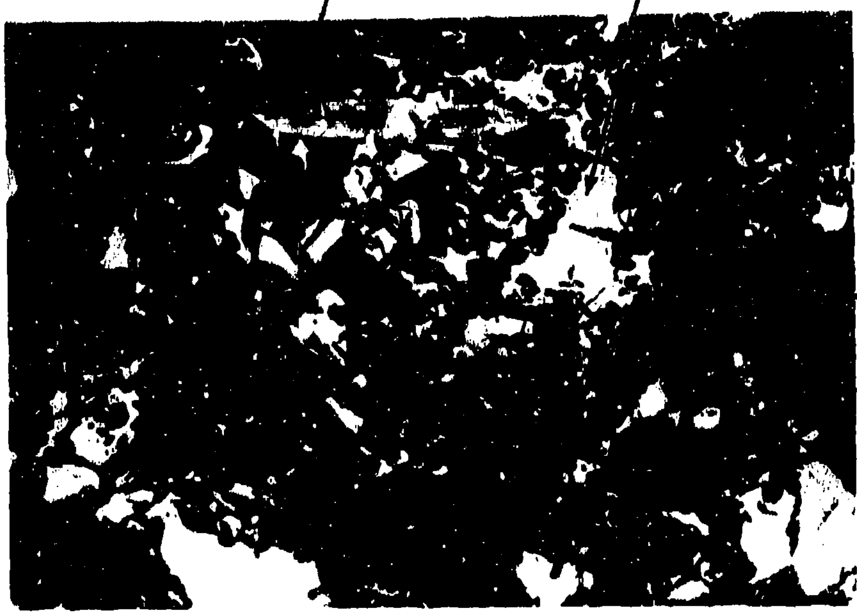

Plate No. 4334

Unetched 500X

Figure 48. JT0981 (F-16), Transverse Section.

Plate No. 4388

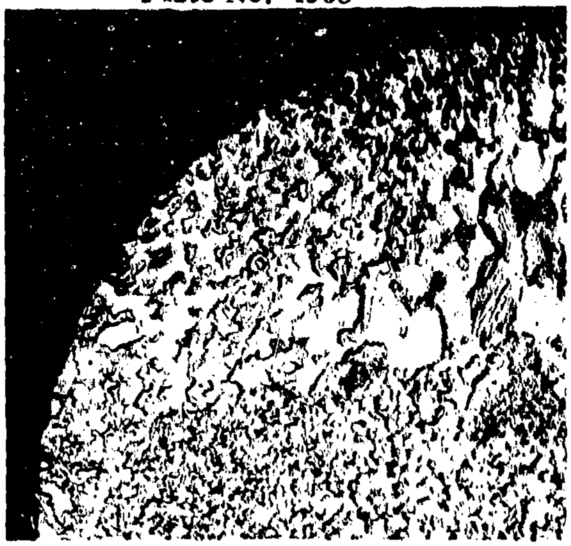

Etched with Murakamis' Reagent ~7X

Figure 49. W (G-18), 1" Diam. Bar, Transverse Section. The Sample Is Symmetric; One Quadrant Is Shown.

Plate No. 4308

Etched with Murakamis' Reagent 100X

Figure 50. W (G-18), 1" Diam. Bar, Transverse Section, Fine Grains of The Diametral Band.

Plate No. 4309

Etched with Murakamis' Reagent 100X

Figure 51. W (G-18), 1" Diam. Bar, Transverse Section, Large Grains.

Plate No. 4489

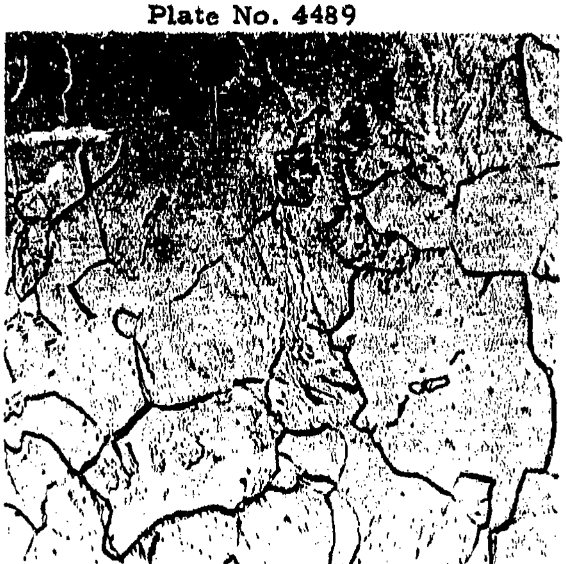

Etched with Murakamis' Reagent 500X

Figure 52. W (G-18), 1/2" Diam. Bar, Transverse Section. The 1/2" Rod Is Uniform Across The Transverse Section.

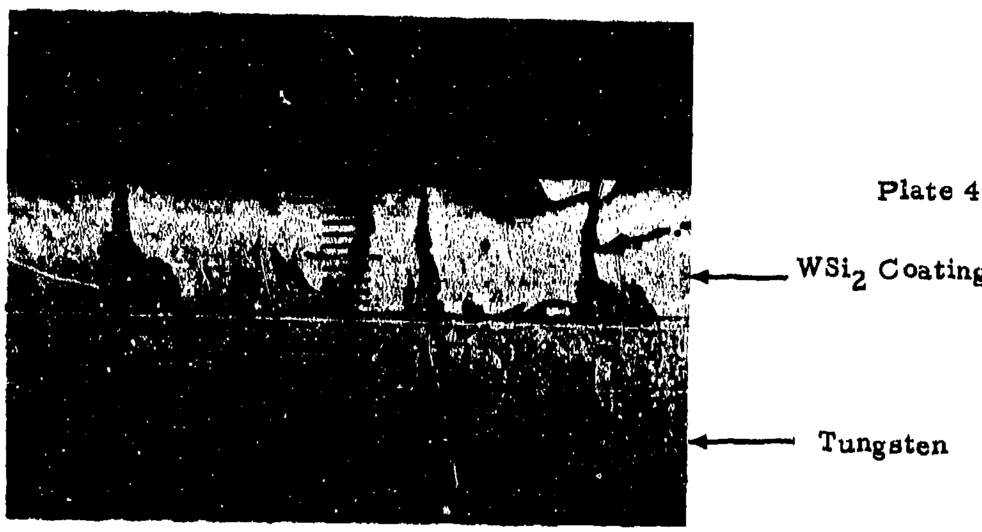

Etched with Murakamis' Reagent X175

Figure 53. WSi_2 Coating on Tungsten (G-18) Longitudinal Section on Top Face of Cylinder. One Division Equals 0.394 Mils.* (Fissures in Coating have been Accentuated by Mechanical Preparation).

*Distance between numbered divisions is equal to 3.94 mils.

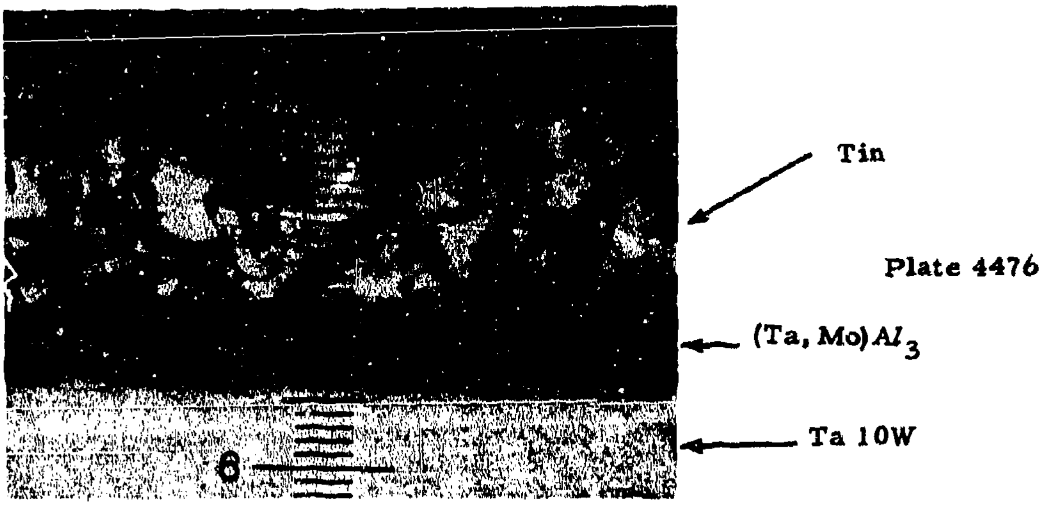

(a)

Etched with 30 cc Lactic Acid, 10cc HNO_3, 5cc HF X200

Figure 54. Sn-Al-Mo Coating on Ta-10W (G-19) Longitudinal Section of Top Face of Cylinder. One Unit Equals 0.394 Mils.

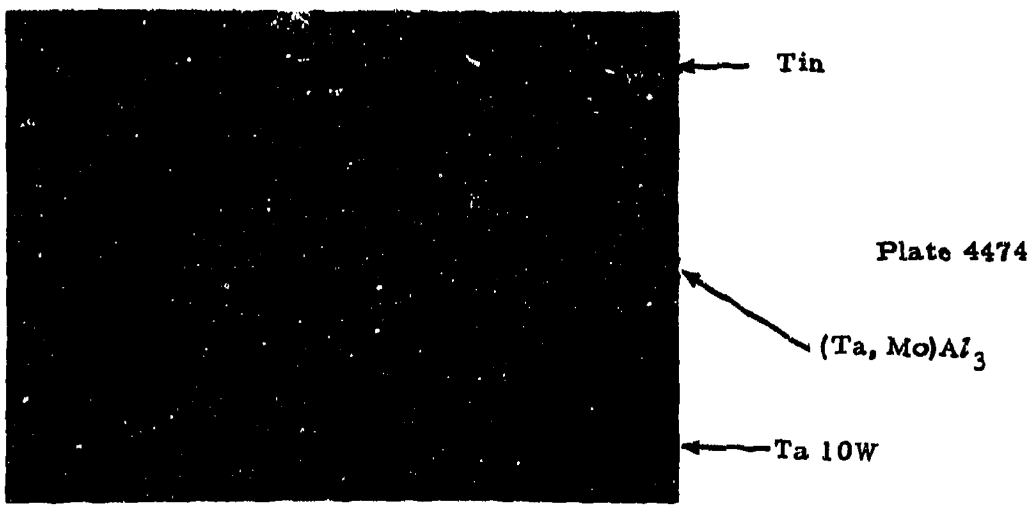

Unetched (b) X250

Figure 55. Sn-Al-Mo Coating on Ta-10W (G-19), Sectioned at an Angle to Cylinder Side.

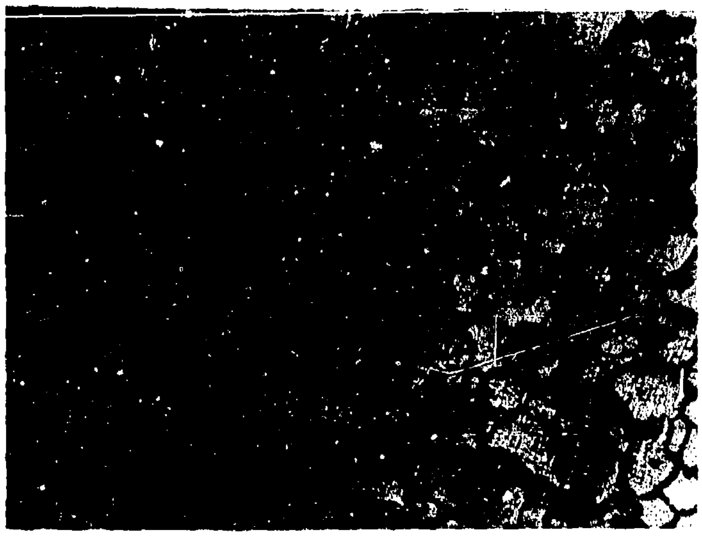

Plate No. 5362

Etched with Murikami's Reagent X500

Figure 56. Microstructural Characteristics of W + Zr + Cu (G-20) Transverse Section. Tungsten Grains are Light.

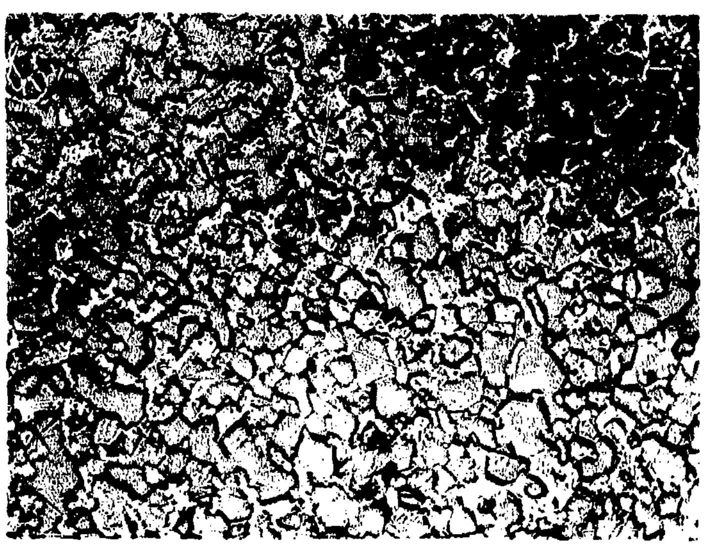

Plate No. 5055b

Unetched X500

Figure 57. Microstructural Characteristics of W + Ag (G-21) Transverse Section. Silver Infiltrant is Light.

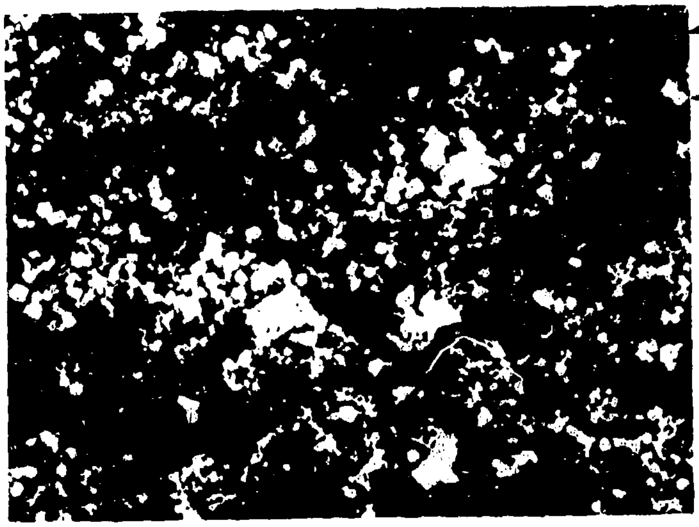

Plate 4722

Unetched (a) X250

Figure 58. Microstructural Characteristics of SiO_2-68.5 w/o W (H-22) (Twenty-One Volume Per Cent W). Density 5.70 gms/cm^3 Longitudinal Section.

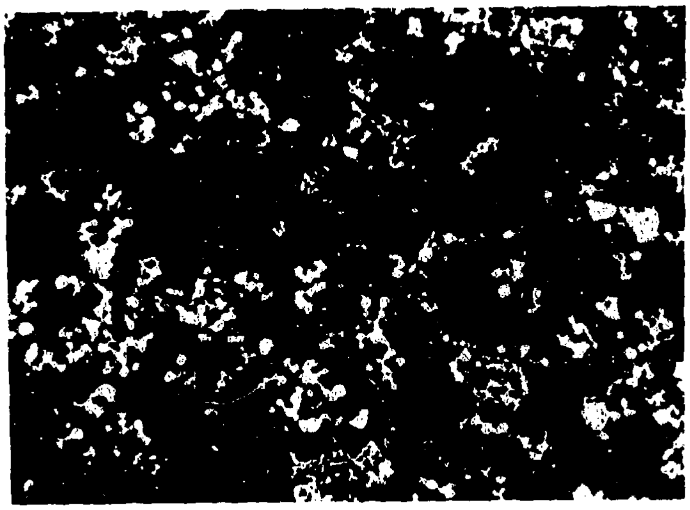

Plate 4721

Unetched (b) X250

Figure 59. Microstructural Characteristics of SiO_2-68.5 w/o W (H-22) (Twenty-One Volume Per Cent W). Density 5.70 gms/cm^3 Transverse Section.

Unetched (a) X250

Figure 60. Microstructural Characteristics of SiO_2-60 w/oW (H-23) (Seventeen Volume Per Cent W). Density 4.80 gms/cm^3 Transverse Section.

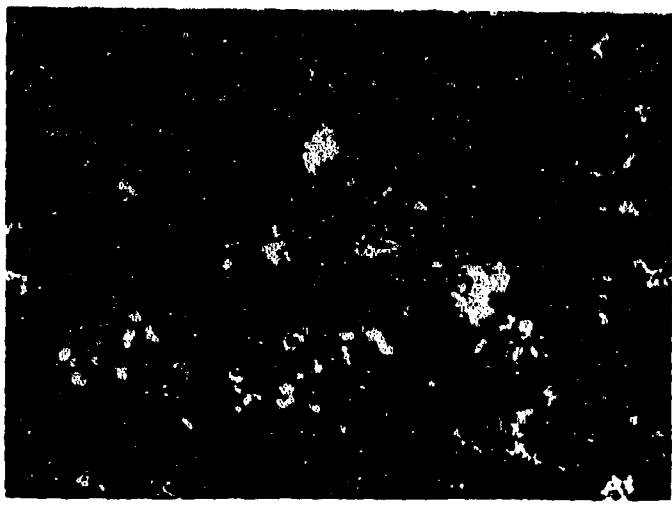

Unetched (b) X250

Figure 61. Microstructural Characteristics of SiO_2-35 w/o W (H-24) (Six Volume Per Cent W). Density 3.20 gms/cm^3 Transverse S . . . .

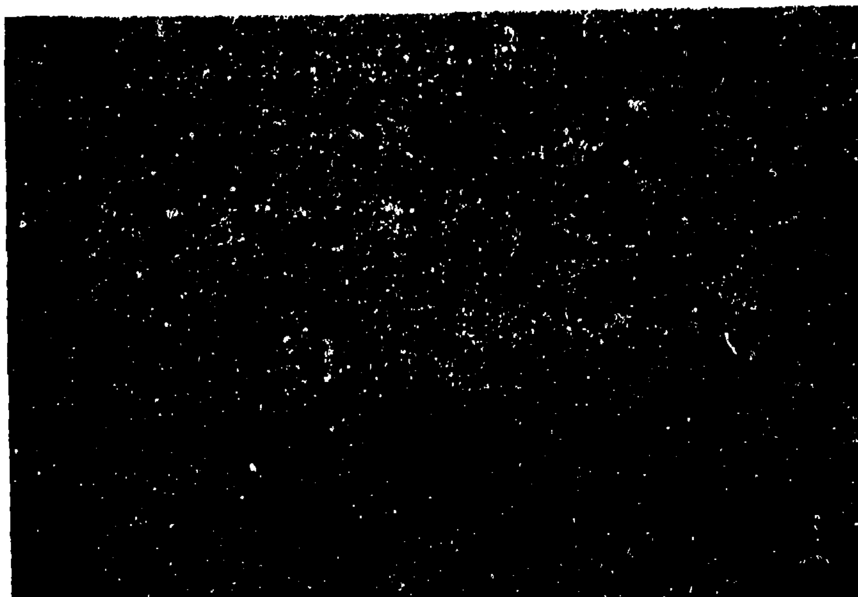

Plate No. 4397

Etched with 30 Lactic 10 HNO_3 1HF 250X

Figure 62. Hf-20Ta-2Mo (I-23), 1" Diam. Bar, Transverse Section. Notice the Outline of the Grain Boundaries of the Preceding Structure.

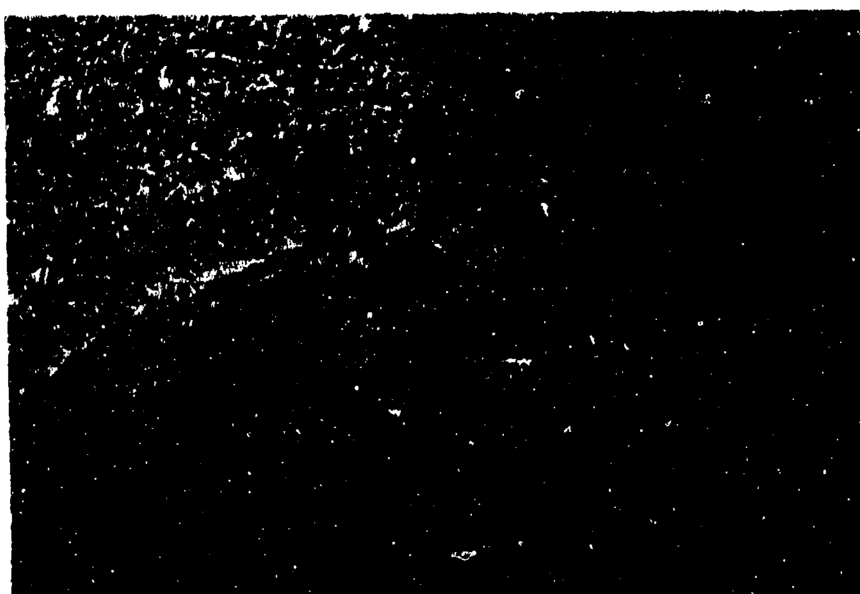

Plate No. 4398

Etched with 30 Lactic 10$HNO_3$1HF 1000X

Figure 63. Hf-20Ta-2Mo (I-23), 1" Diam. Bar, Transverse Section. Platelets are α in a β Matrix. Note Precipitation on Grain Boundaries of Preceding Structure.

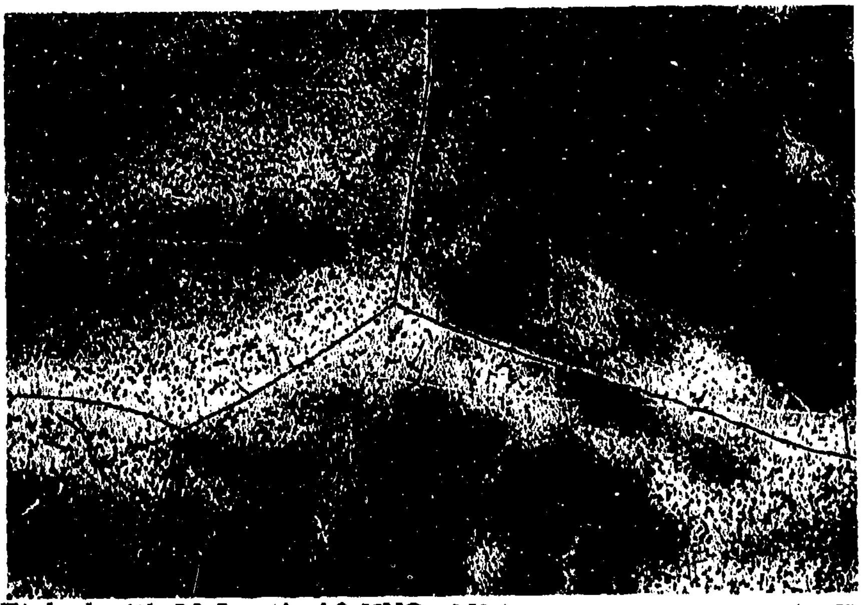

Etched with 30 Lactic 10 HNO_3 1HF 500X

Figure 64. Hf-20Ta-2Mo (I-23), 1/2" Diam. Bar, Transverse Section. This Alloy Is Principally β Hf. Note the Relationship to the Structure Shown in Figures 26-27.

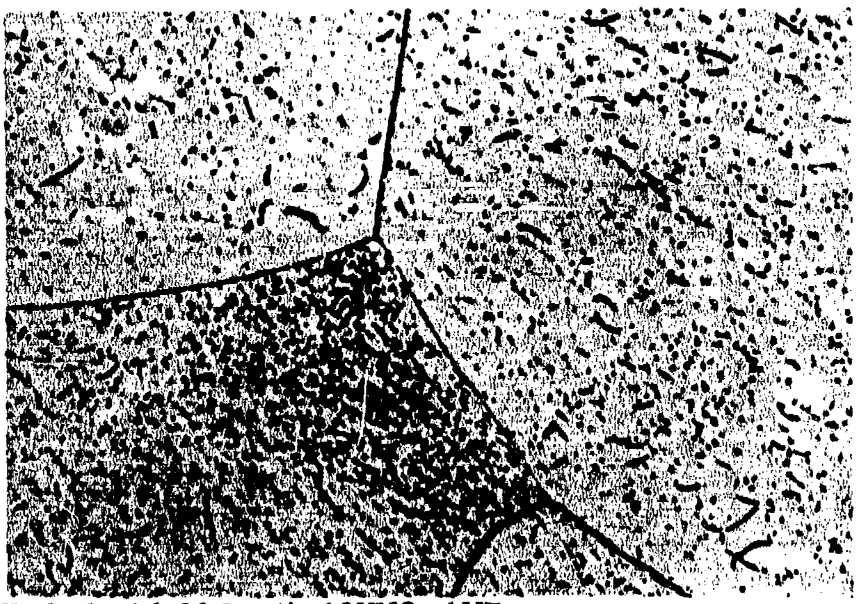

Etched with 30 Lactic 10HNO_3 1HF 1000X

Figure 65. Hf-20Ta-2Mo (I-23), 1/2" Diam. Bar, Transverse Section.

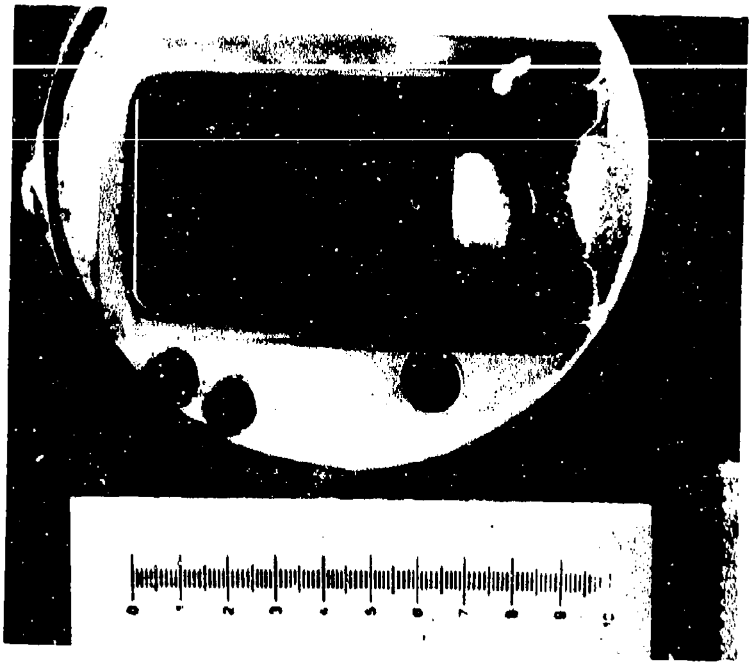

Plate No.
2-0446

Unetched X2.87

Figure 66. Ir/C (I-24) Iridium Coated Poco Graphite Longitudinal Section. One Inch Scale.

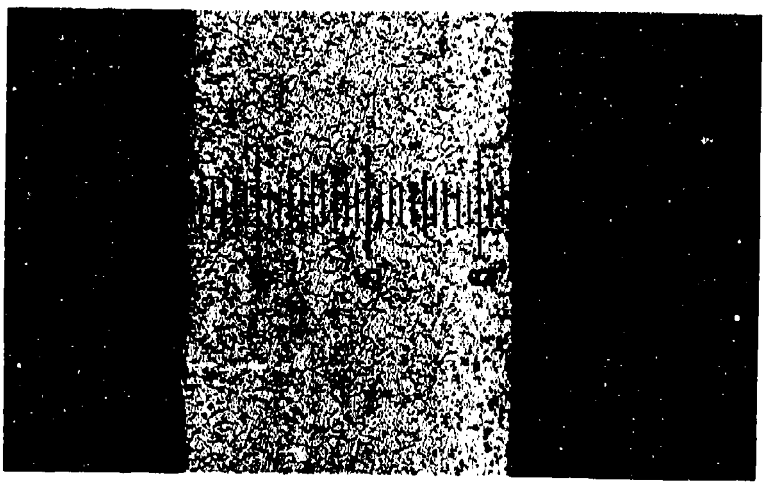

Plate No.
2-0447

Etched Electrolytically in 20% HCl in a Saturated Solution of NaCl in Water X89

Figure 67. Iridium Coating on Top Surface of Ir/C (I-24), One Division Equals 0.788 Mils. Coating Thickness equals 23.6 mils, Graphite at Right.

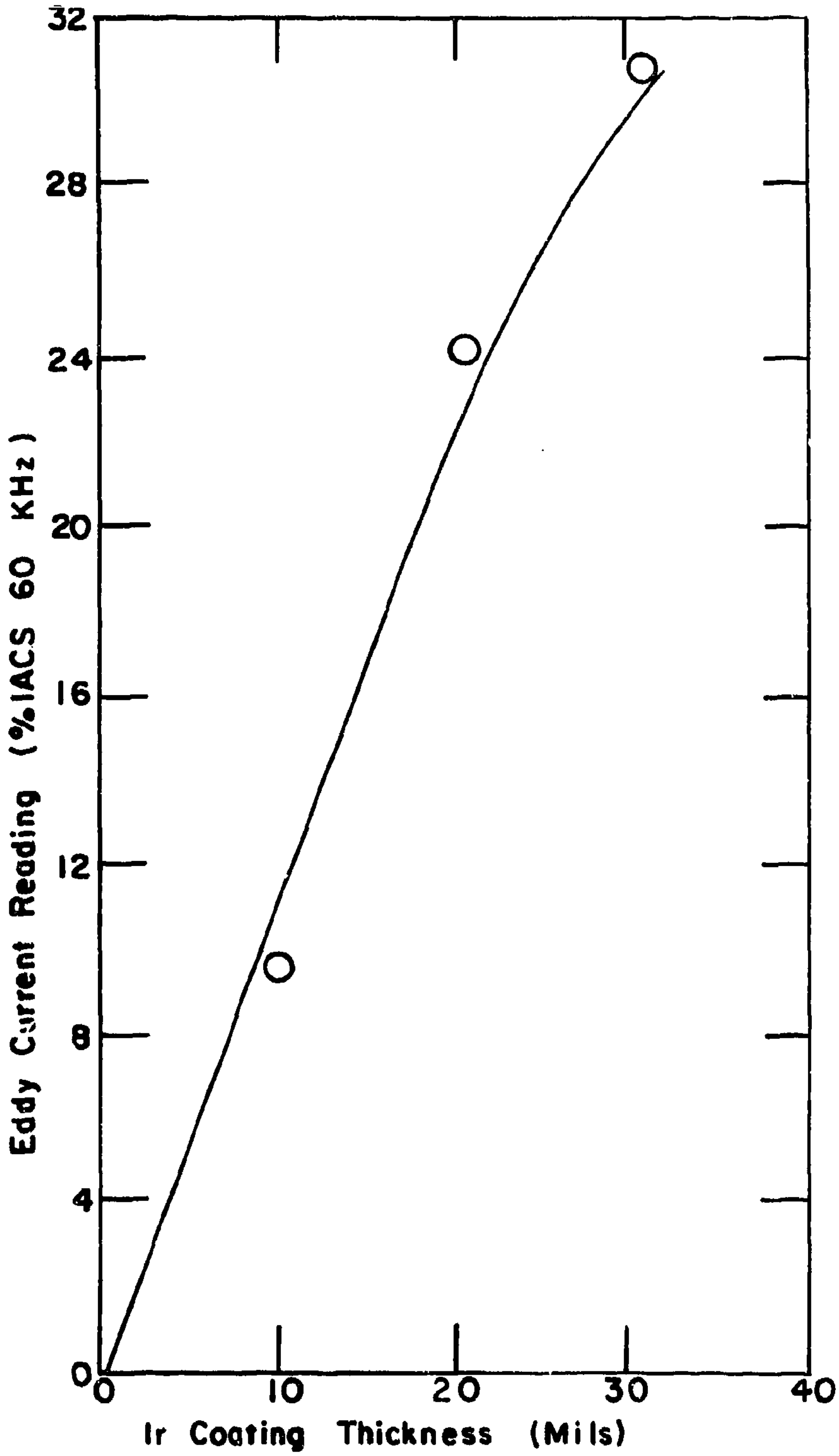

Figure 68. Calibration Curve for Iridium Coating Measurement

TABLE 1

LIST OF CANDIDATE MATERIALS

Material	Code No.	Source
$HfB_{2.1}$	A-2	Carborundum Co., Niagara Falls, New York
ZrB_2	A-3	Carborundum Co., Niagara Falls, New York
HfB_2 + 20v/o SiC	A-4	Carborundum Co., Niagara Falls, New York
Boride Z	A-5	Carborundum Co., Niagara Falls, New York
$HfB_{2.1}$	A-6	ManLabs-Avco AF33(615)-3671
$HfB_{2.1}$ + 20v/o SiC	A-7	ManLabs-Avco AF33(615)-3671
$ZrB_{2.1}$ + 20v/o SiC	A-8	ManLabs-Avco AF33(615)-3671
$HfB_{2.1}$ + 35v/o SiC	A-9	ManLabs-Avco AF33(615)-3671
ZrB_2 + 14v/o SiC + 30v/o C	A-10	ManLabs-Avco AF33(615)-3671
RVA	B-5	Union Carbide Corp., New York, New York
PG	B-6	General Electric Co., Detroit, Michigan
BPG	B-7	High Temperature Materials, Lowell, Mass.
Si/RVC	B-8	Union Carbide Corp., New York, New York
PT0178	B-9	Union Carbide Corp., New York, New York
Poco Graphite (AXF-5Q)	B-10	Poco Graphite Inc., Garland, Texas
Glassy Carbon	B-11	Lockheed M & SC, Palo Alto, California
HfC + C	C-11	Battelle Memorial Institute, Columbus, Ohio
ZrC + C	C-12	Battelle Memorial Institute, Columbus, Ohio
JTA (C + ZrB_2 + SiC)	D-13	Union Carbide Corp., New York, New York
KT-SiC	E-14	Carborundum Co., Niagara Falls, New York
JT0992 (C + ZrC + SiC)	F-15	Union Carbide Corp., New York, New York
JT0981 (C + HfC + SiC)	F-16	Union Carbide Corp., New York, New York
WSi_2/W	G-18	General Electric Co., Cleveland, Ohio (type MK-W)
		TRW, Cleveland, Ohio (WSi_2 coating)
Sn-Al/Ta-W	G-19	National Research Corp., Newton, Mass. (Ta-10W)
		GT & E, Hicksville, New York (Sn-Al coating)
W-Zr-Cu	G-20	Rocketdyne, Canoga Park, California
W-Ag	G-21	Wah Chang Corp., Albany, Oregon
SiO_2 + 68.5w/o W	H-22	Bjorksten Research Labs, Madison, Wisconsin
SiO_2 + 60w/o W	H-23	General Electric Co., Willoughby, Ohio
SiO_2 + 35w/o W	H-24	General Electric Co., Willoughby, Ohio
Hf-20Ta-2Mo	I-23	Wah Chang Corp., Albany, Oregon
Ir/Graphite	I-24	Battelle Memorial Institute, Columbus, Ohio
		General Technologies Corp., Reston, Virginia

TABLE 2

CHARACTERIZATION OF TEST MATERIALS

MATERIAL: $HfB_{2,1}$, CODE (A-2)

SUPPLIER: Carborundum Co., Niagara Falls, New York

Qualitative Analysis (Range w/o)
(Jarrell-Ash Co., Waltham, Mass.)

1.0-0.1	0.1-0.01	0.001-0.0001	< 0.0001
Zr, Ti, Si	Fe, Al, Ca	Mg, V, Cr, Mn	Cu, Ag, Sn

Quantitative Analysis

Element	w/o (Source)
Hf	84.2 (ManLabs)
Zr*	2.6 (ManLabs)
B	10.65 (ManLabs)
O	0.007 (MIT), 0.002 (Luvak)
C	0.28 (ManLabs)

Over-all Atomic Ratio:	$B/(Hf+Zr) = 1.97$
Corrected Atomic Ratio+:	$B/(Hf+Zr) = 2.07$
Calculated Dioxide:	0.06 w/o
Calculated Monocarbide:	4.46 w/o
Calculated Weight Per Cent Diboride:	93.2
Phases Identified by X-ray:	HfB_2, HfC
Metallographic Description:	Two Phase
Bulk Density:	10.02 gms/cm^3

*Based on Zr = 3% Hf.
+Based on (Hf+Zr) pr[illegible] minus (Hf+Zr) present as dioxide and monocarbide. The calc[illegible] oxide based on the oxygen analysis provided by MIT. The Luvak [illegible] appears to be too low.

MATERIAL: $ZrB_{2,1}$, CODE (A-3)

SUPPLIER: Carborundum, Co., Niagara Falls, New York

Qualitative Analysis (Range w/o)
(Jarrell-Ash Co., Waltham, Mass.)

1.0-0.1	0.01-0.001	0.001-0.0001	< 0.0001
Fe	Ti, Si	Al, Ca, Cr, Mg, Ni, V	Co, Cu, Mn, Sn

Quantitative Analysis

Element	w/o (Source)
Zr	79.2, 79.5, 80.1 (ManLabs), 79.8 (MIT)
B	18.36, 18.0+, 18.0- (ManLabs), 18.5 (MIT)
O	0.1700 (MIT), 0.0066 (Luvak)
Fe	1.26, 0.75 (Jarrell-Ash: quantitative spectroscopy)
C	0.26 (MIT), 0.24 (ManLabs)

Over-all Atomic Ratio:	$B/Zr = 1.91$
Corrected Atomic Ratio*:	$B/Zr = 1.97$
Calculated Dioxide:	0.66 w/o
Calculated Monocarbide:	1.98 w/o
Calculated Weight Per Cent Diboride	95.33
Phases Identified by X-ray:	ZrB_2, ZrC
Metallographic Description:	Single phase, equiaxed grain structure
Bulk Density:	5.58 gms/cm^3

*Based on Zr present minus Zr present as dioxide and monocarbide. The calculated dioxide based on the oxygen analysis provided by MIT. The Luvak result appears to be too low.

MATERIAL: $HfB_{2,1}$ + 20 v/o SiC, CODE (A-4)

SUPPLIER: Carborundum Co., Niagara Falls, New York

Qualitative Analysis (Range w/o)
(Jarrell-Ash Co., Waltham, Mass.)

>10	10-1.0	0.1-0.01	0.01-0.001	0.001-0.0001	<0.0001
Hf, B, Si	Ti	Ca, Fe, Zr	Cr, Mn, Sn, V	Al, Cu, Mg, Na, Pb, Zn	Ag

Quantitative Analysis

Element	w/o (Source)
Hf	77.9, 79.9 (ManLabs)
Zr*	2.4 (ManLabs)
B	10.3 (ManLabs)
Si	5.13 (ManLabs)
O	0.09 (MIT)
Fe	-----
C	1.44, 1.72, 1.90 (ManLabs)

Over-all Atomic Ratio:	$B/Me = 2.01$
Over-all Atomic Ratio:	$C/Si = 0.77$
SiC-Diboride Atomic Ratio:	0.228
Calculated Weight Per Cent SiC:	6.5
Calculated Weight Per Cent Diboride:	92.6
Phases Identified by X-ray:	HfB_2, SiC, HfC (trace)
Metallographic Description:	Two phase, uniform distribution of SiC in matrix of equiaxed grains of HfB_2
Bulk Density:	9.36 ± .02 gms/cm^3

*Based on assumption that Zr = 3% Hf.

MATERIAL: Boride Z, CODE (A-5)

SUPPLIER: Carborundum Co., Niagara Falls, New York

Qualitative Analysis (Range w/o)
(Jarrell-Ash Co., Waltham, Mass.)

>10%	10.0-1.0	0.1-0.01	0.01-0.001
B, Zr	Si, Mo	Fe	Al, Ca, Ti, Mn

Quantitative Analysis

Element	w/o (Source)
Zr	70.1 (MIT)
B	17.3 (MIT)
Si	2.74 (MIT)
C	0.83 (MIT)
Mo	6.93 (MIT)
Total	97.90

Over-all Atomic Ratio:	$B/Zr = 2.08$
Over-all Atomic Ratio:	$B/(Zr + Mo) = 1.90$
Over-all Atomic Ratio:	$C/Si = 0.70$
Calculated Weight Per Cent $Zr_{0.9}Mo_{0.1}B_{1.9}$:	94.3
Calculated Weight Per Cent SiC:	2.8
Phases Identified by X-ray:	ZrB_2, SiC
Metallographic Description:	Two Phase
Bulk Density:	5.70 gms/cm^3

TABLE 3

CHARACTERIZATION OF TEST MATERIALS

MATERIAL: $HfB_{2.1}$, CODE (A-6)

SUPPLIER: ManLabs, Inc. and Avco Space Systems Division, Lowell, Mass., AF33(615)-3671 (Material II)

Qualitative Analysis (Range w/o)+
(ManLabs, Inc.)

1.0-0.1	0.01-0.001	0.001-0.0001	<0.0001
Fe, Zr	Al, Cu, Ni, Ti	Si	Ca, Cr, Mg

Quantitative Analysis+

Element	w/o(Source)
Hf	87.1 (ManLabs)
Zr	1.15 (Jarrell-Ash)
B	10.95 (ManLabs)
C	0.18 (MIT)
O	0.10 (MIT)
Si	0.12 (Jarrell-Ash)
Al	0.12 (Jarrell-Ash)

Over-all Atomic Ratio:	B/(Hf+Zr) = 2.02
Corrected Atomic Ratio°:	B/(Hf+Zr) = 2.10
Calculated Dioxide:	0.66 w/o
Calculated Monocarbide:	2.80 w/o
Calculated Weight Per Cent Diboride:	95.87
Phases Identified by X-ray:	HfB_2, HfC
Metallographic Description:	Two phase, equiaxed grains of HfB_2 having a grain size of 15-25 microns.
Bulk Density:	10.69 gms/cm^3

+Qualitative and quantitative analyses performed on different billets.
°Based on (Hf+Zr) present minus (Hf+Zr) present as dioxide and monocarbide.

MATERIAL: $HfB_{2.1}$ + 20 v/o SiC, CODE (A-7)

SUPPLIER: ManLabs, Inc. and Avco Space Systems Division, Lowell, Mass. AF33(615)-3671 (Material III)

Qualitative Analysis (Range w/o)*
(ManLabs, Inc.)

1.0-0.1	0.1-0.01	0.01-0.01	0.001-0.0001	<0.0001
Zr	Fe	Al, Cu, Ni, Ti	Mg	Ca, Cr

Quantitative Analysis*

Element	w/o(Source)
Hf	80.02 (ManLabs)
Zr	1.08 (ManLabs)
B	9.76 (ManLabs)
C	1.18 (ManLabs)
O	0.10 (MIT)
Si	5.98 (ManLabs)

Over-all Atomic Ratio:	B/Me = 1.96
SiC-Diboride Atomic Ratio:	0.228
Calculated Weight Per Cent SiC:	7.16
Calculated Weight Per Cent Diboride:	92.30
Phases Identified by X-ray:	HfB_2, SiC, HfC (Trace)
Metallographic Description:	Two phase, uniform distribution of SiC grains (4-6μ grain size) within equiaxed grains of HfB2 (5μ grain size).
Bulk Density:	9.03 gms/cm^3

*Qualitative and quantitative analyses performed on different billets.

MATERIAL: $ZrB_{2.1}$ + 20 v/o SiC, CODE (A-8)

SUPPLIER: ManLabs, Inc. and Avco Space Systems Division, Lowell, Mass. AF33(615)-3671 (Material V)

Qualitative Analysis (Range w/o)°
(ManLabs, Inc.)

1.0-0.1	0.1-0.01	0.01-0.001
Fe	Al, Ca, Cu, Hf	Ti

Quantitative Analysis*

Element	w/o(Source)
Zr	69.97 (ManLabs)
B	14.90 (ManLabs)
C	2.96 (ManLabs)
O	0.25 (MIT)
Si	8.35 (ManLabs)

Over-all Atomic Ratio:	B/Me = 1.80
SiC-Diboride Atomic Ratio:	0.254
Calculated Weight Per Cent SiC:	11.31
Calculated Weight Per Cent Diboride:	84.16
Phases Identified by X-ray:	ZrB_2, SiC
Metallographic Description:	Two phase, uniform distribution of SiC grains (4-5μ grain size) within equiaxed grains of ZrB_2 (8-10μ grain size).
Bulk Density:	5.47 gms/cm^3 (100% theoretical density)

°Qualitative and quantitative analyses performed on different billets.

MATERIAL: $HfB_{2.1}$ + 35 v/o SiC, CODE (A-9)

SUPPLIER: ManLabs, Inc. and Avco Space Systems Division, Lowell, Mass. AF33(615)-3671 (Material IV)

Qualitative Analysis (Range w/o)
(ManLabs, Inc.)

>10	0.1-0.01	0.01-0.001	0.001-0.0001	<0.0001
B, Hf, Si	Fe, Zr	Cu	Ca, Ni, Ti	Cr, Mg

Phases Identified by X-ray:	HfB_2, SiC, HfC (trace)
Metallographic Description:	Two phase, uniform distribution of SiC grains (4-5μ grain size) within equiaxed HfB_2 grains (10μ grain size).
Bulk Density:	7.78 gms/cm^3

TABLE 4

CHARACTERIZATION OF TEST MATERIALS

MATERIAL: ZrB_2 + 14% SiC + 30% C, CODE (A-10)

SUPPLIER: ManLabs, Inc. and Avco Space Systems Division, Lowell Mass. AF33(615)-3671 (Material VIII)

Qualitative Analysis (Range w/o)
(ManLabs, Inc.)

>10	1.0-0.1	0.1-0.01	0.01-0.001
B, Si, Zr, C	Al, Fe	Cu, Hf	Ti

Phases Identified by X-ray: ZrB_2, SiC, graphite
Metallographic Description: Uniform mixture of SiC grains and graphite flakes within equiaxed grains of ZrB_2.
Bulk Density: 4.50 gms/cm^3

MATERIAL: RVA Graphite, CODE (B-5)

SUPPLIER: Union Carbide Corp., New York, New York

Qualitative Analysis (Range w/o)
(Jarrell-Ash Co., Waltham, Mass.)

10-1.0	1.0-0.1	0.1-0.01	0.01-0.001	0.001-0.0001	<0.0001
Si, Ca	Ti, Zr, Ba	B, Al, Fe	Mg, V	Cr, Cu, Mn, Na, Zn	Ag, Ni, Pb

Quantitative Analysis: Carbon-99.2 w/o (ManLabs, Inc.)
Phases Identified by X-ray: Graphite, no extra lines
Metallographic Description: Typical graphite microstructure, fairly large grain size (~0.1 mm). Substantial porosity with pore size comparable to grain size.
Bulk Density: 1.79 ± 0.02 gms/cm^3

MATERIAL: PG (Pyrolitic Graphite), CODE (B-6)

SUPPLIER: General Electric Co., Metallurgical Products Division Detroit, Michigan

Qualitative Analysis (Range w/o)
(Jarrell-Ash Co., Waltham, Mass.)

Al, B, Ca, Fe, Mg, Si all less than 0.0001% each.
Approximately 0.1% residue on ignition (ManLabs, Inc.)

Phases Identified by X-ray: Graphite, no extra lines
Metallographic Description: Typical PG structure. Section parallel to (001) plane of deposition shows large hills(~1mm) composed of smaller hills. Section parallel to [001] axis is lamellar in appearance.
Bulk Density: 2.18 gms/cm^3

MATERIAL: BPG (Boron Doped Pyrolitic Graphite), CODE (B-7)

SUPPLIER: High Temperature Materials Division, Union Carbide Corp., Lowell, Mass.

Qualitative Analysis (Range w/o)
(Jarrell-Ash Co., Waltham, Mass.)

10-1.0	0.001-0.0001	<0.0001
B	Ca, Fe, Mg, Na, Si	Ag, Al, Cr, Cu

Quantitative Analysis: Carbon-98.6 w/o (ManLabs, Inc.
Phases Identified by X-ray: Graphite
Metallographic Description: Similar to PG (B-6). No second phase observed
Bulk Density: 2.22 gms/cm^3

TABLE 5

CHARACTERIZATION OF TEST MATERIALS

MATERIAL: Si/RVC (Siliconized RVC Graphite), CODE (B-8)

SUPPLIER: Union Carbide Corp., Carbon Products Division, New York, New York

Qualitative Analysis of RVC (Range w/o)
(Kent Laboratories, Newton Falls, Mass.)

0.1-0.01	0.03-0.003	0.01-0.001	0.003-0.0003	0.001-0.0001	< 0.0001
Ca	Fe	Ti, Zr	Si	Al, B, Ba, Mg, V	Ag, Cr, Cu, Ni, Sr

Phases Identified by X-ray: Graphite (matrix), SiC (coating) with no trace of free Si.

Metallographic Description: Matrix-typical graphite microstructure, substantial porosity, randomly oriented grains (~0.1 mm grain size). Coating-extremely nonuniform but continuous, variations in thickness from 1-8 mils, average thickness 4 mils.

Bulk Density: 1.66 gms/cm^3 (RVC only)

MATERIAL: PT0178 Graphite, CODE (B-9)

SUPPLIER: Union Carbide Corp., Carbon Products Division, New York, New York

Qualitative Analysis (Range w/o)
(Kent Laboratories, Newton Falls, Mass.)

0.1-0.01	0.01-0.001	0.003-0.0003	0.001-0.0001	< 0.0003
Fe	B, V	Ca	Si	Ba, Cr, Cu, Mg, Ni

Approximately 0.33% residue on ignition (ManLabs, Inc.).

Phases Identified by X-ray: Graphite

Metallographic Description: Randomly oriented fiberous graphite bundles (50-100μ in size) each composed of oriented graphite fibers (~10μ diam. by 50-100μ long). Considerable porosity.

Bulk Density: 1.29 ± 0.02 gms/cm^3

MATERIAL: AXF-5Q Poco Graphite, CODE (B-10)

SUPPLIER: Poco Graphite, Inc., Garland, Texas

Qualitative Analysis (Range w/o)
(Kent Laboratories, Newton Falls, Mass.)

0.01-0.001	0.003-0.0003	0.001-0.0001	< 0.0003
V	Fe, Si	Al, B, Ca, Zr	Cu, Mg, Ni

Approximately 0.075% Residue on ignition (ManLabs, Inc.).

Phases Identified by X-ray: Graphite

Metallographic Description: Very fine grain size (~5μ), grain orientation random, porosity evenly distributed

Bulk Density: 1.83 gms/cm^3

MATERIAL: HfC + C, CODE (C-11)

SUPPLIER: Battelle Memorial Institute, Columbus, Ohio

Qualitative Analysis (Range w/o)
(ManLabs, Inc.)

0.1-0.01	0.01-0.001	0.001-0.0001
B, Zr	Fe, Mg, Si	Ca, Cu, Ni, Ti

Quantitative Analysis: Carbon-14.4 ± 1.0 w/o (Battelle)

Phases Identified by X-ray: HfC, graphite

Metallographic Description: Long needles of primary graphite (50-100 mils long by 0.7-1.6 mils diam.) in a eutectic matrix.

Radiographic Analysis: Many billets with gas bubbles and voids, some with center-line core-type flaw (Battelle)

Bulk Density: 9.04 ± 0.3 gms/cm^3

TABLE 6

CHARACTERIZATION OF LMSC GLASSY CARBON

MATERIAL: Glassy Carbon, CODE (B-11)

SUPPLIER: Lockheed Missile & Space Co., Palo Alto, California

Supplier Property Analysis (6)

	Grade 2000	Grade 3000
Density (gms/cm^3)*	1.43-1.50	1.36-1.42
Lc(Å)**	19	110
d (Å)	3.56	3.45
Ave. Pore Radius (Å)	23	60
Crystalline Characteristics:	Combination of tetrahedral and trigonal linkages related to the turbostratic precursor polymer structure.	
Phases Identified by X-ray:	Carbon (amorphous), no other phases.	

*Density range related to material thickness, i.e. thicker material has higher density.

** Crystallite Size

TABLE 7

CHARACTERIZATION OF TEST MATERIALS

MATERIAL: ZrC + C, CODE (C-12)

SUPPLIER: Battelle Memorial Institute, Columbus, Ohio

Qualitative Analysis (Range w/o)
(ManLabs, Inc.)

1.0-0.1	0.1-0.01	0.01-0.001	0.001-0.0001
Hf, Fe, Ti	Al, Cu, Mg	Si	Mn

Quantitative Analysis: Carbon-21.25 ± 1.0 w/o (Battelle)
Phases Identified by X-ray: ZrC, graphite
Metallographic Description: Long needles of primary graphite (50-150 mils long by 1.2-1.8 mils diam.) in a eutectic matrix.
Radiographic Analysis: Most billets with gas bubbles and voids, some with center-line core-type flaw (Battelle)
Bulk Density: 5.41 ± 0.1 gms/cm^3

MATERIAL: JTA, CODE (D-13)

SUPPLIER: Union Carbide Corp., Carbon Products Division, New York, New York

Qualitative Analysis (Range w/o)
(Jarrell-Ash Co., Waltham, Mass.)

>10	0.1-0.01	0.01-0.001	0.001-0.0001	<0.0001
Zr, B, Si	Ba, Ca, Co, Fe, Mo, Hf, Ti	Al, Mg, Mn, V	Cr, Cu, Ni	Ag

Quantitative Analysis (ManLabs, Inc.)

Element	w/o
C	47.9
Si	8.1
Zr	30.2
B	8.2

Phases Identified by X-ray: Graphite, ZrB_2, α-SiC
Metallographic Description: White ZrB_2 particles and grey SiC particles embedded in a graphite matrix.
Bulk Density: 3.00 ± 0.04 gms/cm^3 (varies with billets)

MATERIAL: KT-Silicon Carbide, CODE (E-14)

SUPPLIER: Carborundum Co., Niagara Falls, New York

Qualitative Analysis (Range w/o)
(Jarrell-Ash Co., Waltham, Mass.)

1.0-0.1	0.1-0.01	0.01-0.001	0.001-0.0001
Fe	Al, B, Ca, Cr, Mn, Ti	Ba, Cu, Mg, Ni, Pb, V	Ag, Bi, Na, Sn

Quantitative Analysis (ManLabs, Inc.)

Element	w/o
Si	72.5
C	26.9

Fe, Al, Ti and Cr amount to approximately 1% of remainder.

Phases Identified by X-ray: α-SiC(II), Si, graphite
Metallographic Description: Irregularly shaped SiC grains with considerable amounts of free silicon and small amounts of graphite randomly interspersed.
Bulk Density: 3.10 gms/cm^3

MATERIAL: JT0992, CODE (F-15)

SUPPLIER: Union Carbide Corp., Carbon Products Division, New York, New York

Qualitative Analysis (Range w/o)
(Jarrell-Ash Co., Waltham, Mass.)

>10	1.0-0.1	0.1-0.01	0.01-0.001	0.001-0.0001	<0.0001
Hf, Si	Ti	Al, B, Ca, Mn	Co, Cr, Cu, Fe, Zr	Mg, Mo, Ni, Sn, V	Ag

Quantitative Analysis (ManLabs, Inc.)

Element	w/o
Si	11.1
Hf	53.8
C	31.9

Phases Identified by X-ray: Graphite, HfC, SiC
Metallographic Description: Similar to JTA (D-13), HfC and SiC particles embedded in a graphite matrix
Bulk Density: 4.63 gms/cm^3

TABLE 8

SUMMARY OF DATA ON HYPEREUTECTIC CARBIDES HfC + C(C-11) AND ZrC + C(C-12) SUPPLIED BY BATTELLE MEMORIAL INSTITUTE

Material (Code)	Billet No.	Diameter (inches)	Length (inches)	Weight (grams)	Density* (gms/cm^3)	Composition by Density (wt % C)
HfC+C(C-11)	1400A	1.001	4.004	466.5	9.063	14.40
	1400B	1.000	4.006	467.7	9.085	14.30
	1402A	1.004	4.004	470.7	9.159	14.05
	1402B	1.001	4.001	470.2	9.149	14.10
	1402C	1.001	4.005	470.9	9.146	14.10
	1403A	1.001	4.004	465.5	9.059	14.40
	1415A	1.000	3.985	453.3	8.833	15.10
	1415B	1.000	4.009	450.3	8.724	15.50
	1415C	1.000	4.005	446.9	8.692	15.60
	1416A	1.000	4.004	466.9	9.081	14.35
	1416B	1.001	3.996	467.0	9.100	14.25
	1416C	1.001	4.008	469.5	9.096	14.25
	1422A	1.001	4.005	478.2	9.322	13.60
					9.04 Average	14.40 Average
ZrC+C(C-12)	1405A	0.999	4.008	284.0	5.523	20.25
	1419A	1.000	4.006	283.0	5.504	20.50
	1419B	1.003	4.006	280.4	5.453	21.00
	1420A	0.999	3.909	272.5	5.341	22.10
	1467A	1.000	4.008	275.5	5.349	22.00
	1467B	1.012	4.002	281.5	5.362	21.90
	1467C	1.016	4.007	282.4	5.358	21.90
					5.41 Average	21.25 Average

*By immersion techniques.

TABLE 9

CHARACTERIZATION OF TEST MATERIALS

MATERIAL: JT-PT, CODE (F-1)

SUPPLIER: RTD, Dayton, Ohio

(Processed by Union Carbide Corp.*, June 1966)

As Charged Composition*	ManLabs Analysis
30.9 w/o Graphite cloth	C = 53.4 w/o
15.4 w/o G-7 resin	B = 5.8 w/o
11.4 w/o 175° M. P. pitch	Si = 8.2 w/o
34.6 w/o Si	Zr = 30.3 w/o

Qualitative Spectrographic Analysis (MIT)

1.0 - 0.1	0.1 - 0.01
Cr, Al	Ca, Cu, Mn

X-ray Analysis: Graphite, ZrB_2, ZrC, β SiC

Bulk Density: 1.65 ± .10 g/cm^3

Metallographic Description: Discrete white particles in a graphite matrix. Polishing results in substantially more relief between the graphite and the particles than encountered in JTA, JT0981 or JT0992.

*P.G. Lafyatis and M.S. Carter "Exploratory Development of Graphite Materials" AFML-TR-65-324, June 1966.

TABLE 10

CHARACTERIZATION OF TEST MATERIALS

MATERIAL: JT0961, CODE (F-16)

SUPPLIER: Union Carbide Corp., Carbon Products Division, New York, New York

Qualitative Analysis (Range w/o)
(Jarrell-Ash Co., Waltham, Mass.)

>10	1.0-0.1	0.1-0.01	0.01-0.001	0.001-0.0001
Si, Zr	Ti, Hf	B, Ba, Ca	Al, Cr, Fe, Mn, Sn, V	Ag, Co, Cu, Mg, Ni

Quantitative Analysis (ManLabs, Inc.)

Element	w/o
Si	16.8
Zr	29.6
C	48.1

Phases Identified by X-ray: Graphite, SiC, ZrC
Metallographic Description: Similar to JTA(D-13) and JT0992 (F-15). ZrC and SiC particles embedded in a graphite matrix.
Bulk Density: 3.10 gms/cm^3

MATERIAL: WSi_2/W (WSi_2 Coating on W), CODE (G-18)

SUPPLIER: General Electric Co., Cleveland, Ohio (Type MK-W); TRW, Cleveland, Ohio (WSi_2 Coating)

Qualitative Analysis of MK-W (Range w/o)
(Jarrell-Ash Co., Waltham, Mass.)

0.01-0.001	0.001-0.0001	< 0.0001
Cu, Mg, Si	Al, B, Fe	Ag, Cr, Mn

Qualitative Analysis of Entire Sample (Range w/o)
(Kent Laboratories, Newton Falls, Mass.)

10-1.0	0.1-0.01	0.001-0.0001	< 0.0003
Si	Ca	Al, Cr, Cu, Fe, Zr	Mg, Mn, Ni

Quantitative Analysis of MK-W

Element	w/o (Source)
O	0.00053 (Luvak)
C	0.008 (MIT)

Phases Identified by X-ray: Tungsten (matrix), WSi_2 plus trace of W_5Si_3 (coating)
Metallographic Description: Typical hot-worked W structure, fine grained and uniform, grains elongated in one direction in transverse section. Coating quite uniform, thickness approximately 4.5 mils.
Bulk Density: 18.86 gms/cm^3 (W only)

MATERIAL: Sn-Al/Ta-W (Sn-Al-Mo coating on Ta-10%W), CODE (G-19)

SUPPLIER: National Research Division, Norton Co., Newton, Mass. (Ta-W); General Telephone and Electronics Corp., Hicksville, New York (Sn-Al coating)

Qualitative Analysis of Ta-W (Range w/o)
(Jarrell-Ash Co., Waltham, Mass.)

>10	0.01-0.001	0.001-0.0001	<0.0001
W	Cr, Nb, Zr	Cu, Fe, Mg, Mn, Na, Ni, Si	Ag, Al, B, Pb, Sn

Qualitative Analysis of Entire Sample (Range w/o)
(Kent Laboratories, Newton Falls, Mass.)

10-1.0	3.0-0.3	0.003-0.0003	0.001-0.0001	< 0.0003
W	Al, Mo, Sn	Cr, Cu, Fe	Ca, Mg, Mn, Ni, Si, Zr	Ag, Pb

Quantitative Analysis of Ta-W: W = 8.8 w/o (MIT)
Supplier Analysis of Ta-W: W = 10.4 w/o
Supplier Designation of Sn-Al Coating: Sn-27Al-6.9 Mo (R505F Coating)
Phases Identified by X-ray (coating): Complex pattern, β-Sn, Al, Al_3Ta present, plus other unidentified phases.
Metallographic Description: Very fine grained, worked structure, uniform and apparently single phase. Coating uniform, 6 mil outer layer and 2 mil diffusion zone.
Bulk Density: 17.08 gms/cm^3 (Ta-W only)

MATERIAL: SiO_2 + 68.5 w/o W, CODE (H-22)

SUPPLIER: Bjorksten Research Laboratories, Madison, Wisconsin

Supplier Analysis: Tungsten - 99.9%+ purity
Silica - 99.9%+ purity
Samples - 20 v/oW (68.5 w/oW)*
Quantitative Analysis: 69.3 w/oW (ManLabs, Inc.)
Phases Identified by X-ray: W(SiO_2 vitreous)
Electron Probe Microanalysis: Oxidized samples showed little or no inter-diffusion between W and SiO_2
Metallographic Description: Fine, approximately spherical, discrete particles of W embedded in a continuous SiO_2 matrix.
Bulk Density: >5.70 gms/cm^3

*Based on lineal analysis and density (20.5-21 v/o W observed).

TABLE 11

CHARACTERIZATION OF INFILTRATED TUNGSTEN COMPOSITES

MATERIAL: W + Zr + Cu, CODE (G-20)

SUPPLIER: Rocketdyne, Canoga Park, California

Supplier Analysis:	Porous powder metallurgical grade tungsten product 76% of theoretical density was infiltrated with Cu-75w/o Zr alloy. Composite density is 15.7 gms/cm^3 (97% of expected value) (2).
Quantitative Analysis:	16.5v/o Cu-Zr phase.*
Phase Identified by X-ray:	Tungsten plus a Cu-Zr compound, $CuZr_2$ or $CuZr_3$, no free Zr or Cu.
Metallographic Description:	Equiaxed grains of tungsten (approx. 15 micron grain size) with randomly interspersed regions of Cu-Zr phase.
Bulk Density:	15.81 gms/cm^3

MATERIAL: W + Ag(G-21)

SUPPLIER: Wah Chang Corp., Albany, Oregon

Quantitative Analysis:	19.4v/o Ag*.
Phases Identified by X-ray:	Tungsten and silver.
Metallographic Description:	Equiaxed grains of tungsten (approx. 10 micron grain size) with randomly interspersed regions of silver.
Bulk Density:	17.49 gms/cm^3.

*Based on lineal analysis..

TABLE 12

CHARACTERIZATION OF TEST MATERIALS

MATERIAL: SiO_2 + 60 w/oW, CODE (H-23)

SUPPLIER: General Electric Co., Willoughby, Ohio

Qualitative Analysis (Range w/o)
(Kent Laboratories, Newton Falls, Mass.)

0.1-0.01	0.01-0.001	0.003-0.0003	0.001-0.0001	<0.0003
Al, Fe, Ti	Ni	Mg, Mo, Zr	Ca, V	Ba, Cu

Quantitative Analysis:	60.3 w/oW (MIT) 61.1 w/oW (ManLabs, Inc.)*
Phases Identified by X-ray:	W(SiO_2 Vitreous)
Metallographic Description:	Fine W particles embedded in a continuous SiO_2 matrix, some agglomeration.
Bulk Density:	4.80 gms/cm^3

*Based on lineal analysis and density (15.2-18 v/oW observed).

MATERIAL: SiO_2 + 35 w/o W, CODE (H-24)

SUPPLIER: General Electric Co., Willoughby, Ohio

Qualitative Analysis (Range w/o)
(Kent Laboratories, Newton Falls, Mass.)

0.3-0.03	0.1-0.01	0.01-0.001	0.003-0.0003	0.001-0.0001	<0.0003
Al, Ti	Fe	Ni	Mg, Zr	Ca, Mo, V	Ba, Cu

Quantitative Analysis:	35.8 w/o W (MIT) 35.3 w/o W (ManLabs, Inc.)*
Phases Identified by X-ray:	W (SiO_2 vitreous)
Metallographic Description:	Fine W particles embedded in a continuous SiO_2 matrix, some agglomeration
Bulk Density:	3.20 gms/cm^3

*Based on linear analysis and density (5-6 v/o W observed).

MATERIAL: Hf-20Ta-2Mo, CODE (I-23)

SUPPLIER: Wah Chang Corp., Albany, Oregon

Qualitative Analysis (Range w/o)
(Jarrell-Ash Co., Waltham, Mass.)

>10	0.01-0.001	0.001-0.0001	<0.0001
Hf, Ta, Mo	Fe, Ti	Cu, Mn, Zr	Al, B, Cr, Mg, Si, Sn, Ag

Quantitative Analysis (MIT)

Element	w/o
Hf	79.4
Ta	19.6
Mo	1.4
O	0.0075 and 0.0078

Nominal Composition:	Hf-19.7Ta-2.15 Mo (2.6% Zr)
Phases Identified by X-ray:	α-Hf, β-Ta, α-Hf lines shifted, strongly preferred orientation (1" bar). β-Hf (a_o = 3.47 Å) (1/2" bar).
Metallographic Description: 1" Bar	Recrystallized structure of fine α-Hf-rich plates in β-Ta-rich matrix. Old grains large and clearly visible.
Metallographic Description: 1/2" Bar	Large β-Hf-Ta grains. Etchant causes a pattern of pitting reminiscent of the α-Hf-β-Ta platelet structure. In some regions a dendrite-like structure appears from staining by the etchant.
Bulk Density:	13.47 gms/cm^3 (1" bar) 13.48 gms/cm^3 (1/2" bar)

MATERIAL: Ir/Graphite (Iridium coating on Poco Graphite), CODE (I-24)

SUPPLIER: Battelle Memorial Institute, Columbus, Ohio

Phases Identified by X-ray:	Graphite (matrix), Ir (coating). In some cases coating contained α-Fe_2O_3 and looked rusted in appearance.
Coating Thickness (Battelle):	33 mils average on length of specimens with variations from 23.8-53.7 mils. 37.4 mils average on top diameter with variations from 29.5-51 mils.
Coating Weight (Battelle):	10.3 gms average
Radiographic Analysis:	Some inhomogeneities in coatings (such as thinning at junctions, cracks and spotty surface build up) in 7 out of 19 specimens.

TABLE 13

SUMMARY OF DATA ON Ir/GRAPHITE (I-24) SUPPLIED BY BATTELLE MEMORIAL INSTITUTE

Specimen No.	Parameters before Coating of Poco Graphite (B-10)			Parameters after Coating and Bonding			Coating Parameters		
	length (inches)	diameter (inches)	weight (grams)	length (inches)	diameter (inches)	weight (grams)	thickness (length/diam)		weight
2	0.9704	0.4858	5.3261	1.0175	0.5221	16.2297	0.0471	0.0363	10.9036
3	0.9695	0.4859	5.3033	0.9955	0.5198	14.9326	0.0300	0.0339	9.6301
4	0.9704	0.4852	5.2716	0.9986	0.5191	14.5108	0.0282	0.0339	9.2392
6	0.9699	0.4851	5.2902	1.0025	0.5344	18.9378	0.0326	0.0493	13.6476
9	0.9693	0.4851	5.0921	1.0027	0.5206	14.8195	0.0334	0.0355	9.7274
10	0.9687	0.4851	5.0180	1.0014	0.5209	15.2073	0.0327	0.0358	10.1893
11	0.9707	0.4850	5.0414	1.0013	0.5250	15.5233	0.0306	0.0400	10.4819
12	0.9699	0.4860	5.2064	------	------	-------	------	------	-------
13	0.9703	0.4853	5.0511	0.9992	0.5234	14.5677	0.0289	0.0381	9.5166
16	0.9707	0.4851	5.1561	1.0004	0.5212	14.8760	0.0297	0.0361	9.7166
17	0.9710	0.4854	5.0307	1.0025	0.5208	14.5865	0.0315	0.0354	9.5558
18	0.9702	0.4854	5.0121	1.0024	0.5215	15.4184	0.0312	0.0361	10.4063
19	0.9695	0.4856	5.0918	1.0028	0.5199	14.9219	0.0333	0.0343	9.8300
22	0.9706	0.4860	5.1442	0.9965	0.5255	15.8383	0.0259	0.0395	10.6941
23	0.9798	0.4860	5.2344	1.0036	0.5370	17.2547	0.0238	0.0510	12.0203
24	0.9695	0.4852	5.1076	1.0022	0.5202	14.6589	0.0327	0.0350	9.55[illegible]3
25	0.9708	0.4856	5.2280	1.0029	0.5151	13.7218	0.0321	0.0295	8.4938
27	0.9696	0.4855	5.2553	1.0071	0.5215	14.8181	0.0375	0.0360	9.5628
29	0.9699	0.4852	5.3068	1.0017	0.5265	17.0008	0.0318	0.0413	11.6940
30	0.9697	0.4850	5.2076	1.0234	0.5178	16.0019	0.0537	0.0328	10.7943
						Averages -	0.0330	0.0374	10.2978

TABLE 14

SUMMARY OF DATA ON Ir/GRAPHITE(I-24) SUPPLIED BY GENERAL TECHNOLOGIES CORP.

Specimen No.	Coating Thickness (mils)	Finished Diameter (in.)	Visual Inspection	Eddy Current Thickness (mils)
1	4.7	.512	1 tree pit	5.55
2	4.4	.511	2 tree pits	5.15
3	3.5	.509	no defects	4.95
4	3.8	.510	no defects, treed	5.65
5*	4.8	.512		<2.00
6	3.6	.510	1 tree pit	2.75
7	4.9	.512	no defects	5.10
8*	3.8	.513		3.40
9	3.2	.509	3 tree pits	5.40
10	6.5	.515	excellent	5.20
11	3.9	.508	excellent	3.05
12*	1.3	.506		<2.00
13	4.3	.512	excellent	4.05
14	4.6	.511	excellent	4.60
15	4.1	.510	excellent	4.20
16	3.8	.508	no defects, treed	5.60
17*	3.1	.508		3.8
18*	2.3	.509		<2.00
35*	3.4	.509		3.05
46	5.7	.513		6.05
61*	---	.508		<2.00
66	8.0	.518	excellent	6.00
69*	---	.520		4.85
71*	1.3	.509		<2.00
73*	0.8	.506		<2.00
75	2.7	.507	excellent	3.70
76	---	----	no defects, treed	<2.00

*Samples considered rejects but supplied for evaluation.

TABLE 15

SUMMARY OF NONDESTRUCTIVE TEST RESULTS ON ZrB_2 (A-3)

Specimen Number	V_L inches/microsec	Density gms/cm^3	Per Cent IACS Top	Per Cent IACS Bottom
A-3-1	0.342	5.52	18.8	19.8
A-3-2	0.346	5.56	19.6	19.6
A-3-3	0.345	5.59	19.6	19.4
A-3-4	0.348	5.65	19.3	19.8
A-3-5	0.346	5.59	19.3	19.0
A-3-6	0.345	5.64	19.6	20.0
A-3-7	0.345	5.60	19.6	19.4
A-3-8	0.346	5.63	19.7	20.0
A-3-9	0.347	5.65	18.8	19.6
A-3-10	0.345	5.57	19.5	19.6
A-3-11	0.347	5.48	19.2	19.4
A-3-12	0.346	5.61	19.7	20.2
A-3-13	0.343	5.62	19.5	19.8
A-3-14	0.342	5.62	19.8	19.7
A-3-15	0.339	5.56	19.1	19.4
A-3-16	0.340	5.57	19.0	19.5
A-3-17	0.343	5.64	19.5	19.6
A-3-18	0.342	5.61	18.8	18.9
A-3-19	0.343	5.62	19.3	19.1
A-3-20	0.339	5.59	19.0	19.3
A-3-21	0.347	5.68	19.7	20.0
A-3-22	0.346	5.75	19.5	20.0
A-3-23	0.350	5.64	19.7	19.7
A-3-24	0.346	5.60	19.2	19.7
A-3-25	0.343	5.56	19.3	19.1
A-3-26	0.344	5.67	19.5	19.6
A-3-27	0.344	5.58	19.0	18.8
A-3-28	0.343	5.61	19.3	19.3
A-3-29	0.344	5.56	19.5	18.9
A-3-30	0.345	5.60	19.3	18.2

TABLE 16

RESULTS FOR $HfB_{2.1}$ (A-2) SPECIMENS FROM NDT EVALUATION

Specimen[1] Designation	Longitudinal Velocity[2] (inches/microsecond) Axial Direction	Radial Direction	Relative Eddy Current 60 KHz[3] Top	Bottom	500 KHz[3] Top	Bottom	8MHz[4] Top	Bottom
(A-2) - 1	0.265	0.303	15.4	Counter Bored	10	Counter Bored	6	Counter Bored
- 2	0.264	0.303	15.1		10		8	
- 3	0.263	0.301	14.8		10		8	
- 4	0.265	0.309	14.8		10		8	
- 5	0.263	0.303	15.2		10		6	
- 6	0.264	0.305	15.0		10		6	
- 7	0.263	0.305	15.2		10		6	
- 8	0.265	0.303	15.2		10		6	
- 9	0.265	0.309	14.7		10		10	
-10	0.265	0.307	15.4		10		6	
-11	0.264	0.307	15.4		10		8	
-12	0.264	0.307	15.0		10		6	
-13	0.263	0.301	15.2	15.4	10	10	8	8
-14	0.263	0.299	13.6	15.2	10	10	10	8
-15	0.263	0.303	15.2	14.7	10	10	10	10
-16	0.263	0.299	15.2	15.2	10	10	10	6
-17	0.259	0.294	15.2	14.9	10	10	6	10
-18	0.265	0.301	15.2	15.3	10	10	6	6
-19	0.265	0.302	15.0	15.3	14	10	>100	10
-20	0.264	0.299	14.8	15.0	10	10	10	8
-21	0.268	0.311	14.6	15.1	19[5]	18	80	44
-22	0.265	0.305	15.4	15.2	10	10	6	6
-23	0.264	0.305	15.2	15.1	10	10	8	10
-24	0.265	0.301	15.0	12.8	10	18	10	16
Average	0.264	0.303	15.0	14.9	10	11	11[6]	12
Maximum	0.268	0.311	15.4	15.4	19	18	>100	44
Minimum	0.259	0.294	14.6	12.8	10	10	6	6
Range	3.6%	5.5%						

1. End surfaces not flat and parallel.
2. Velocity technique: through transmission; equipment = Arenberg PG 650-C high voltage pulsed oscillator, General Radio power amplifier (20 KHz 1.5 MHz), Tektronix 545A scope; frequency 1.0 MHz; accuracy = 1.0 per cent, precision better than 1 per cent.
3. Eddy current technique for 60 KHz: equipment = Magnatest FM-100; precision better than 3 per cent (± 0.4).
4. Eddy current technique for 500 KHz and 8MHz: equipment = Boonton Metal Film Gauge Type 255A; precision better than 20 per cent (± 1).
5. Surface not machined.
6. Excluding the point >100.

TABLE 16 (CONT)

RESULTS FOR $HfB_{2.1}$ (A-2) SPECIMENS FROM NDT EVALUATION

X-rays[7]	Dye Penetrant[9]	Visual Inspection[10]	Specimen Designation
All specimens exhibit low density regions extending radially from the axis at the specimen's midsection[8].	Porous band around center of cylinders	No cracks. Edges are chipped.	(A-2) - 1
	Porous band around center of cylinders	No cracks. Edges are chipped.	- 2
	Porous band around center of cylinders	No cracks. Edges are chipped.	- 3
	Crack along bottom edge approx. 1/4" long. No porous band.	No cracks. Edges are chipped.	- 4
	Two small cracks along bottom edge. Porous band around center of cylinder.	No cracks. Edges are chipped.	- 5
	Crack at top approx. 1/5" long. Porous band around center.	Crack approx 1/8" long at top near chip. Edges are chipped.	- 6
	Porous band around center.	No cracks. Edges are chipped.	- 7
	Porous band around center.	No cracks. Edges are chipped.	- 8
	Shallow crack at top. No porous band.	Shallow crack at top. Edges chipped.	- 9
	Porous band around center.	No cracks. Edges are chipped.	-10
	Small crack at top edge. Porous band around center.	No cracks. Edges are chipped.	-11
	Crack along bottom edge approx. 1/4" long. Porous band around center.	No cracks. Edges are chipped.	-12
	Porous band around center.	No cracks. Edges are chipped.	-13
	Several shallow cracks. Porous band.	Several shallow cracks. Edges chipped.	-14
	Several shallow cracks. Porous band.	Several shallow cracks. Metallic (copper?) part. on cylinder surface.	-15
	Porous band around center.	Several shallow cracks. Edges chipped.	-16
	Porous band around center.	No cracks. Edges are chipped.	-17
	Porous band around center.	No cracks. Edges are chipped.	-18
	Porous band around center.	No cracks. Edges are chipped.	-19
	Porous band around center.	No cracks. Edges chipped	-20
	Shallow crack. No porous band.	No cracks. Edges chipped	-21
	Porous band around center.	No cracks. Edges chipped	-22
	Porous band around center.	Shallow crack. Edges chipped	-24

7. X-ray radiographic technique: 1 Mevp, TFD = 36", Eastman Type M film; 3 exposures for each specimen (2 radial at 0° and 90° and 1 axial).
8. Low density regions are attributed to pressing technique.
9. Dye penetrant technique: post emulsification using Zygloe ZL-22.
10. Visual inspection employed 40X microscope. Anomalies indelibly marked on specimens.

TABLE 17

RESULTS FOR JTA (D-13) SPECIMENS FROM NDT EVALUATION

Specimen[1] Designation D-13 Billet No. Sample No.	Longitudinal Vel.[2] (inches/microsecond) Axial Direction	Radial Direction	Relative Eddy Current[3] 500 KHz[4] Top	Bottom	X-ray[5]	Alcohol Wipe	Visual Inspection[6]
5/E/17/2-1	0.134	0.199	56	Counter Bored	No Defects Observed	No Cracks Observed	
5/E/17-2-2	0.129	0.208	44				
5/E/17-2-3	0.125	0.202	44				Scratches on end surface
5/E/17-2-4	0.123	0.199	60				Chip along inner diam.
5/E/17-2-5	0.126	0.202	44				Flat spot-some scratches
5/E/17-2-6	0.129	0.214	42				Discoloration along inner edge
5/ /17-2-7	0.128	0.200	58				Scratches on end surface
5/E/17-2-8	0.127	0.189	62				Discoloration along inner edge
5/E/17-2-9	0.121	0.185	70				Chips-1 end
5/E/17-2-10	0.123	0.191	68				
Average	0.127	0.199	55				
Maximum	0.134	0.214	70				
Minimum	0.121	0.185	42				
Range	10%	13.6%					

1. End surfaces not flat and parallel. Surface contact poor. Ends slightly sanded to facilitate measurements.
2. Velocity technique: same as used for $HfB_{2.1}$.
3. Testing not possible at 60 KHz. Conductivity outside range of test instrument.
4. Eddy current technique for 500 KHz: same as used for $HfB_{2.1}$; precision = $\pm$ 1 unit.
5. X-ray radiographic technique: 120 kvp, 10 mA for 2 minutes, TFD = 60", Eastman Type T (between A and M) film and 5 mil lead screens.
6. Visual inspection employed using 40X microscope.

TABLE 18

RESULTS FOR JT0981 (F-16) SPECIMENS FROM NDT EVALUATION

Specimen[1] Designation F-16 Billet No. Sample No.	Longitudinal Vel.[2] (inches/microsecond) Axial Direction	Radial Direction	Relative Eddy Current 500 KHz[4] Top	Bottom	X-rays[5]	Alcohol Wipe	Visual Inspection[6]
5/F/2/1-1	0.130	0.210	62	Counter Bored	No Defects Observed	No Cracks Observed	Flat spot along outside wall
5/F/2/1-2	0.135	0.211	54				Flat spot along outside wall
5/F/2/1-3	0.142	0.222	52				Scratching on end surface
5/F/2/1-4	0.143	0.231	50				Scratching on end surface
5/F/2/1-5	0.138	0.226	52				Scratching on end surface
5/F/2/1-6	0.140	0.214	60				Scratches on end surface
5/F/2/1-7	0.141	0.218	56				Small chip end surface
5/F/2/1-8	0.139	0.214	56				
5/F/2/1-9	0.139	0.0220	50				Small chip end surface
5/F/2/1-10	0.139	0.220	56				Small chip end surface
5/F/2/1-11	0.130	0.207	60				Small chip end surface
Average	0.138	0.218	55				
Maximum	0.143	0.231	62				
Minimum	0.130	0.207	50				
Range	9%	10.4%					

1. End surfaces not flat and parallel. Surface contact poor. Ends slightly sanded to aid measurements.
2. Velocity technique: same as used for $HfB_{2.1}$.
3. Testing not possible at 60 KHz. Conductivity outside range of test instrument.
4. Eddy current technique for 500 KHz: same as used for $HfB_{2.1}$; precision = $\pm$ 1 unit.
5. X-ray radiographic technique: 120 Kvp, 10 mA for 2 minutes, TFD = 60", Eastman Type T (between A and M) film and 5 mil lead screens.
6. Visual inspection . mployed 40X microscope.

TABLE 19

NONDESTRUCTIVE TESTS OF WAVE SUPERHEATER MODELS

Sample Code ManLabs No. /CAL No.	Run Number Sting Number	Comments
ZrB_2 (A-3)-1-2	67-473- 1	Edges of bore are chipped
KTSiC (E-14)-1-8	2	No Imperfections
KTSiC (E-14)-3-18	3	No Imperfections
Hf-Ta-Mo (I-23)-4-19	4	No Imperfections
W (G-18) Uncoated-X-11	5	No Imperfections
RVA (B-5)-X-5	6	Large pit and porous area in hemispherical cap
JTA (D-13)-X-7	7	Contained high density flecks through volume
JT0992 (F-15)-X-9	8	Contained high density flecks through volume
Hf-Ta-Mo (I-23)-1-12	67-474- 1	Tool marks on wall
$HfB_{2.1}$ (A-2)-X-1	2	Edges of bars are chipped
HfB_2 + SiC (A-4)-X-4	3	Edges of bore are chipped
PG (B-6)-X-6*	4	Large pit and porous area on wall
BPG (B-7)-X-16*	5	Surface porosity, chipped base
JT0981 (F-16)-X-10	6	Contained high density flecks through volume
ZrB_2 (A-3)-24-3	7	Contained two high density flecks 300 mils from nose and one fleck 700 mils from nose. Edges of bore are chipped.
Sn-Al/Ta-10W (G-19)-3-22	8	No Imperfections
Hf-Ta-Mo (I-23)-2-0	No Test	No Imperfections
Hf-Ta-Mo (I-23)-3-0	No Test	Contained 40 mil diameter low density region in front face
KT SiC (E-14)-4-0	No Test	No Imperfections
KT SiC (E-14)-2-0	No Test	No Imperfections

*"C" axis perpendicular to cylinder axis.

TABLE 20

INTERNAL FEATURES OF WAVE SUPERHEATER MODELS

DISCLOSED BY RADIOGRAPHY

Sample Code ManLabs No/CAL No.	Diameter/Length/Wall Thickness (mils) (mils)	Comments
ZrB_2(A-3)-1-2	492/1021/139	Twenty-five mil protrusion on inner wall of front face
KTSiC (E-14)-1-8	488/1000/135	Counter bore 1/8" diameter 1/16" deep
KT SiC (E-14)-3-18	944/994/130	Inside of front cap is stepped
Hf-Ta-Mo (I-23)-4-19	997/1167/129	No defects
W(G-8) Uncoated-X-11	491/992/152	Twenty-five mil protrusion on inner wall of front face
RVA (B-5)-X-5	488/996/112	No defects
JTA (B-13)-X-7	489/957/125	No defects
JT0992 (F-15)-X-9	490/945/96	No defects
Hf-Ta-Mo (I-23)-1-12	491/1000/155	No defects
$HfB_{2.1}$ (A-2)-X-1	491/937/144	Fifteen mil protrusion on inner wall of front face
HfB_2 + SiC (A-4)-X-4	492/963/154	Twenty-five mil protrusion inner wall of front face
PG (B-6)-X-6 **	488/1061/122	No defects
BPG (B-7)-X-16**	490/836/157	No defects
JT0981 (F-16)-X-10	488/946/141	No defects
ZrB_2 (A-3)-24-3	492/989/163	Fifty mil protrusion on inner wall of front face
Sn-Al/Ta-10W(G-19)-3-22	1001/1001/146	No defects
Hf-Ta-Mo (I-23)-2-0*	1001/1062/122	No defects
Hf-Ta-Mo (I-23)-3-0*	503/943/110	No defects
KT SiC (E-14)-4-0*	491/1004/336	Core drill islands at base of hole
KT SiC (E-14)-2-0*	972/959/164	Core drill islands at base of hole

*All samples were hemispherical caps except those noted by asterisk. The latter were flat faced cylinders.

**"C" axis perpendicular to cylinder axis.

TABLE 21

RESULTS OF ACOUSTIC VELOCITY AND EDDY CURRENT MEASUREMENTS FOR BORIDE AND BORIDE COMPOSITE HIGH FLUX CYLINDERS

ACOUSTIC VELOCITY MEASUREMENTS

Material (Code)	Longitudinal Wave Velocity at 1.0MHz (in/μ sec) axial	radial	Transverse Wave Velocity (in/μ sec) axial at 1.0MHz	axial at 2.25MHz	Attenuation dB/in 5.0 MHz	15.0 MHz
HfB_2, 1(A-2)						
HF-1	0.272	0.286	0.1785	0.1785	2.10	10.29
-2	0.268	0.282	0.1785	0.1785	2.12	8.21
-3	0.268	0.284	0.1765	0.1785	2.80	13.06
-4	0.272	0.286	0.1785	0.1785	2.72	8.45
Average	0.270	0.284	0.1777	0.1785	----	-----
Maximum	0.272	0.286	0.1785	0.1785	----	-----
Minimum	0.268	0.282	0.1765	0.1785	----	-----
Range	1.5%	1.4%	1.1%	------	----	-----
ZrB_2(A-3)						
HF-5	0.354	0.374	0.234	0.234	2.57	1.33
-6	0.357	0.377	0.238	0.234	2.91	1.37
-7	0.357	0.377	0.238	0.234	2.73	0.93
-8	0.354	0.371	0.234	0.234	2.37	0.89
Average	0.355	0.375	0.236	0.234	----	-----
Maximum	0.357	0.377	0.238	0.234	----	-----
Minimum	0.354	0.371	0.234	0.234	----	-----
Range	0.84%	1.6%	1.7%	-----	----	-----
Boride Z(A-5)						
HF-9	0.357	0.384	0.234	0.238	1.71	2.35
-10	0.357	0.380	0.238	0.238	0.263	1.43
-11	0.350	0.380	0.238	0.238	2.37	4.57
-12	0.357	0.380	0.238	0.238	1.37	2.66
Average	0.355	0.381	0.237	0.238	----	-----
Maximum	0.357	0.384	0.238	0.238	----	-----
Minimum	0.350	0.380	0.234	0.238	----	-----
Range	1.9%	1.0%	1.7%	-----	----	-----

ACOUSTIC VELOCITY MEASUREMENTS

Material (Code)	Longitudinal Wave Velocity at 1.0 MHz (in/μ sec) axial	radial	Transverse Wave Velocity (in/μ sec) axial at 1.0MHz	axial at 2.25MHz	Attenuation dB/in 5.0 MHz	15.0 MHz
ZrB_2 (A-3)						
HF -13	0.345	0.371	0.231	0.234	0.811	1.36
-14	0.351	0.374	0.234	0.234	0.91	0.421
-15	0.345	0.371	0.231	0.235	1.65	0.985
-16	0.345	0.371	0.231	0.234	1.76	0.718
Average	0.347	0.372	0.232	0.234	----	-----
Maximum	0.351	0.374	0.234	0.235	----	-----
Minimum	0.345	0.371	0.231	0.234	----	-----
Range	0.7%	0.8%	1.3%	-----	----	-----
ZrB_2*						
HF -17	0.360	0.380	0.230	0.234	3.33	1.33
HfB_2 + SiC (A-7)						
HF -18	0.291	0.302	0.184	0.189	6.19	3.12
-19	0.291	0.302	0.184	0.189	5.50	5.50
HfB_2 (A-6)						
HF -20	0.271	0.280	0.1735	0.1755	2.58	4.87
-21	0.269	0.279	0.1735	0.1755	1.08	2.62
ZrB_2*						
HF -22	0.353	0.370	0.211	0.232	2.56	1.08
ZrB_2 + SiC (A-8)						
HF -23	0.384	0.400	0.235	0.246	2.68	1.17
-24	0.384	0.400	0.241	0.254	1.67	1.67

*ManLabs-Avco material.

EDDY CURRENT RESPONSE

% IACS

Material (Code)	f = 60 KHz top	bottom	f = 500 KHz top	bottom	f = 8 MHz top	bottom
HfB_2, 1(A-2)						
HF-1	14.6	14.3	46	46	56	52
-2	15.4	15.8	46	46	56	56
-3	15.4	15.3	46	46	56	54
-4	14.4	14.2	46	46	54	52
Average	14.9	14.9	--	--	55	53
Maximum	15.4	15.8	--	--	56	56
Minimum	14.4	14.2	--	--	54	52
Range	6.9%	6.2%	--	--	3.6%	7.2%
ZrB_2(A-3)						
HF-5	23.1	21.75	52	50	64	62
-6	22.9	21.7	52	50	64	62
-7	22.75	22.8	52	50	62	62
-8	23.1	22.1	52	50	64	60
Average	22.9	22.1	--	--	63	61
Maximum	23.1	22.8	--	--	64	62
Minimum	22.75	21.7	--	--	62	60
Range	1.1%	4.8%	--	--	3.1%	3.3%
Boride Z(A-5)						
HF-9	1.76	2.19	22	8	64	44
-10	1.79	2.15	20	8	56	46
-11	2.52	2.17	2	10	28	46
-12	1.77	2.17	20	10	52	48
Average	1.96	2.17	16	9	50	46
Maximum	2.52	2.19	22	10	64	48
Minimum	1.76	2.15	2	8	28	44
Range	30%	1.8%	--	--	--	--

EDDY CURRENT RESPONSE

% IACS

Material (Code)	f = 60 KHz top	bottom	f = 500 KHz top	bottom	f = 8 MHz top	bottom
ZrB_2 (A-3)						
HF-13	19.8	22.15	50	50	60	62
-14	20.25	22.25	50	50	60	62
-15	19.7	22.1	50	50	60	62
-16	19.7	22.1	50	50	60	62
Average	19.9	22.15	--	--	--	--
Maximum	20.25	22.25	--	--	--	--
Minimum	19.7	22.1	--	--	--	--
Range	2.7%	0.6%	--	--	--	--
ZrB_2*						
HF-17	21.3	21.6	50	52	62	60
HfB_2 + SiC(A-7)						
HF-18	15.3	16.0	46	48	54	56
-19	15.6	16.1	48	48	54	54
HfB_2 (A-6)						
HF-20	22.75	23.8	52	50	62	62
-21	23.1	23.9	52	50	62	62
ZrB_2*						
HF-22	21.75	22.1	50	50	62	60
ZrB_2 + SiC(A-8)						
HF-23	16.1	16.2	48	48	54	54
-24	15.6	14.8	48	48	56	54

*ManLabs-Avco material.

TABLE 22

RESULTS OF VISUAL, DYE PENETRANT AND RADIOGRAPHIC INSPECTIONS FOR HYPEREUTECTIC CARBIDE BILLETS AND HIGH FLUX CYLINDERS

HYPEREUTECTIC CARBIDE BILLETS

Material (Code)	Billet No.	Visual Inspection of Surface	Radiographic Inspection*
HfC + C (C-11)	1400A	Small voids	Internal gas holes
	1400B	Good	No internal voids
	1402A	Slight flaws	Small pipe 1/2" long
	1402B	Bubbles, voids	No internal voids
	1402C	Good	Small pipe 1/2" long
	1403A	Small voids	Small pipe 1/4" long
	1415A	Hole on end	Small gas hole near end
	1415B	Voids	Possible gas holes
	1415C	Bubbles, voids	Possible gas holes
	1416A	Slight flaws	Possible gas holes
	1416B	Voids	No internal voids
	1416C	Good	Possible gas holes
	1422A	Good	No internal voids
ZrC + C (C-12)	1405A	Small voids	Possible gas holes
	1419A	Small voids	Small pipe
	1419B	Small voids	Possible gas holes
	1420A	Small voids	No internal voids
	1467A	Small voids	Internal pipe
	1467B	Holes	No internal voids
	1467C	Small voids	No internal voids

*Radiographs supplied by Battelle Memorial Institute.

Ir/GRAPHITE (I-24) SPECIMENS

Specimen No.	Fluorescent Penetrant	Radiography*
2	Porous side wall	Low density (thin coating) at junction of front face.
3		Low density at junction of front face.
4		Low density at junction of front face.
6	Scale on front	Unusually thick coating.
9		No significant indications.
10		No significant indications.
11		No significant indications.
13	Crack on side wall	Crack at bottom of side wall extending into sting hole.
16	Heavy porosity at junction of front face and side wall	No significant indications.
17		No significant indications.
18	Crack in coating	Surface crack in coating, substrate appears exposed.
19		No significant indications.
22		Heavier coating.
23		Much heavier coating.
24		No significant indications.
25		Spotty surface build-up of coating.
27	Scale and porous spots on side wall	Spotty surface build-up of coating.
29	Extreme porosity throughout specimen	Heavier coating.
30		No significant indications.

*All specimens exhibit porosity at junction of front face and side wall.

VISUAL AND FLUORESCENT PENETRANT TESTS

Material (Code)	Visual 40X	Fluorescent Penetrant Before Testing	Fluorescent Penetrant After Testing
$HfB_{2.1}$ (A-2)			
HF -1	chipped edges	no cracks	large cracks
-2	chipped edges	no cracks	fine cracks
-3	chipped edges	no cracks	
-4	chipped edges	no cracks	
ZrB_2 (A-3)			
HF -5	chipped edges	no cracks	not tested
-6	chipped edges	no cracks	not tested
-7	chipped edges	no cracks	not tested
-8	chipped edges	no cracks	not tested
Boride Z (A-5)			
HF -9	1/8" crack on face, chipped edge	1/8 crack on face	
-10	chipped edges	no cracks	
-11	chipped edges	no cracks	not tested
-12	1/2" large chip	no cracks	not tested
ZrB_2 (A-3)			
HF -13	chipped edges	no cracks	not tested
-14	chipped edges	no cracks	not tested
-15	chipped edges	no cracks	not tested
-16	chipped edges	no cracks	
ZrB_2*			
HF -17	chipped edges, microcracks	microcracks at edge	fine cracks
HfB_2+SiC (A-7)			
HF -18	chipped edges	no cracks	fine cracks
-19	chipped edges	no cracks	not tested
HfB_2(A-6)			
HF -20	chipped edges, microcracks	cracks at both faces	not tested
-21	chipped edges	no cracks	fine cracks
ZrB_2*			
HF -22	chipped edges	no cracks	not tested
ZrB_2+SiC (A-8)			
HF -23	chipped edges	no cracks	not tested
-24	chipped edges	no cracks	
HfB_2+SiC (A-4)			
HF -25		porous band	not tested
-26		porous band	not tested
-27		porous band	no cracks
-28		porous band	no cracks
HfB_2 + SiC (A-7)			
HF -29		no cracks	
-30		no cracks	
-31		no cracks	
-32			no cracks
-33			cracked
-34			no cracks
HfB_2 + SiC (A-4)			
HF -35			fine cracks
-36			large crack
-37			no cracks
-38			large crack

*ManLabs-Avco material.

*ManLabs-Avco material.

TABLE 22 (CONT)

COMPILATION OF EDDY CURRENT MEASUREMENTS OF IRIDIUM COATINGS ON GRAPHITE (I-24) SUPPLIED BY BATTELLE MEMORIAL INSTITUTE

Sample No.	(% IACS)	Thickness (mils)	Predicted Thickness Based on Eddy Current Measurement (mils)	Comments
Calibration				
A	(9.0)	10 (measured)	--	--
B	(24.0)	20 (measured)	--	--
C	(31.0)	30 (measured)	--	--
2**	(14.0)	24 (estimated)*	14	--
3**	(21.0)	15 (estimated)	17	--
4	(23.0)	14 (estimated)	18	--
6**	(----)	16 (estimated)	--	--
11	(18.0)	16 (estimated)	15	Exposed 11M
16**	(25.5)	14 (estimated)	21	Exposed 16M
17	(24.0)	16 (estimated)	20	Exposed 17R
18	(24.0)	16 (estimated)	20	--
23	(24.0)	12 (estimated)	20	--
24	(14.0)	16 (estimated)	14	Exposed 24R
25	(18.5)	16 (estimated)	15	--
27	(23.0)	19 (estimated)	18	--
29	(20.0)	16 (estimated)	16	--
30	(24.0)	27 (estimated)	20	Exposed 3R

*Estimated from Table 13 on the assumption that coating thickness equals 1/2 length thickness.
**Denotes rough or irregular surface. Eddy current reading may be doubtful.

UNCLASSIFIED

Security Classification

DOCUMENT CONTROL DATA - R & D

(Security classification of title, body of abstract and indexing annotation must be entered when the overall report is classified)

1. ORIGINATING ACTIVITY (Corporate author) ManLabs, Inc. 21 Erie Street Cambridge, Massachusetts 02139	2a. REPORT SECURITY CLASSIFICATION UNCLASSIFIED 2b. GROUP N/A

3. REPORT TITLE

Stability Characterization of Refractory Materials Under High Velocity Atmospheric Flight Conditions - Part II-Volume I Facilities and Techniques Employed for Characterization of Candidate Materials

4. DESCRIPTIVE NOTES (Type of report and inclusive dates)

Technical Documentary Report, April 1966 to July 1969

5. AUTHOR(S) (First name, middle initial, last name)

Larry Kaufman and Harvey Nesor

6. REPORT DATE	7a. TOTAL NO. OF PAGES	7b. NO. OF REFS
December 1969	86	12

8a. CONTRACT OR GRANT NO. AF33(615)-3859 b. PROJECT NO. 7312 Task 731201 c. 7350 Tasks 735001 and 735002 d.	9a. ORIGINATOR'S REPORT NUMBER(S) N/A 9b. OTHER REPORT NO(S) (Any other numbers that may be assigned this report) AFML-TR-69-84, Part II-Volume I

10. DISTRIBUTION STATEMENT This document is subject to export controls and each transmittal to foreign governments or foreign nationals may be made only with prior approval of the Air Force Materials Laboratory (MAMC), Wright-Patterson Air Force Base, Ohio 45433

11. SUPPLEMENTARY NOTES	12. SPONSORING MILITARY ACTIVITY
N/A	Air Force Materials Laboratory (MAMC) Wright-Patterson Air Force Base Ohio 45433

13. ABSTRACT

This report describes the candidate materials which were obtained from commercial sources and represent state of the art materials. Available processing information is included. Characterization of materials was performed by qualitative spectrographic, wet chemical and vacuum (or inert gas) fusion, metallographic, X-ray, electron microprobe and pycnometric analysis. Standard analysis of refractory boride, carbide and silicide composites were employed.

Nondestructive testing of candidate materials included radiography, gamma radiometry, die penetrant inspection and measurement of ultrasonic velocity. Film radiography was used to detect the presence of voids, inclusions and local gross changes in composition. Radiometric density gauging used to measure local densities within each specimen and alcohol penetrant tests were employed to disclose tight surface cracks which are not visible at moderate magnifications.

The results of nondestructive testing of samples prior to arc plasma testing is reported. Test results are provided for a series of hemispherical shells of diboride composites. Graphite composites, silicon carbide and hafnium-tantalum alloy were also tested prior to exposure. In several instances, flaws which caused failures on exposure were detected by means of dye penetrant and radiographic techniques. The latter methods proved to be most effective of the NDT techniques employed in this study.

This abstract is subject to special export controls and each transmittal to foreign governments or foreign nationals may be made only with prior approval of the Air Force Materials Laboratory (MAMC), W-PAFB, Ohio 45433

DD FORM 1 NOV 65 1473 REPLACES DD FORM 1473, 1 JAN 64, WHICH IS OBSOLETE FOR ARMY USE.

UNCLASSIFIED

Security Classification

UNCLASSIFIED
Security Classification

14. KEY WORDS	LINK A		LINK B		LINK C	
	ROLE	WT	ROLE	WT	ROLE	WT
Oxidation Refractory Borides Graphites JT composites Hypereutectic carbide-graphite composites Refractory metals Coated refractory metals Metal oxide composites Iridium coated graphites Characterization Nondestructive testing						

UNCLASSIFIED
Security Classification